Czech Technical University in Prague
Faculty of Electrical Engineering
Department of Electrotechnology

STUDY OF MECHANISMS OF THE SPARK PLASMA SINTERING TECHNIQUE

Doctoral Thesis

Jakub Cinert

Prague, February 2018

Ph.D. Programme: Electrical Engineering and Information Technology (P2612)

Branch of study: Electrotechnology and Materials (2602V009)

Supervisor: prof. Ing. Václav Bouda, CSc.

Supervisor-Specialist: Ing. Tomáš Chráska, Ph.D.

Acknowledgements

First of all, I would like to thank prof. Václav Bouda and Dr. Tomáš Chráska for supervising my scientific work. Their mentoring greatly affected the quality of my scientific results. The thesis has been done in very close collaboration with the Department of Materials Engineering at the Institute of Plasma Physics of the Czech Academy of Sciences. I would also like to thank all my colleagues from the department for our discussions and for their support during the measurements, namely Jakub Klečka for the polishing of samples and hardness testing. I greatly appreciate Dr. Radek Mušálek, Dr. Monika Vilemová, Jan Medřický and Jan Maňák (from the Institute of Physics of the Czech Academy of Sciences) for their help with the SEM imaging. I thank to Dr. František Lukáč for XRD analysis.

This work was partially supported by Czech Academy of Sciences Strategy AV21 and by the grant GA15-15609S (Ultrafine-grained and nanocrystalline metals with high strength prepared by pulsed electric current sintering) provided by the Czech Science Foundation.

Declaration

I hereby declare that this thesis is the result of my own work and all the sources I used are in the list of references, in accordance with the Methodological Instructions on Ethical Principles in the Preparation of University Theses.

In Prague 28th of February 2018 .....

Jakub Cinert

Table of Contents

Abstract

This Doctoral thesis is written for the purpose of a deeper understanding of the spark plasma sintering processes. The main objective of the work is to deeply evaluate how the change of sintering parameters (length of electric pulse, heating rate and sintering pressure) can affect the material properties of a sintered sample. The sintering process was investigated in detail, especially the reliability of temperature measurement. It was found that the measured temperature is different to the real temperature of the sintered sample, moreover this temperature difference depends on the parameters of sintering and the electrical conductivity of sintered powder. On the base of measured data, the sintering process was optimised and the reproducibility of sintering was investigated. While samples sintered by non-pulsed current showed relatively a good reproducibility, the reproducibility of samples sintered by pulse current was significantly worse. The influence of the sintering parameters were studied on a carefully selected materials with regard to the previous measurement. The mechanical properties of the sintered samples were studied through a measurement of porosity, hardness and flexural strength. The phase composition of samples was characterised by XRD analysis. It was found that the pulsed current has not improved any mechanical properties of the sintered samples and contrarily its usage might result in worsening of mechanical properties of the sintered samples. All measurements in this work provide new knowledge about the Spark Plasma Sintering process and thereby contribute to a better understanding of the spark plasma sintering processes. These results might be well used in a further research.

Keywords:

Spark plasma sintering, SPS, Field Assisted Sintering Technology, FAST, Sintering, Reproducibility, Sintering mechanism, Influence of pulsed current

Abstrakt

Předložená doktorská práce se zabývá hlubším porozuměním problematiky Spark Plasma Sintering, hlavním cílem práce je vyhodnocení vlivu parametru slinování (jako je například délka elektrického pulzu, rychlost ohřevu nebo sekvence ohřevu a aplikovaného tlaku) na mechanické vlastnosti slinutých vzorků. Proces byl detailně studován, zejména pak přesnost měření procesních teplot. Bylo zjištěno, že se teplota slinovaného prášku a teplota měřená výrazně liší. Tento teplotní rozdíl závisí na parametrech slinování, zejména na rychlosti ohřevu a na elektrické vodivosti slinovaného prášku. Na základě naměřených dat byl slinovací proces zoptimalizován a byla vyhodnocena jeho reprodukovatelnost. Jak ukazují naměřené údaje, při slinování stejnosměrným proudem lze dosáhnout poměrně dobré opakovatelnosti výroby, ovšem při použití pulzního proudu se reprodukovatelnost procesu znatelně zhoršuje. Vliv parametrů slinování byl vyhodnocován na široké řadě prášků a při vyhodnocení byly využity poznatky z předchozích měření, zejména byl brán ohled na reprodukovatelnost procesu slinování. Mechanické vlastnosti, respektive jejich změny byly u jednotlivých vzorků vyhodnocovány pomocí měření pórovitosti, tvrdosti a pevnosti v ohybu. U vzorků bylo dále zkoumáno jejich fázové složení a byla pozorována jejich mikrostruktura. Bylo zjištěno, že slinování pulzním proudem nepřináší oproti slinování stejnosměrným proudem žádné prokazatelné vylepšení materiálových vlastností vzorků, naopak u některých typů materiálů bylo prokázáno jejich zhoršení. Všechna tato měření přináší nový pohled na problematiku Spark Plasma Sintering a do značné části prohlubují současný stav znalostí této metody. Tyto výsledky mohou být využity při dalším výzkumu.

Klíčová slova:

Spark plasma sintering, SPS, Field Assisted Sintering Technology, FAST, slinování, reprodukovatelnost, mechanismus slinování, pulzní proud

1 Introduction

Sintering is one of several processes for compacting and forming powder materials (metal or ceramics) into solid-state objects by heat and pressure at temperatures below their melting point. The sintered particles are bonded together by atomic transport mechanisms and the particle growth results in a decrease in porosity[1] [2] [3].

The driving force for a sintering process is the reduction of system enthalpy by reducing of the specific surface area or by a decreasing structural enthalpy (e.g. by the process of re-crystallization).

The result of a sintering process is affected by several points [4] which can be divided into two basic categories. The first one is called the "process variables" and contains all parameters that may be affected by a change of a sintering process (sintering temperature and holding time, sintering pressure, furnace atmosphere etc.). The second category is known as "material variables" (geometrical structure of particles, their size and size distribution) [5] [6] .

Structure and size distribution of particles have a significant effect in sintering processes. It has been established that particle size affects the sintering kinetics, especially at the neck forming areas among the grains[7] [8].

Mathematical models of a sintering process are usually based on the joining of two spherical particles [9] [10]. But in fact any industrial production of spherical particles is relatively difficult. The powder particles in industrial use as seen in *Figure 1-1* are mostly in the form of angular (after grinding), spongy (metal splashing), and flakey particles (grinding thin film by ultrasound). The process of spherical or rounded particle production is mostly used for creating metal particles. A pulsated orifice ejection method has been developed for mass-production of monosized micro particles [11].

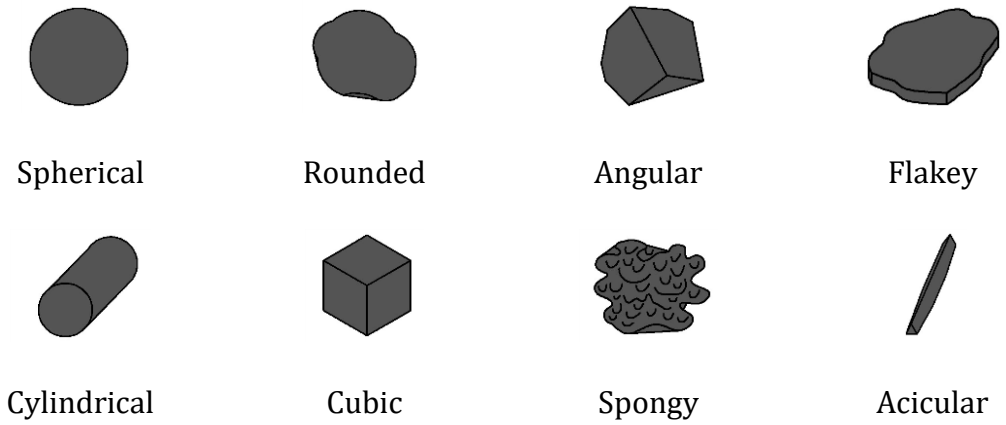

Figure 1-1 Powder particle shapes

1.1 Methods of powder compaction

The "process variables" are given by the chosen sintering methods, which can be divided into two basic groups as shown in *Figure 1-2*. The first group contains techniques where the samples are produced without applied pressure

(except gravity). The second group includes all techniques where the powder is compacted by applied pressure; the pressure is mostly in the order MPa.

Each of these techniques can be divided according to sintering temperatures. In the "Cold pressing" category, the heat is generated by an external pressure or a chemical reaction. The "Hot pressing" category represents all techniques where the heat is generated by an external source [12] [13] [14].

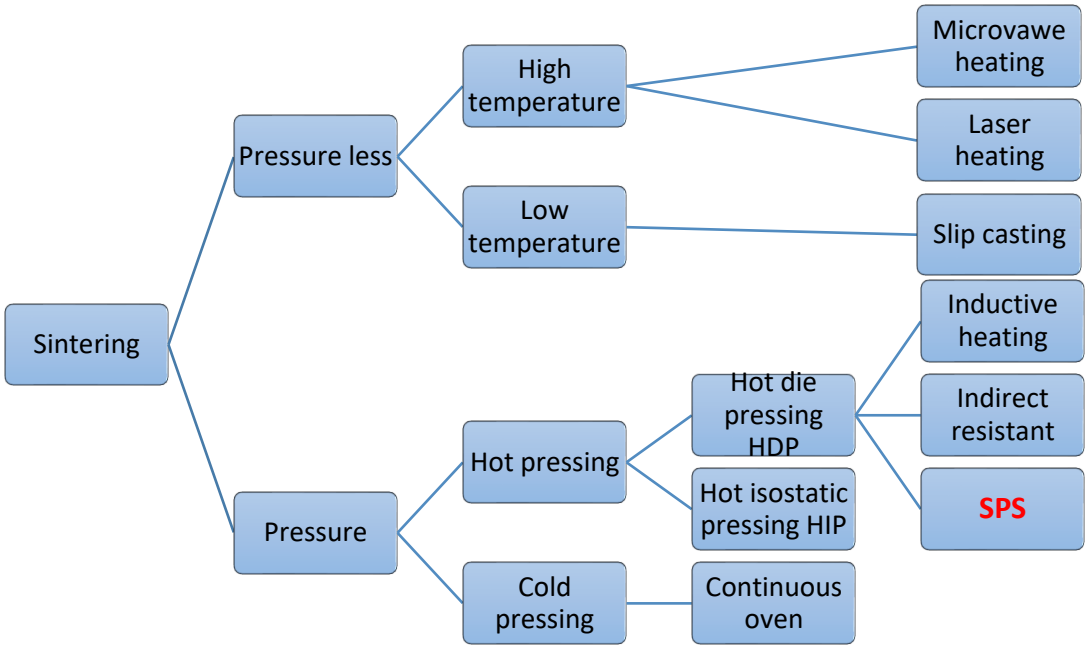

Figure 1-2 Standard classification of the sintering process

1.2 Pressure less sintering

Pressure less sintering is one type of a powder compacting process without applied pressure (except gravity). High component density can be obtained by using fine-grained starting powder (<3µm) and different additives [15].

Two basic processes have been developed up to now. The main difference is whether the final product needs to be burned by high temperature.

1.2.1 Slip-casting

The slip-casting method provides relatively good surface quality, density and uniformity of sintering parts. This technique is mostly commonly used for mass-producing identical ceramic parts, that cannot have simple shapes. A big advantage of the slip-casting method is that the final product mostly does not need a surface finish.

The sintering material for slip-casting is a suspension prepared from micro ceramic powder and a convenient liquid. After the suspension is mixed, a mould is filled up by this suspension.

A mould is composed of a block of plaster (or a different material with high porosity) that has the desired carved inside. The mould can be created from one piece (mostly as single-purpose) or from two halves which then can be used more times.

When the cast piece is removed from the mould, it is neatly trimmed and allowed to dry. This process usually takes between minutes to hours, depending on the size and thickness of the piece.

This technique is commonly used for the mass-production identical ceramic parts [16] [4].

1.2.2 Pressureless/high temperature sintering

This type of sintering requires a high temperature furnace, but does not need any preconditioning of the powder [17]. The initial powder (metal or ceramics) is poured or mechanically vibrated into a mould. The mold is heated up to a sintering temperature. Microwave heating is the most common heat source [18].

The disadvantage of this method is that this process cannot be used for the production of complex-shaped parts and the mathematical model of this type of sintering predicts a much faster rate of grain-growth during pressureless sintering than during HIP [19].

1.3 Pressure-assisted sintering

Dense ceramic or metal parts are mostly created from nano or micro powder pressed and heated by pressure-assisted methods. The powder is basically placed into a closed die and pressured between two or more punches. The high sintering temperature and relatively long sintering time often results in extreme grain growth [20]. Published works show that WC grains grew after HP process from 50 nm to 200-500 nm [21].

Two main types of pressure-assisted sintering methods are shown in *Figure 1-3*.

1.3.1 Cold pressing

The powder is formed into the required shape by applying pressure in a mould with mechanical or hydrostatic pressure. This process bonds the powder particles together (into a so-called “green body”) and allows the green body parts to be handled during the successive high temperature sintering process [13]. The density of the resulting green body compact material increases to around 95 % or more of the theoretical density. When the powder is pressed, the mould is removed [22].

High temperature sintering goes on without the presence of external pressure. The biggest advantage of this method is that a higher heating rate can be achieved because only the powder is heated (not punches and dies). The

process is mostly used for producing very simple shapes – meaning without re-entrant angles in solid form.

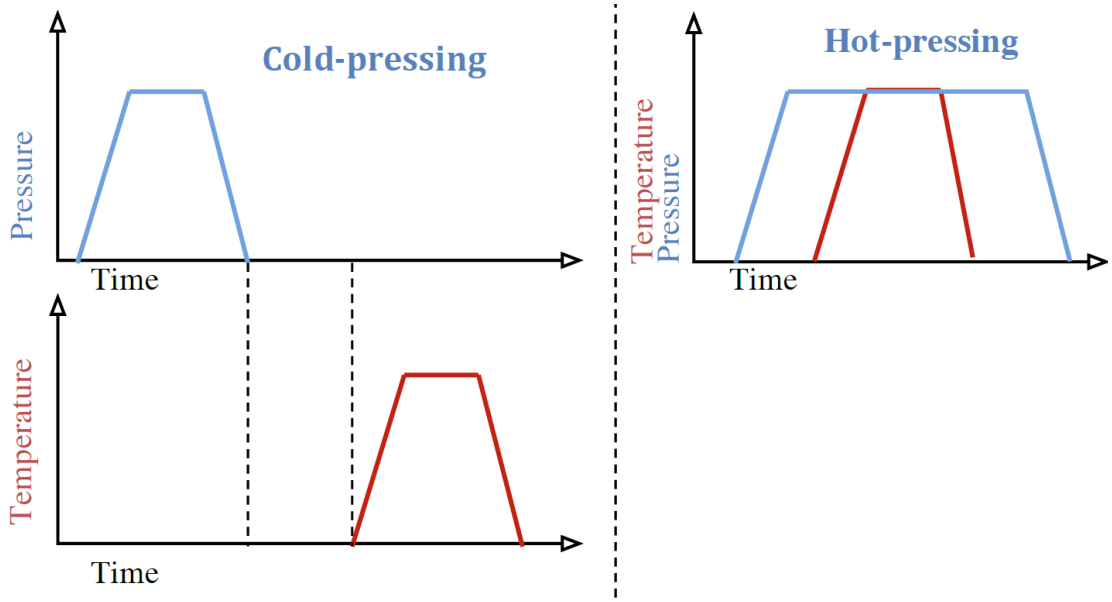

Figure 1-3 Consolidation methods - cold pressing and hot pressing

1.3.2 Hot pressing (HP)

The biggest advantage of HP is that pressure increases the driving force for densification, reducing the temperature required for any sintering process and it results in slower grain growth [23]. On the other hand, HP is suited to produce relatively simple shapes and the sintered part usually requiring diamond grinding to achieve the finished tolerances.

Hot pressing technologies are divided according to type of heating (Hot isostatic pressing, induction heating, indirect resistance heating, and FAST / SPS, Direct hot pressing).

1.3.2.1 Hot isostatic pressing (HIP)

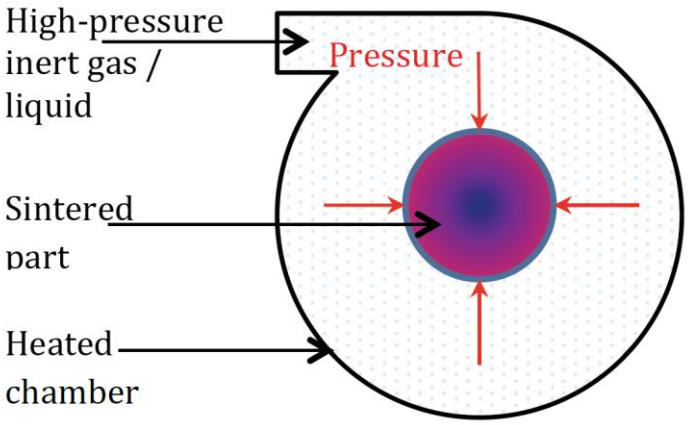

Figure 1-4 HIP technique

HIP shown in *Figure 1-4* is one type of heat treatment that uses high pressure and temperature to improve material properties where the pressure is applied by an inert gas or liquid with a very high thermal conductivity [24]. The big advantage of this method is that it provides fully dense bonded material [22], secures uniform products quality if the product is of a complicated shape [25] and HIP minimalizes the finishing operations as well. But the powder must be held in a required shape before the HIP process; for that reason it mainly uses the Slip casting technique. The heating of the chamber and raising the pressure is a very slow process, resulting in a several hours-long machine cycle [26].

1.3.2.2 Hot Die Pressing

In the hot pressing die sintering process, pressure and heat are applied together at the same time to the sample, but the sample is placed into a heated die [27]. Hot pressing die sintering is mainly used to produce relatively simple shapes from very hard and brittle materials like diamond metal composites, cutting tools and technical ceramics. This technique is limited by the mould material, which is mostly graphite, that allows heating up to maximal temperatures around 2.500 °C [28].

1.3.2.3 Indirect resistance heating

With indirect resistance heating technology, the mould is placed in a heating chamber. The mould is heated by graphite heating elements generating the heat by Joule heating. The heat is then transferred into the die by heat convection. The advantages of this type of sintering are independence of the warming and pressure, high achievable temperatures and punches and mould can be made from non-conductive materials. However, the heating process is relatively slow [29].

1.3.2.4 Inductive heating

The heat is produced in a high frequency electric field by an induction coil and HF power source. The mould must be made from conductive materials, mostly graphite or steel. The advantage is that the pressure and the induced current are totally independent and the heating up process is very fast. But a too high heating rate will result in high temperature differences between the surface and core of the mould, because the electric field can penetrate the mould only between 0.5 mm to 3 mm. The heat is transferred, by thermal conductivity, from the surface into the powder, which is located in the middle of mould [29].

1.4 **Spark Plasma Sintering Technique (SPS)**

Classic sintering techniques as HP, HIP or slip-casting have many disadvantages. The most significant one is the very slow heating rate (in the range 5 – 10 °C per minute [30], depending on the sintering part's volume), because the powder is heated by radiation and conduction from external heating elements. The slow heating rate results in a substantial particle growth [31].

For that reason, a new method of powder compacting called Spark Plasma Sintering (SPS) was developed and patented (US patent NO. 3 241 956) in the

1960s. This technique was further developed during 1980s to 1990s [20] and nowadays it is also known as Field Assisted Sintering Technology (FAST), Plasma Activated Sintering (PAS) and Electric Current Activated/Assisted Sintering (ECAS). The first commercial SPS machine was developed by Sumitomo Heavy Industries Ltd. in 1990 [32]. There have been many publications focused on the advantages of SPS from the point of developing new materials, but only few papers have focused on the specific mechanisms occurring during the sintering process [33]. SPS offers many advantages over traditional sintering techniques like HP, HIP or atmospheric furnaces. For example, the heating rate around 1000 °C per min [34] can be achieved (depending on the geometry of die, punches and on power supply). Further advantages are the lower sintering temperature, short holding time, no need of pre-compaction and shorter sintering time results in the possibility to sinter nanometric powder to near theoretical density. But, on the other hand, the SPS technique can be used only for the production of very simple shapes [35]

1.4.1 Basic SPS configuration

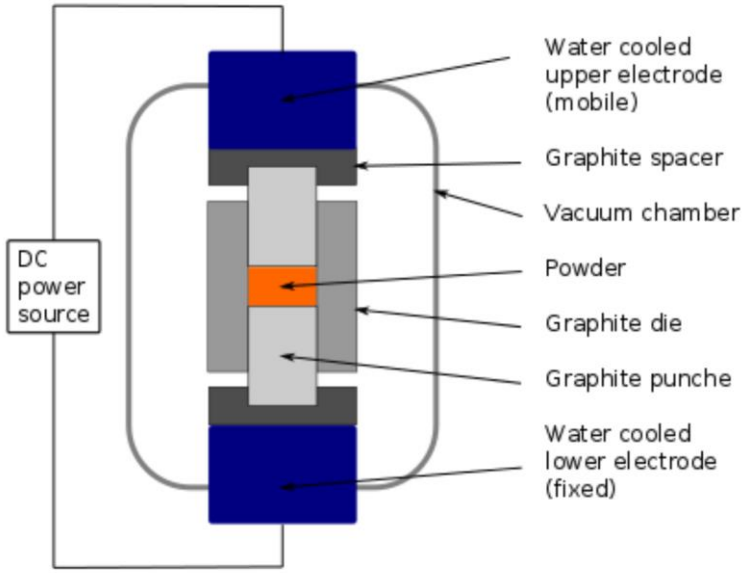

Figure 1-5 Schematic of SPS furnace

SPS is shown in *Figure 1-5*. The SPS system consists of a hydraulic press with a (mostly) vertical single pressurization axis. The pressure is transferred via two steel cylinders (rams) that are also simultaneously used as electrodes. There are two graphite spacers and two graphite punches between upper and lower punch electrodes. The sintered powder is stacked in a cylindrical die and pressed between the punches. Everything is built in a water cooled vacuum chamber. The water cooled electrodes are connected to an electric power supply. The power supply produces electric current flowing through graphite punches, sintered powder and particularly through graphite die. Therefore, the die and the punches are made from an electrically conductive material, which must be able to resist high temperature and pressure. The material of choice is mostly

graphite and thungsten carbide. The powder is placed in the middle of the die. The mechanical load is independent on the generated heat and may be constant or changing during one sintering process. The electric current might be non-pulsed DC or pulse DC (PDC).

1.4.2 Plasma generation and pulse current effect

The ON-OFF DC pulsing might create Joule heat point and spark discharges as seen in *Figure 1-6*. The formation of the spark discharges is located in the gaps between particle surfaces. The spark discharges create points of high temperature area up to 10000 °C that results in the vaporization and melting of the surface of both particles in the area of the spark and secondly necks are formed around the area of contact between particles [36]. The pulse frequency should lead to homogenous temperature distribution through sintering powder, because the heat which is generated during a pulse on the surface of the particle is conducted to the volume of the sintered powder during the "pulse off time" [37] [38].

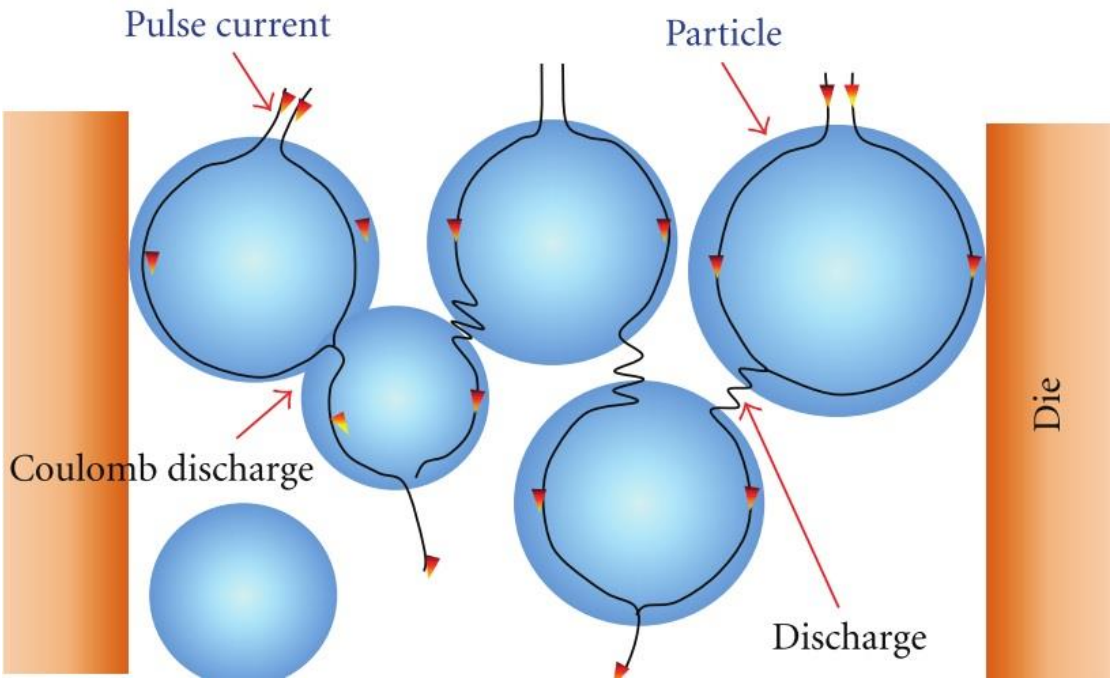

Figure 1-6 A model of SPS process, published in [36] *by Nouari Saheb*

1.4.3 Electro plastic effect

The electro plastic effect is related only to metals, because the valence electrons of metal atoms have small ionization energy. Metals in the solid state contain valence electrons, which are relatively free to leave the atom. These valence electrons can be moved due to the influence of an electric field. Metal powders have been observed to exhibit lower yield strength under an electric field [39]. The microscopic mechanism of electroplastic is still unclear at the present time. Three main models have been described that account for the electroplastic effect [40]. The first article claims that the electroplastic effect in metals is the depinning of dislocations from paramagnetic obstacles by the

magnetic field induced by the electric current (in our case this field is created by a DC pulse electric current) and was published in 1995 [41] [40]. Another publication showed that an electrostatic field applied during plastic deformation of metals reduced the flow stress and retarded cavitation and grain growth. It is possible that the influence of electric field reflects the migration of charged vacancies or may solute atom vacancy complex along particle boundaries to the charged surface [42]. And finally the drift electrons can generate a force on dislocations and affect the plastic flow of metals [40].

1.4.4 Joule heating

Joule heating is a form of resistive heating; it is the process by which the passage of an electric current through a conductor releases heat. The amount of heat Q is given by Equation 1: Joule-Lenz law.

$$Q = I_{rms}^2 . R . t$$

Equation 1: Joule-Lenz law

The resistance between two particles depends on their geometry. It is known that resistance is indirectly proportional to the size of contact area of two particles and to the cross-section of particles. If the contact size of two particles is smaller than their cross-section, more heat is generated on the border of the particles. It might be one mechanism of neck growing in an early sintering step.

1.5 **Challenges and opportunities for spark plasma sintering**

The recent widespread use of the SPS method has been described by many papers demonstrating numerous benefits of this method in relation to other conventional techniques. The main benefits of SPS have been identified and include:

- effect of the current flow (*Chapter 1.5.1)*
- effect of DC pulsing (*Chapter 1.5.2*)
- the effect of rapid heating (*Chapter 1.5.3*)
- the effect of pressure (*Chapter 1.5.4*)

SPS is to a considerable extent similar in several ways to hot-press sintering (HP), but on the other hand, the SPS process is different from hot pressing by the application of the electrical current heating leading to a higher heating rate [43]. Therefore these effects described above will be investigated and the results will be discussed with regard to my results.

1.5.1 Effect of the current (and role of DC pulsing below)

As mentioned before, the fundamental difference between the conventions HP and SPS is the high heating rate, which is caused by the Joule heating from current floating through punches, sintered powder (if it is electrically conductive) and particularly through the die. In addition to the Joule heating, some authors describe another process of the heat generation: generation of plasma between sintered particles. The plasma is proposed to be a

source of a very localized heating between two particles. The generation of plasma was described by several authors. One of the first authors who published the influence of plasma effect was Tokita [44] in the year 1999. In this work, neck formation between particles is described as an influence of the plasma generation: "*When a spark discharge appears in a gap or at the contact point between the particles of a material, a local high temperature-state (discharge column) of several to ten thousands of degrees centigrade is generated momentarily. This causes evaporation and melting on the surface of powder particles in the SPS process, and "necks" are formed around the area of contact between particles."* However, the experiment was carried out with material Si_3N_4, which is not electrically conductive and no electrical current can flow through the sample, as is explained in *Chapter 4.3.1*. Older mentions of the plasma generation were written mostly by Japanese authors between the years 1993-1995 [45], but many articles were written in Japanese [46], [47].

Another older publication by Makino [48] measured the current passing through sintered Al_2O_3 powder and it was found that at the temperature 1000 °C, the current was around 100 mA in comparison with the peak total current of 1000 A.

A very similar work with contradictory results was written by H. Tomino et el. [49]. One of their experiments was the sintering of alumina powder in graphite die and punches. They concluded that no current flowed through the alumina powder and therefore there was a lack of any discharge generation within the non-conducting sample.

Another work published by G.Xie [50] described the sintering of pure Al where the pulse frekvency 40 kHz was used. The result of the work is that there was no discharge presence during a sintering cycle.

Many publications [51] [52] [53]dealing with the SPS process are referenced to the experiment done by O. Yanagisawa [54]. Copper spherical powder (550μm) was placed in a non-conductive die with a cross-section of 2 x 1.45 mm and pressed by two copper punches. The experiment was carried out under pressure of 7 - 16 MPa and applied current density of 17- 170 A mm^{-2}. Observable discharges arose after the current density exceeded 100 $A.mm^{-2}$ at the pressure of 6.9 MPa. The experiment was repeated at higher pressure of 10.1 MPa and the discharge was determined after exceeding the current density 117 $A.mm^{-2}$. However, a normal SPS process uses electrically conductive die and sintered samples are usually much bigger (normally 1-2 cm in diameter). The attainment of the critical current density of 100 $A.mm^{-2}$ within sintering by SPS would require a sintering current above 31.5 kA (for a sample with 10mm radius); however, SPS power supplies are usually not so powerful.

The fundamental principle of spark plasma sintering was investigated in publication [55]. The aim of this work was to confirm if the SPS sintering process involves the presence of momentary plasma or sparks generated between particles of various types of powder summarized in *Table 1-1.*

Powder	Temperature (°C)	Atmosphere
None	650	Vacuum
Al	500	Vacuum
Al_2O_3	650	Vacuum
NaCl	650	Vacuum
Mg	450	Vacuum
Zn	225	Vacuum
Zn	225	Ar

Table 1-1 Used powder in the publication [55]

The experiment was an in situ observation of powder sintering by atomic emission spectroscopy (AES) and consisted of a high- temperature fiber optic flame probe connected by a fiber optic patch cable connected to a very sensitive spectrometer. The fiber optic flame probe was protected by a borosilicate glass capillary tube and placed directly in wide variety of sintered powders. Moreover, the in situ voltage measurement between upper and lower punches was made. The voltage was measured by an oscilloscope with a sampling rate of 5 GHz. Applied pressure on the sintered powder was held as low as possible to maximize the presence of the point contacts between sintered particles and reduce their plastic flow. A wide variety of conductive or non-conductive powders and SPS conditions were used in this investigation.

All of the experimental methods indicate that there was no plasma or sparks present during the sintering processes.

1.5.2 Role of DC pulsing

Only few publications dealt with the effect of pulse length and frequency on material properties of sintered samples.

One paper [56] investigated the influence of pulse pattern parameter (on:off - 12:2, 2:2 and 2:6) on the reactive sintering of α-$Al_{2-2x}Fe_{2x}O_3$ where **X** a variable. A reactive spark plasma sintering process might produce materials with surface-layer composition and microstructure different to that of the core. The pulse current influence on the change of the surface microstructure and the surface layer position to the core of sample was discussed. Average composite layer thickness was about 38 μm for pulses ratio 12:2 and 48 μm for pulses 2:2 and 2:6. The bottom thickness was 32 μm for all samples. The observed asymmetry of the sintered samples, where upper and bottom sites had different thickness of the same composition, was described as unidirectional cationic

migration. On the other hand, the results were not compared with samples sintered by not pulsing DC current. In addition, it is disputable if the change in the layer thickness would prove to be the same for more samples sintered by identical pulse patterns.

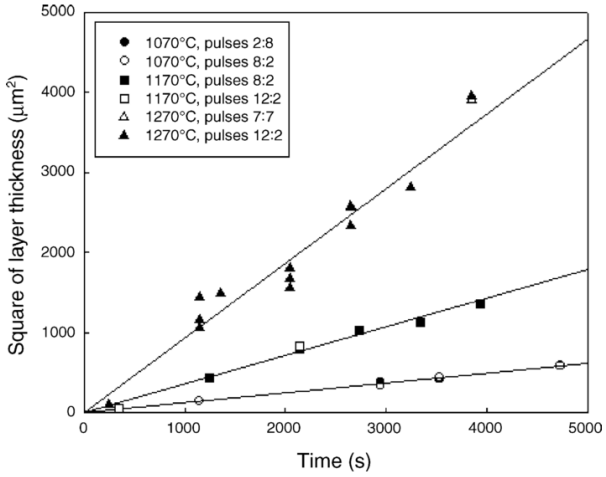

Figure 1-7 The growth of $MoSi_2$ layer in the SPS at different temperatures and under different pulse patterns [57]

A very similar approach is used by Anselmi-Tamburini et al. [57]. The paper *Figure 1-7* investigates the influence of a DC pulsing current on the reactivity between Si wafer and Mo foils. Pulse waveforms for patterns of (on:off ms) 6:24, 21:21, 36:6, and 24:6) were chosen for the current generated by the SPS and measured in real-time. To determine the effect of pulsing, the authors preferred to investigate the solid-state reactivity rather than the sintering of a powder as the boundary between two flat foils (Mo and Si) is well defined. The interaction between Mo and Si layers resulted in the formation of a product layer, primarily $MoSi_2$. SEM images of the product layer revealed that the direction of the current and the pulse pattern had no effect on the thickness of the product layer.

Another publication dealing with the effect of pulsed current was written by Chakraborty [58] in 2015. ZrB_2 ceramic powder was sintered and the influence of current pulse on its densification, mechanical and tribological properties was investigated. The electrical conductivity of ZrB_2 is surprisingly high $>10^6$ $S.m^{-1}$ [59], which is in contrast to the property of any typical ceramic. ZrB_2 powder was sintered at 2100 °C in argon atmosphere at 35 MPa with different DC pulse on–off patterns (the shortest pulse 1ms, the longest 100 ms). The paper concludes that the maximum relative density (98.65 %, measured by the Archimedes method) is achieved by 50 ms pulse on and 5ms pulse off and the Vickers hardness (1 kgf) of the sample was 16.64 ± 1.48 GPa. On the other hand, the minimal density was achieved by pulses 10 ms on and 1 ms off. The minimal density was 97.41 % and the Vickers hardness was 15,32 ± 1,29 GPa. The values for sintering by direct current (without any pulses) are 98.58 % for relative density and 15,69 ± 1,33 GPa for hardness. The analysis of XRD patterns of ZrB_2 samples SPSed either without pulses or with (T_{on} 50ms and t_{off} 5 ms)

shows different crystallite size of samples, which was 99 nm for the sample sintered by direct current and 83 nm for pulsed current. As seen from these results, the hardness is approximately the same for all tested samples after taking the measurement uncertainty into account. Although the reported data are an average of five local hardness measurements, it would be appropriate to compare two identical samples if their hardness is equal.

Sl no.	Pulse (ms)		RD %	Hardness (GPa)
	t_{on}	t_{off}		1 kgf
1	Direct current		98.58	15.69 ± 1.33
2	10	1	97.41	15.32 ± 1.29
3	10	5	98.25	16.14 ± 1.42
4	10	10	98.30	15.88 ± 1.34
5	10	15	96.12	15.39 ± 1.22
6	50	5	98.65	16.64 ± 1.48
7	50	25	97.91	16.50 ± 1.38
8	50	50	98.05	16.09 ± 1.29
9	100	5	98.03	16.02 ± 1.31
10	100	50	97.87	16.25 ± 1.32
11	100	100	98.10	16.29 ± 1.30

Figure 1-8 ZrB2 samples under different pulse schedules of spark plasma sintering at 2100 °C for 15 min dwell time [58]

The relative density of a carbon fiber-reinforced aluminum matrix (Al–CF) composite fabricated by SPS in various pulse conditions was investigated in publication [60]. They used DC pulsed current with on:off ratio 24:1, 12:2, 6:4 and 3:3, one amplitude of pulse was 3 ms. Two types of samples were prepared by mixing 50 vol% of carbon fibers (CF), where the first type was 80 μm long CF and the second one was 500 μm long CF.

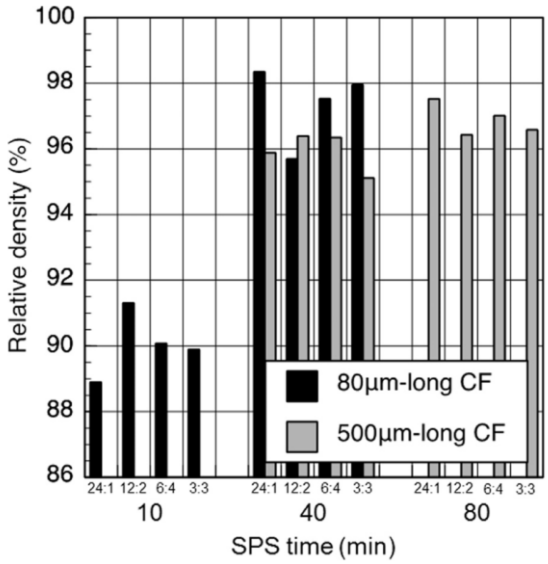

Figure 1-9 The relative densities of Al–CF 50 vol% composites fabricated by SPS with various pulse conditions [60]

Sintered samples were prepared with uniaxial pressure of 50 MPa, the heating rate of 40 °C/min at maximum temperature 600 °C. Dwell time was

10 min for samples with 80 μm CF, 40 min for samples 80 and 500 μm CF and 80 min for samples with 500 μm CF. The results of porosity are obvious from *Figure 1-9*. The Al–CF samples were annealed at 650 °C for 6 h under argon atmosphere and the thermal expansion behaviour was tested. The authors reached the conclusion that the pulse condition of SPS is one of the significant factors which might control the Al/CF interfacial condition and in turn determines the thermal expansion behaviour of the Al–CF composite.

1.5.3 The heating rate effect

One of the biggest differences between conventional hot pressing and SPS method is a very rapid heating rate of 1000 °C/min that can be achieved by using the SPS method. The effect of heating rate on grain growth and densification was investigated and described by several authors. The influence of SPS heating rates on the synthesis reaction of tantalum diboride was investigated in [61]. The SPS technique was used to realise reactive sintering processes of powders where the final product was TaB_2. The mixture of powders was sintered at 2200 °C, 48 MPa for dwell time 5 min. Heating rates were chosen from 50 °C/min up to 400 °C/min.

Heating rate	**Apparent density**	**Relative density**	**Young's modulus**	**Hardness**	**Mean grain size**
(°C /min)	(g/cm^3)	(%)	(GPa)	(GPa)	[μm]
50	11.74 ± 0.03	93	577 ± 10	17.4 ± 0.4	3.8 ± 0.3
100	11.70 ± 0.06	93	559 ± 10	20.5 ± 0.9	4.2 ± 0.5
200	11.96 ± 0.03	95	571 ± 13	20.7 ± 0.8	3.8 ± 0.1
300	11.49 ± 0.03	91	532 ± 9	20.6 ± 0.7	4.0 ± 0.2
400	11.77 ± 0.03	93	571 ± 10	19.1 ± 0.2	4.0 ± 0.2

Table 1-2 Influence of different heating rate on the reaction of Ta + 2B mixture, obtained at 2200 °C during 5 min. [61]

All sintered samples had a relative density of 91–95 % and Young's modulus 532-570 GPa. The Vickers hardness for samples heated at the rates from 100 °C/min to 400 °C/min was around 20 GPa, the samples heated at the rate of 50 °C/min had the hardness of 17.4 GPa. The XRD patterns for all materials were similar with no significant differences.

The influence of heating rate on superconducting characteristics of MgB_2 was investigated in [62]. Other material properties and analyses as crystallite size, magnetic moment, critical current density, SEM and XRD were done as well. The MgB_2 powder was sintered by several heating rates (20, 100, 235, 355, and 475 °C/min). The different heating rates were applied from room temperature

up to 1100 °C. From 1100 to 1150 °C the heating rate were constant of 50 °C/min. The uniaxial pressure applied on samples was 95MPa. The relative samples density was above 95.1 % (for heating rate 100 °C/min) up to 99.5 % (for heating rate 355 °C/min). XRD identified the main phase, which was MgB_2, and two secondary phases MgO and MgB_4. Higher heating rate (355 and 475 °C/min) promoted formation of a lower amount of secondary phases. The critical temperature for superconductivity is approximately 38.8 K for all SPS samples. The most significant difference is in the morphology of samples as was observed by SEM. For samples sintering with lower heating rate (as 20 °C/min) straight grain boundaries were defined. On the other hand, samples sintered 355 and 475 °C/min grain boundaries between particles can be observed with difficulty and often they show round shape edges.

But some publications investigated the effect of heating rate on densification and grain growth gave conflicting results *Table 1-3*. Two types of powder were sintered [63] by different heating rates from 50 °C/min to 700 °C/min. One powder was eclectically conductive $MoSi_2$ and the second was insulating α-Al_2O_3.

Heating rate	**Final density (g/cm³)**		**Grain size (μm)**	
(°C/min)	Al_2O_3	$MoSiO_2$	Al_2O_3	$MoSiO_2$
50	3.95	5.73	6 to 9	2 to 4
250	3.95	5.73	3 to 4	2 to 4
700	3.93	5.76	0.5 to 0.6	2 to 4

Table 1-3 Density and grain sizes of SPS sintered samples as a function of heating rate [63]

Powders were sintered at 1100 °C for 2 minutes under the pressure of 45 MPa. As seen in *Table 1-3*, there is no effect on the final density for samples sintered by different heating rate. Alumina showed a dependence on heating rate -the grain size grew with lower heating rate but this dependence is not convincing for $MoSiO_2$ where the grain size and heating rate were independent. This results are with contradiction to another study [64] published that heating rate had a measurable impact on density of alumina samples. The density decreased as the heating rate increased up to 600 °C/min.

1.5.4 Effect of pressure

Sintered powders are heated by floating current and higher densification is also achieved by uniaxial pressing applied simultaneously to the heating. The pressure has a direct mechanical effect on particle rearrangement and destruction of agglomerates. Secondly, the pressure is a driving force for sintering which might lead to a decrease in sintering temperature and a limitation of grain growth. Validation of the effect of applied pressure was provided in many of the recent SPS investigations.

Effect of pressure on the densification and grain size was evaluated in publication [65]. TaC and TaC–1wt.% B_4C were consolidated by SPS at 1850 °C and varying pressure of 100, 255 and 363 MPa. The effect of pressure on the densification and grain size was evaluated by XRD, SEM and high resolution TEM.

The density increased with the pressure and a 100 % density was achieved for 255 MPa and 363 MPa for TaC. The reason for observed densities higher than true density is the reaction between B_4C and TaC leading to formation of new products with higher density than TaC. Samples sintered at 255 MPa and 363 MPa were without any porosity. The grain size was calculated through SEM images and their average size was compared with the starting powder particles size (0.36±0.13 μm). It was observed that the sintering pressure 100 MPa had only a little impact on particles size growth while with the particle growth was significant under higher pressure loading. Validation of these conclusions was provided by [66]. In conformity with this result, it was found that higher pressurizing conditions can decrease the sintering temperatures.

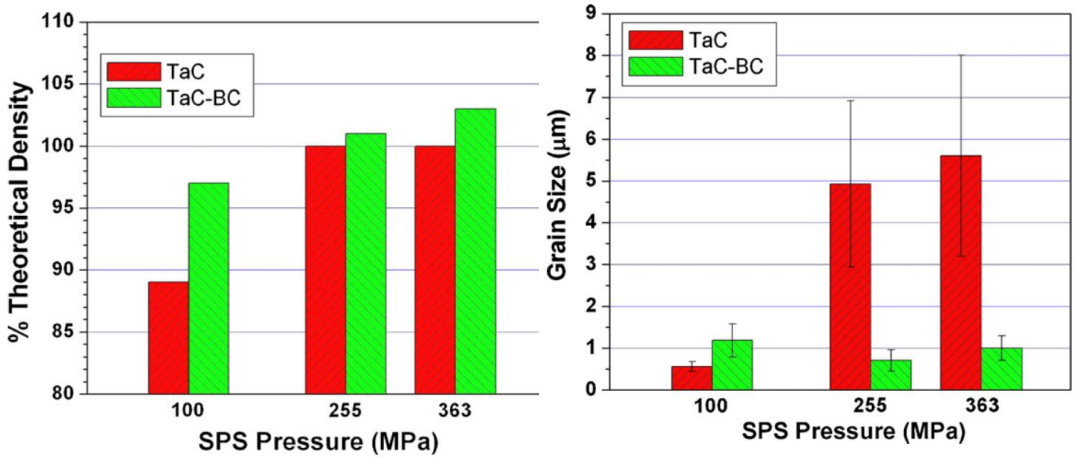

Figure 1-10 Variation of % of theoretical density and grain size of sintered TaC and TaC–B_4C samples within various SPS pressures [65]

2 Motivation for the thesis and design of experiments

As shown in the previous research, the influence of sintering parameters on the mechanical properties has been investigated in many publications; nevertheless the results are very often in contradiction. The main problem of published results is the lack of reliable data collection and statistical evaluation. Measurement of reliability on one sample and repeatability of the sintering process over a wider range of samples are not sufficiently addressed. This work aims to obtain a deeper and reliable understanding of the influence of the electric current on the structure and mechanical properties of samples consolidated by the SPS technique.

The design (and sequence) of all experiments are seen in *Figure 2-1.* The influence of sintering parameters on the mechanical properties of SPSed samples will be investigated on a carefully selected materials (electrically conductive and non-conductive powders, different powder sizes distribution, single element powders and alloys), which are chosen with regard to the previous experiments described in the introduction.

The SPS process is regulated by the temperature measured by a thermocouple or pyrometer. However, this temperature is not measured directly in the sintered powder, but in the bottom punches or in a hole in the die. Therefore, the measured temperature and the temperature inside the compacted powder might be different. This temperature difference and its dependence on heating rate and electrical conductivity of sintered powder will be investigated. Based on the obtained result, an optimised sintering course will be implemented. As a result, the difference between the set point temperature and the real temperature of the sintered powder will be minimised.

The next step is to determine suitable sintering temperatures for all used powders. The aim of this work is to evaluate the effect of current pulsing on sintering. Therefore, it is appropriate to evaluate this effect on not fully dense samples. Since the samples will be compacted by a non-pulsed and pulsed current, the benefits of pulsed current should be observable in lower porosity of the compacted samples (compared to the porosity of samples compacted by a non-pulsed current). Therefore, the temperatures of sintering are determined as the temperatures when the porosity of the SPSed samples is around 5 %.

It was proved [67] that the microstructure of SPSed samples is not homogeneously distributed. The porosity of samples is higher around their circumference than in the centre, thus the material properties (hardness, grain size) of samples might not be homogeneously distributed as well. The hardness measurement will therefore take this inhomogeneity into consideration and all hardness measurements will be designed to provide a reliable result.

Because the difference in mechanical properties of samples sintered by a pulsed or non-pulsed current is in order of percent (*Chapter 1.5.2*), the reproducibility of the sintering process must be carefully investigated as well.

After the reproducibility of the SPS process and measurement reliability of selected samples properties is verified, the influence of different sintering parameters (electric pulse length, sequence of heating and applied pressure and different heating rate) on the mechanical properties of sintered samples might be studied in detail.

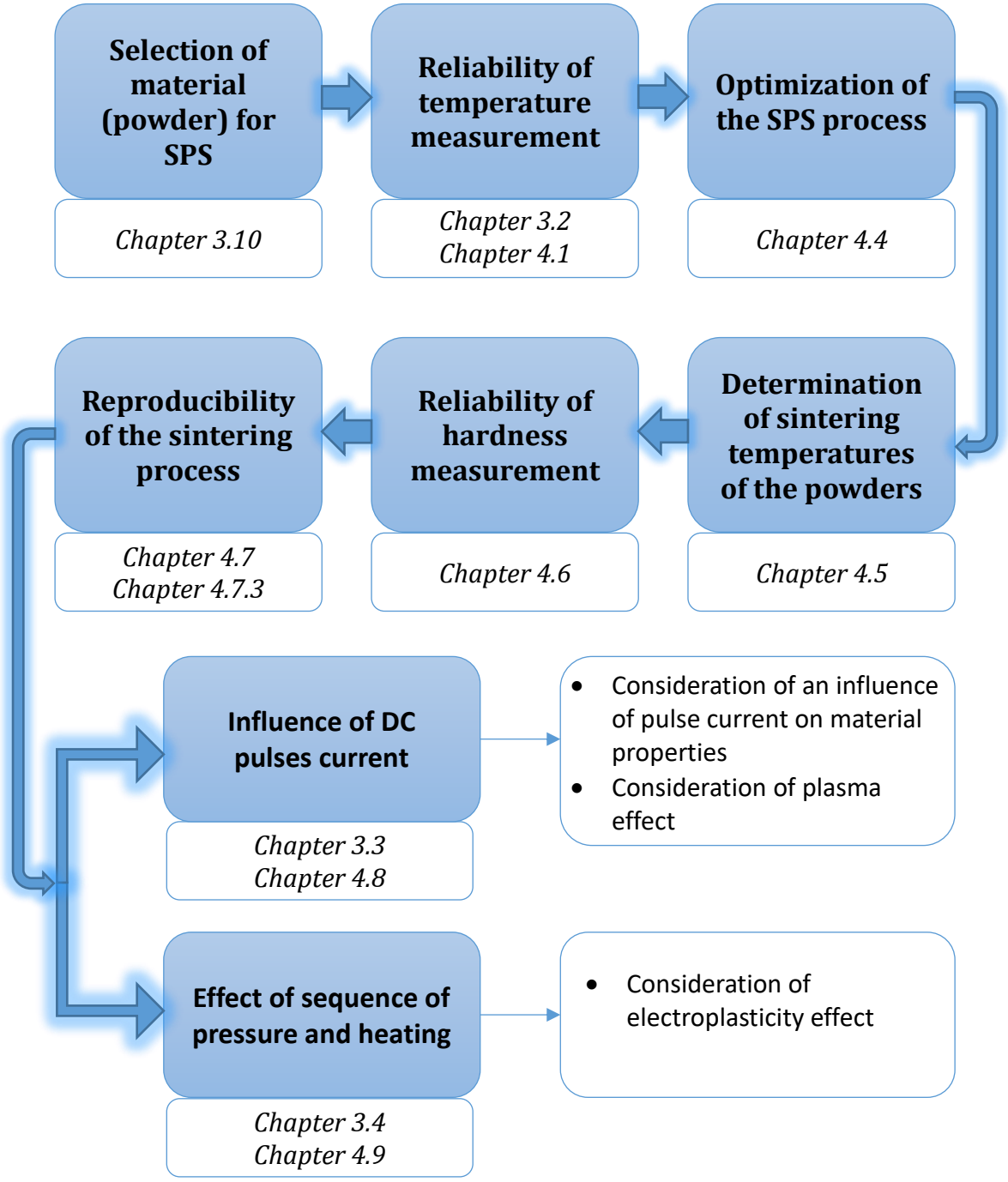

Figure 2-1 Design of experiments

3 Materials and experimental method

3.1 **Experimental SPS device**

All measurements have been carried out by the SPS *Thermal Technology LLC, SPS 10-4 10Ton* as seen in the *Figure* 3-1. This SPS machine is composed of four DC power supplies (1), one control unit (2) and a vacuum chamber (3).

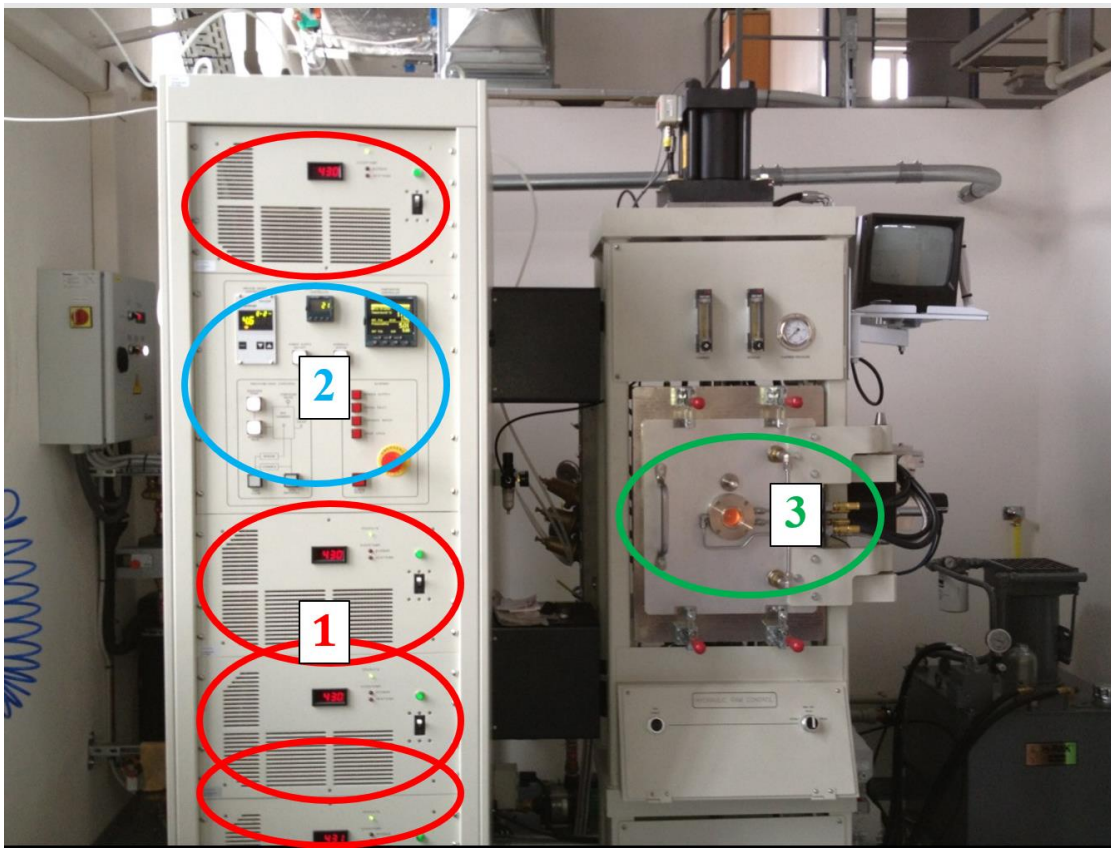

Figure 3-1 SPS Thermal Technology LLC, SPS 10-4 10Ton

The power supplies are connected in parallel, their maximum voltage is 10 V and the maximum output current is 4 kA (1 kA each of them). The pulse of current pulse can be 1ms or longer and the hydraulic press force by force up to 10 t.

The process of sintering is controlled by the Eurotherm unit regulating temperature, uniaxial pressure and sintering time. The process temperature is measured by a thermocouple or a pyrometer. The optical pyrometer is focused into a hole in a side of the die and the thermocouple is placed in the bottom punches, as shown in *Figure 3-2*. This controller reads the process parameters, which are a change of upper punch position (this value is equal to the sintered sample compaction), the vacuum value, temperature and uniaxial pressure set, voltage and current. The sampling rate of measurement is 1 Hz.

The vacuum chamber is cooled by a water-cooling system. The sintering process can be operated in a vacuum (for sintering temperature bellow 1200 °C)

and an inert atmosphere (for sintering temperature above 1200 °C). The final samples' diameter is usually 2 or 3 cm, depends on the used punches and die diameter.

The SPS process is limited by used graphite parts, which can be loaded by a pressure of no more than 100 MPa, Thermocouple type K can be used up to the temperature of 1200 °C and pyrometer in the temperature range of 500 °C to 2000 °C. Thermocouple C probe is designed for use in extreme temperatures, up to 2000 °C. However, the thermocouple is placed into a molybdenum sleeve and its usage is not recommended in applications where the probe would be exposed to carbon, including graphite. The molybdenum sleeve was sprayed by a thin layer of boron nitride. Nevertheless, its reaction with graphite parts was significant. For that reason, the durability of the thermocouple "C" is limited and its usage is suggested only for the verification of sintering temperatures (up to 1500 °C), not as a SPS process controller. Thermocouples type K and type C cannot be combined, as only one type of thermocouple can be used per sintering cycle.

3.2 Reliability of temperature measurement

The aim of the following procedure is to verify the reliability of the SPS temperature measurements by using three thermocouples and one pyrometer. Two new holes were drilled into one die. One hole was drilled into the same depth (7 mm from the sample) as the hole for the pyrometer and the second hole is deeper (3 mm from the sample). The temperature was measured in three holes by thermocouples and compared with the pyrometer value. As seen in *Figure 3-2,* the thermocouple "Term2_pyro" and the pyrometer measure the temperature in the die at the same depth, but the holes are turned by 90°. The thermocouple "Term3_deep" is located in the die and is closer to the sample - it is placed in the bottom punch, 4 mm vertically from the sample.

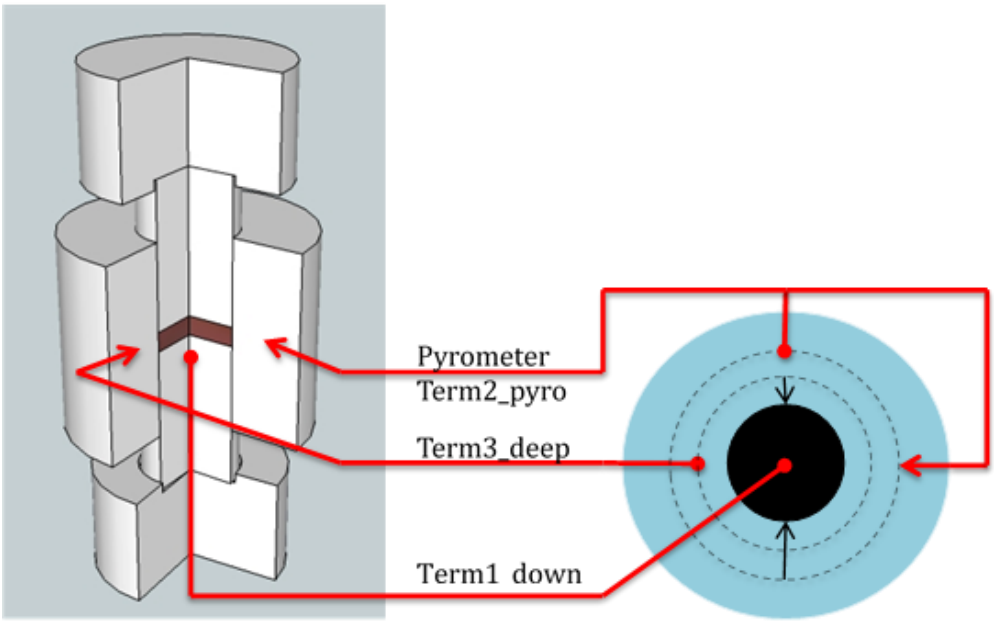

Figure 3-2 Set of SPS die and punches with highlighted position of measured points

The SPS process temperature might be regulated by the pyrometer or by the thermocouple "Term1_down". It is evident that the temperature in these points can be different from the temperature of consolidated powder. In our case, the temperature for the process regulation was measured by the pyrometer and temperature was verified in three different places by type K thermocouples. The sintering process was limited by a used thermocouple at the temperature of 1200 °C. A 100 °C/min heating rate was chosen. After the first sintering cycle, the punches and die were disassembled and for the next measurement the new powder Al_2O_3 was used and the sintering cycle was then repeated. The measurement of repeatability fulfilled all conditions described in the Guidelines for Evaluating and Expressing the Uncertainty of NIST Measurement Results [68], which are

- The same measurement procedure and measuring instrument
- The same observer
- Repetition over a short period of time

This measurement is highly important, because the error of temperature measurement might be caused by:

- A thermocouple which is not in direct contact with the bottom of the hole. It might be eccentric to the hole centre line and touches one side of the hole. Or the thermocouples cannot be pressed correctly to a measured object and the end of the thermocouples are not in contact with the hole surface.

- The effect of interfering fields - the thermoelectric voltage is very small (in the order of mV). A small change of the thermoelectric voltage by 4μV corresponds to a temperature change of about 0.1 °C. Due to interfering elements like the magnetic, electric and electromagnetic fields, parasitic capacitance bonds and current parasitic loops might change the thermoelectric voltage and cause the measured temperature to be inaccurate.

3.3 Effect of pulse current

All samples will be compacted with a non-pulsed current and pulsed current. The material properties of all samples will be compared and thus the effect of pulse current will be investigated. The difference between both current conditions shown in *Figure 3-3.* The heat generated during a sintering cycle is proportional to the RMS (effective) value of electric current. Therefore, the same RMS current evolution responds to the sintering cycle (temperature evolution) under various pulse conditions. Although the RMS current evolution is identical for all pulse patterns, their value of maximal current will be higher.

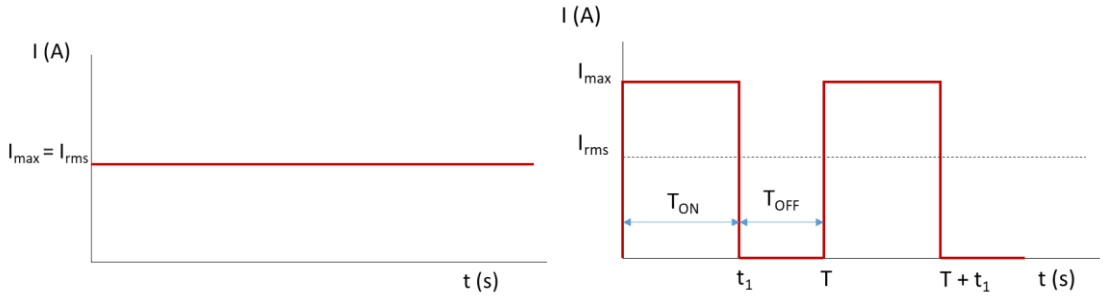

Figure 3-3 SPS non pulsed current and pulsed current

The RMS value of the pulse current can be calculated from the following equation as a general RMS definition which is an integral over the signal period

$$I_{rms} = \sqrt{\frac{1}{T}\int_0^T i(t)^2 \,.\, dt}.$$

Equation 2 I_{rms}

The Equation 2 applied on the pulse current, where the time variable and the maximum value of the I_{max} is a constant

$$I_{rm} = \sqrt{\frac{1}{T}\int_0^{t_1} I_{max}^2 . dt + \int_{t_1}^{T} 0^2 . dt}.$$

Equation 3 I_{rms} of pulsed current

Therefore, the RMS value of pulse is expressed Equation 4

$$I_{rms} = I_{max}\sqrt{\frac{t_1}{T}},$$

Equation 4 Final IRM

and the duty cycle D is given as a ratio of dwell time of one pulse and a signal period.

$$D = \frac{t_1}{T} = \frac{T_{ON}}{T_{ON} + T_{OFF}}$$

It is noticeable that the values of a maximal current and the value of a duty cycle are dependent on each other. The maximal value of an electric current increases with decreasing value of duty cycle (for constant RMS value of electric current). The powder is heated in the time "T_{ON}" and during the time "T_{OFF}", the generated heat is conducted into its volume. However, the powder is heated at a higher temperature with a decreasing duty cycle and the generated heat is conducted through its volume for a longer time.

Various pulse conditions are compared in this thesis. The pulse conditions have been chosen with regards to the duty cycle and to pulse length shown in *Table 3-1*. The combination of various duty cycles and pulse period includes all

variants of pulse patterns which can be used for a spark plasma sintering process.

Pulse pattern	5-15	15-5	5-5	25-75	75-25	50-50	Non-pulsed
T_{ON} (ms)	5	15	5	25	75	50	-
T_{OFF} (ms)	15	5	5	75	25	50	-
Duty cycle	0,25	0,75	0,5	0,25	0,75	0,5	1

Table 3-1 Current pulse patterns used in this thesis and their marking in graphs

3.4 Effect of sequence of pressure and heating

The influence on the heating and applied pressure respective to their sequence impact has been investigated. Under most conditions, the uniaxial pressure is applied on the sintered powder before or after [69] the sintered temperature is reached or in some cases the temperature and pressure are increasing together [70]. As was described in the theoretical part, three different processes might be of major relevance to the result of sintering, the plasma presence between grains, the electroplastic effect and the diffusion along dislocation cores.

All the phenomena mentioned above are to a certain extent reliant on the applied uniaxial pressure. The electro plastic effect depends on the current density in a sample. Many contact points between particles are present only when the sintered powder is not loaded by the maximum uniaxial pressure. When the particles are not deformed, but connected only in a single point, the current density in these point contacts will be high and it might lead to the electro plastic presence. The presence of plasma required high current density and no direct contact between particles as well, this would be fulfilled if the powder is not pressed by a uniaxial pressure.

But on the other hand, one of the driving forces of sintering is the reduction in the free surface energy of a sintering compact. During sintering, the mass transport, usually mediated by vacancies, is driven by the difference in vacancy concentration. The vacancies might be present in the powder due to the grinding process or as a result of a uniaxial pressure, where the particles are pressed in their touching point over the yield.

As described, the electro plastic effect and a plasma presence are in contradiction to the vacancies formation by a uniaxial pressure therefore the sequence of applying a uniaxial pressure and heating will be investigated.

3.5 Density and porosity measurement

The density of samples was measured in order to classify and identify the influence of sintering parameters on material properties. Compared to the three-point bending test, the density measurement does not vary with the amount or shape of testing materials. The determination of the solid density was carried out by several methods.

The most commonly used method for density determination was the Archimedean immersion method. This method is based on measuring the weight loss of an object when suspended in a fluid of known density that is equal to the mass of fluid displaced from which its volume and density can be calculated. All measuring was carried out with regards to ASTM B962 – 17 and ISO 2738:1999. Samples were determined on the Satorius CPA225D-0CE scale using the Density determination kit YDK03. All samples were measured in a laboratory with a constant air temperature of 20 °C.

Samples were rid of the graphite foil grounded with P220 SiC paper, cleaned in acetylene and distilled water. After drying 1.5 hours at 100 °C and cooling off in room temperature, the dry mass $\boldsymbol{m_d}$ of samples was measured.

As the SPS consolidated samples contained open porosity, appropriate conditioning of the samples is important before distilled water immersion to eliminate the residual gas content. A container with immersed samples was evacuated under the pressure of 50 Pa and samples were saturated for 45 minutes until the open pores were filled with the water. After the evacuation and cooling to room temperature, the samples weighted $\boldsymbol{m_i}$ after being immersed in the water. Then the weight of the saturated sample $\boldsymbol{m_s}$ is determined by weighing in air. Any drops remaining on the surface of the sample are removed with a damp sponge before weighing. The weighing operation is performed quickly in order to avoid loss of mass due to evaporation. The bulk density $\boldsymbol{\rho_b}$ was calculated from three previous measurements as:

$$\rho_b = \frac{m_d}{m_i - m_s} \cdot \rho_{H_2O}$$

The apparent porosity $\boldsymbol{\pi_a}$, which is the sum of open and closed porosity of consolidated samples, is calculated as a ratio of the bulk density and table density $\boldsymbol{\rho_t}$.

$$\pi_a = \frac{\rho_t - \rho_b}{\rho_t} \cdot 100$$

The value and standard deviance of the porosity measurement are based on 10 measurements. If the standard variance is highlighted by red colour in the graph, the value of porosity was measured only once and the standard deviance of an approximate value (±0.2 %) - which is obtained from all measurements - was used. The porosity was also evaluated via SEM and light microscopy image analysis. The proper magnification and number of fields of view are crucial to obtain relevant data of porosity. If the magnification is too low, the obtained data

of pores are not very detailed which might result in an inaccurate measurement. However, if the magnification is too high, one field of view might contain one large pore and only a little microstructure and another field of view contains only microstructure without any pore. For that reason, more magnifications were chosen with regard to particle sizes.

3.6 Hardness testing

SPSed samples were cut as seen in *Figure 3-4*. Materialographic samples were prepared with a Tegramin-25 (Struers, DK) polisher using standard grinding and polishing ending with a 1 μm diamond suspension and OP-S (colloidal silica suspension for final polishing).

The Vickers hardness was evaluated by a Qness Q10a+ hardness tester with 1 or 2 kg load with respect to the samples hardness and grain sizes - the indents were larger than is the size of several grains and thus macro the hardness was investigated.

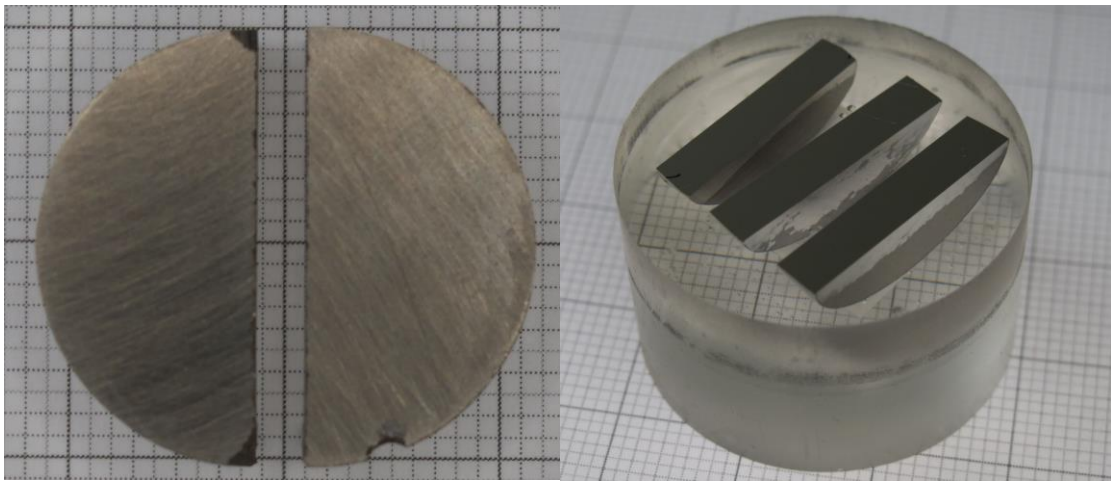

Figure 3-4 Samples prepared for hardness measurement and for metallography analysis

3.7 The Three Point Bend Test

Bend testing (or flexural testing) is commonly performed to measure the flexural strength and modulus of elasticity. The tested sample is laid horizontally over two points of lower supporting pins and the load is applied to the top of the sample through one upper pin until the testing beams cracks.

The parameters of the test are the geometry of upper and lower spans, the speed of the loading, and the maximum sample deflection.

All samples were prepared by the same procedure and tested with same parameters. SPSed samples in *Figure 3-5* (the grid is 1mm) were rid of graphite foil and were cut by a low speed saw to minimalize induced damage. A cut Nickel sample with its cross-section is in *Figure 3-5*. The yield stress was evaluated on beams with typical dimensions about 4 x 5 x 20 mm (the tested beams dimensions were precisely measured before each testing, two tested beams (#1 and #2) are obtained from each SPSed sample). The testing was carried out

according to ASTM C1161-02, though slightly modified with respect to the character of available samples and equipment. All surfaces of the samples were grounded with P220 SiC paper in order to remove any possible material damage caused by the cutting process. The four long edges of each specimen were uniformly chamfered at 45° on SiC grinding paper.

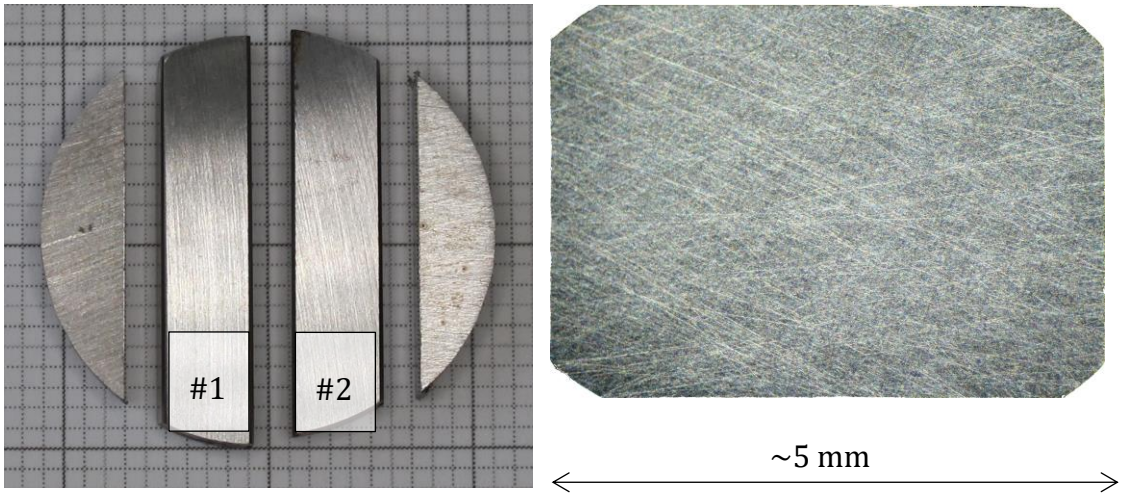

Figure 3-5 Cut SPS'ed sample - two final tested beams and their crossection

All experiments were evaluated by a three-point bending test using the universal testing machine Instron 1362 (Instron, UK) upgraded with 8800 series electronics. The lower and upper support spans are made of hardened steel that is 5 mm in diameter and the spacing of spans was 14.55 mm as seen in *Figure 3-6*. A load force with constant crosshead speed of 0.2 mm/min was applied until a sudden fracture of the specimen.

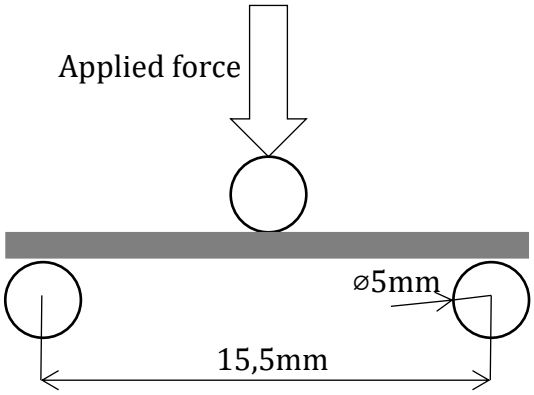

Figure 3-6 Schema of three-point bending test

3.8 XRD analysis

Identification of crystalline phases and quantification of their amount was done by X-ray diffraction (XRD). The measurements were carried out on vertical powder θ-θ diffractometer D8 Discover (Bruker AXS, Germany) using CuKα radiation and 1D LynxEye detector (Ni β filter in front of the detector). A parallel X-ray beam with the radius of 1 mm was formed by polycapillary unit and aimed

at the cross sections of vertically cut samples. Subsequent quantitative Rietveld refinement analysis [71] was performed in TOPAS V5 [72].

3.9 SEM analysis

The microstructure of samples was observed in scanning electron microscope EVO® MA 15 (Carl Zeiss SMT, D) and FEI Quanta 3D FEG. All microstructure was observed on metallographic samples as seen in *Figure 3-4*.

3.10 Materials

Materials were chosen with regards to their melting point temperature and their electrical conductivity. Basically, the chosen powders cover most of typical SPS applications (sintering of ceramic, pure metals and alloys). Two types of metal powders were chosen. Nickel (nano nNi and micro powder uNi) and Al7075 are electrically conductive powders sintering at lower temperatures and the SPS process will be regulated by using thermocouple. Nono sized molybdenum powder (nMo) and AlNi are conductive powders sintered at higher temperatures (by using a pyrometer). Ceramic nano sized powder Al_2O_3 was chosen as one type of non-conductive ceramic. In addition, the difference between micro and nano powders can be investigated by changes in microstructure of nNi and uNi. Two alloys (AlNi and Al7075) were chosen and their changes in phase composition before/after sintering will be investigated. Sintered parameters (especially temperature) were chosen on the base of published papers.

Nano-powders had to be stored under an inert atmosphere due to their reactivity with air and the samples preparation for sintering was carried in a glovebox (under Ar atmosphere).

Material	Size of powder	Alloy / pure metal	Electrical conductive
Nickel (uNi)	micron	pure metal	yes
Nickel (nNi)	nano-sized	pure metal	yes
Molybdenum (nMo)	nano-sized	pure metal	yes
Al7075	micron-sized	alloy	yes
AlNi	micron-sized	alloy	yes
Al_2O_3	nano-sized	ceramic	no

Table 3-2 Used powders

3.10.1 Al7075

Al7075 is an aluminum alloy with strength comparable to many steels, and has good fatigue strength and average machinability. This alloy is widely used in transportation and construction industry. Its strength is deduced preferentially from precipitation strengthening, however, fine grain size can further improve its properties. The powder was chosen because a change in SPS processing parameters might have a significant impact on the microstructure, phase composition, precipitation of secondary phases and microhardness.

The commercial powder utilised in the research was produced by nitrogen atomizing and the powder was supplied by Nanoval GmbH & Co. KG, Berlin.

Element	**Zn**	**Mg**	**Cu**	**Fe**	**Si**	**Al**
Wt. (%)	5.3	2.1	1.3	0.4	0.65	balance

Figure 3-7 The chemical composition of atomised Al7075 powder determined by energy dispersive spectroscopy [73]

Al7075 powder was already sintered in several publications at the temperature in the range from 325 °C to 450 °C. A fully dense sample was obtained at the temperature of 452 °C.

3.10.2 Al_2O_3

Aluminium oxide was chosen as one type of non-conductive powder. It is very often used as a transparent polycrystalline ceramic. Commercial IOLITEC powder (Product Nr.: NO-0008-HP) was used with an average particle size of 40 nm the powder purity is 99.9 %.

SPS compaction of Al_2O_3 has been described by many papers. Al_2O_3 powder (0.4 μm) was densified using SPS at the temperature range from 1350 °C to 1700 °C at a heating rate of 600 °C/min, without a dwell time in [74]. Al_2O_3 structure ceramics have been also investigated in the publication [7]. Several powders' particle distributions were studied in order to compare the sintering behaviour of micron and submicron powders. Medians of the used powders were 0.15 μm, 0.43 μm and 1.8 μm. Powders were compacted at the temperature range from 1000 °C to 1400 °C.

3.10.3 AlNi (alloy)

AlNi metal alloys are often used as a thermal barrier [75]. Powder AlNi 50/50 (atm%) powder was supplied by Amperit® Herman C. Starck Berlin (Order No. 712 2714/KE). The compound provides high thermal stability up to 1638 °C (*Figure 2-9,* red highlighted*)*. If the powder is compacted under this temperature, its phase compound should not be changed. If a different phase compound in sintered samples, it would be evidence of temperature exceeding the temperature at 1638 °C. It would be a significance of presence of discharges

between sintered grains, because the localised heat given by the discharges should be higher than the temperature of 1638 °C as published in many papers.

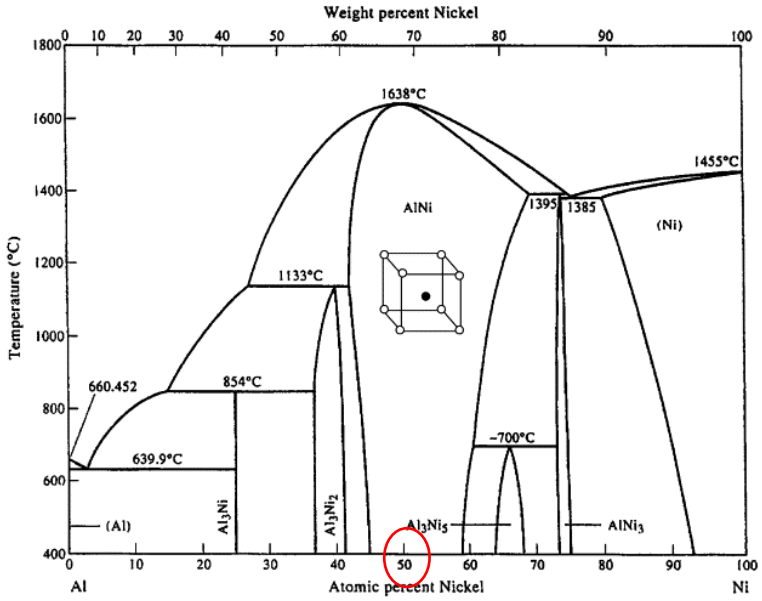

Figure 3-8 Phase diagram of AlNi

Sintering of pure AlNi powder has not been described yet.

3.10.4 Nano and micro sized Nickel

Nickel and nickel alloys are widely used in aerospace applications due to their high flexural strength, toughness and their high corrosion resistance. Two different distributions of powder (both 99.9 %) are used in this work.

The first used power is Nano powder supplied by Skyspring Nanomaterials, Inc., Houston with particle distribution of d_{50}=180 nm and the second is micropowder with the particle distribution from 45 to 90 μm supplied by SVUOM s.r.o., Prague.

The sintering of nickel powder was published by several authors. The sintering temperature depends on the particle size. Borkar [75] investigated the influence of sintering temperature on average grain size and relative density of sintered nickel. They use pure (99.99 %) nickel powder with particle size 1-5 μm. Density measurements were performed in a helium pycnometer. They found out that density increases with sintering temperature from 97.7 % at 700 °C to 99.2 % at 1000 °C. However, the optimal sintering temperature was determined at 850 °C (1 % of porosity) due to the best mechanical sample properties. On the other hand, powder particle size of 4.3 μm was sintered [67] within different die diameter and various heating rates under uniaxial pressure of 70 MPa and at temperature of 1350 °C. The density of the samples was in the range from 97.9±0.1 % to 98.9±0.1 %. It is obvious that the sintering temperatures strongly depends on particle size and so each author achieved different results.

3.10.5 Nano sized Molybdenum

Molybdenum is an alloying agent in various steels, as it not only contributes to their toughness, but also improves the corrosion resistance of the steels. Pure molybdenum is often used for the densification of materials sensitive to surface contamination or as parts for high-temperature furnaces. In this thesis, the nano molybdenum powder (99.99 %), produced by Skyspring Nanomaterials, Inc., Houston with particle size of 500-800 nm, is used.

Pure molybdenum powders with particle size of 3 – 5 μm (produced by Plansee Metall GmbH Austria) were consolidated by SPS in [76]. Mo powder was precompacted by a uniaxial pressure of 29, 57 and 67 MPa and, respectively, followed by heating up to temperatures between 850 °C and 2000 °C under vacuum. The heating rate was diversified between 130 and 360 °C/min, and the holding time at maximum temperature was 3 min for all batches. The pulse pattern of the electric current was adjusted 2:1 (10 ms pulse time, 5 ms pause time). A relative density of 95 % and higher was reached when the sintering temperature exceeded 1600 °C.

4 Experiment Results

4.1 Reliability of temperature measurement

The measurement for verification of reliability of temperature measurement was controlled by a pyrometer, therefore this value of temperature is meant as a reference and the value is the same for both sintering processes in *Figure 4-1*. Another temperature verification took place by thermocouples located as seen in *Figure 3-2*. The pyrometer can be used only for measuring temperatures higher than 500 °C. The initial temperature (the first set point temperature) was set at 700 °C. After 5 min of dwell time, the temperature was raised by 100 °C with a heating rate of 100 °C/min followed with the 5 min dwell time up. This step was repeated up to the set point temperature of 1100 °C. The second, repeated measurement is represented by the dashed line.

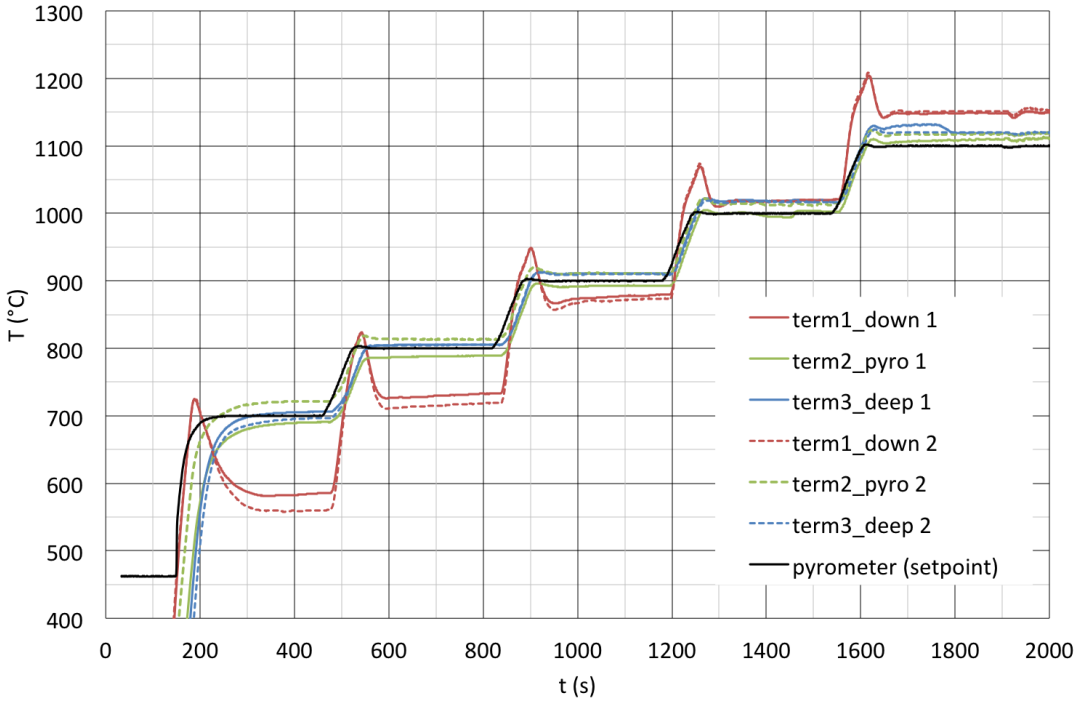

Figure 4-1 Temperatures distribution in die and punches during two SPS sintering cycles

As can be seen in *Figure 4-1*, temperatures "term2_pyro" and "term3_deep" are similar to the set point temperature, but the "term2_pyro" indicates few degrees higher temperature than "term3_deep". However, the temperatures are very close above the temperature 900 °C. It is evident that the most significant difference in temperature is between the values obtained in the bottom punch by "term1_down" and other temperatures measured in the die. Significant temperature peaks are evident in the lower punch; their value increases with higher sintering temperature. The temperature overshot (maximal recorded temperature) between the set point temperature (1100 °C) and the temperature measured by the thermocouple "Term1_down" is 101 °C; the exceeded temperature when the temperatures are stabilized is 48 °C.

There is a small observable difference in temperatures shapes obtained by thermocouples from two repeated measurements. This difference is studied in detail in *Chapter 4.7*.

4.2 Temperature Verification

As the process temperature is measured indirectly, it is very difficult to determine the real temperature in the sintered material, because it is not possible to measure the temperature directly on the surface of the sintered sample. The aim of the next measurement is therefore to determinate differences between the measured and the real temperature. The experiment is based on the comparison of the define Nickel melting point (1455 °C) with temperatures measured by a pyrometer (the type C thermocouple was not available at the time).

The experimental sample is shown in *Figure 4-2*. It is composed of two Al_2O_3 plates that are 2.5 mm thick. A hole was grinded between them. The Ni thin strip was placed into the created cavity. This sample was then sintered like a normal specimen. The aim of this measurement was to verify the temperature when the Ni strip would be melted.

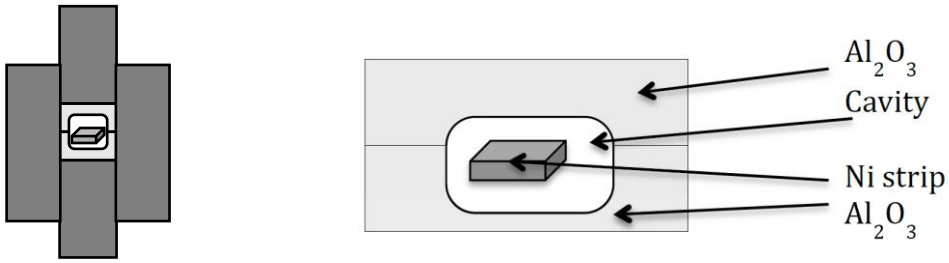

Figure 4-2 Verification of sintering temperatures

The heat rate was chosen 100 °C/min up to 1300 °C and above this temperature the heating was rate only 50 °C/min. After the maximal temperature was reached the specimen was cooled down at the room temperature, dismantled and the strip was inspected. If the temperature of the Ni strip crossed the melting point temperature, the strip was formed into a ball due to surface tension.

Temperature (pyrometer °C)	Result
<1348	Metal strip
>1353	Ball

Table 4-1 Verification of melting point of Ni strip, temperatures measured by pyrometer

It was proved that the Nickel strip melts between 1348 °C and 1353 °C (temperature measured by a pyrometer). It means that the pyrometer measures temperatures at least 100 °C lower (for non-conductive materials) than the real temperature of the sintered sample. As seen in *Figure 4-1*, the temperature measured by thermocouple is higher than the temperature measured by the

pyrometer. Therefore, the temperature measurement by the thermocouple "Term1_down" is more accurate compared to the temperature measured by pyrometer.

4.3 Compacting of electrically conductive and nonconductive powder. Temperature measurement of different heating rates

It was proved that the real temperature of sintering is accurately measured by the thermocouple placed in the bottom punch. However, the difference between temperatures measured by a pyrometer and by a thermocouple depends on the electrical resistivity of a sintered powder.

All measurements were realized under 1200 °C (as the thermocouple type K was used) and it was predicted that the higher sintering temperature, the bigger difference between values measured by pyrometer and thermocouples as was proved by previous measurements in *Figure 4-1*. All samples (both conductive and non-conductive) were measured by heating rate of 50 °C/min and 150 °C/min. This range of heating rates was chosen on the basis of many publications where these heating rates are most frequently used.

4.3.1 Temperature measurement of Non-Conductive materials

If the electrical resistivity of a sintered powder is significantly higher than the resistivity of graphite, the electric current (red arrows) does not flow through the sintered powder (green), but it is conducted from punches (light grey) through the die (dark grey). It is noticeable that the sample is not heated directly, but the heat is transferred from punches and the die by thermal conduction as seen in *Figure 4-3 a)*.

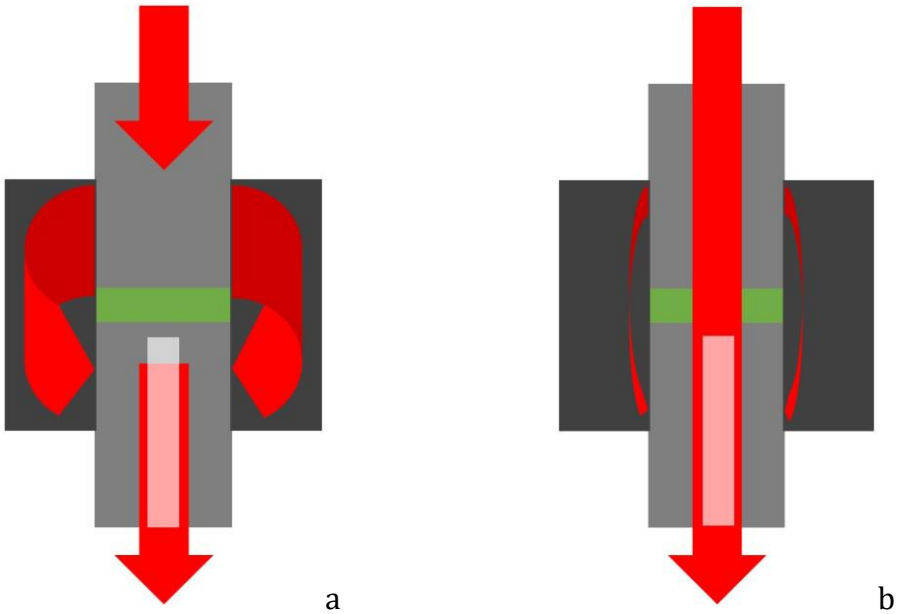

Figure 4-3 a) Schema of heating mechanism of non-conductive samples, b) Schema of heating mechanism of conductive samples

The verification of temperature distribution in the die and punches was realized by sintering Al_2O_3. The die and punches were assembled according to *Figure 3-2*. The sintering process for verifying temperature distribution is regulated by the pyrometer focused on the die hole named "*pyrometer*". The difference between temperatures measured by thermocouples in different places and the values obtained from the pyrometer is investigated. The process was stopped when the measured temperature by the thermocouple was 1200 °C because 1200 °C is the maximum working temperature for a type K thermocouple.

As seen in *Figure 4-4*, the graph can be divided into two parts by 900 °C. The temperature on the surface of the die (*term2_pyro*) is higher than the temperature deeper in the die (*term3_deep* and *term1_pyro*). Above 1000 °C the temperature "*term1_down*" is higher than the temperature measured by a pyrometer. There are noticeable momentary temperature overshoots (peaks in temperature) of "*term1_down*" and the temperature exceeding over the set point where the temperatures are stabilised. The temperature overshoot is around 100 °C higher than the set point where the stabilised temperature is higher by around 50 °C. It is noticeable that the difference between values measured by a pyrometer and thermocouple (*term1_down*) increases with higher set point temperature.

The sintering process was repeated, but with the heating rate of 150 °C/min. The maximum set temperature point was decreased at 1050 °C on the ground of maximum operation temperature of thermocouple type K, because the temperatures overshoots were expected higher than during the heating rate 50 °C/min. The process graph is in *Figure 4-5*. It is noticeable that the temperature overshoots (*term1_down*) over the set temperature point are around 100 °C - 150 °C and the temperature exceeding when temperatures are stabilised also decreases with increasing temperature – it is 25 °C at 1000 °C and 50 °C at 1050 °C.

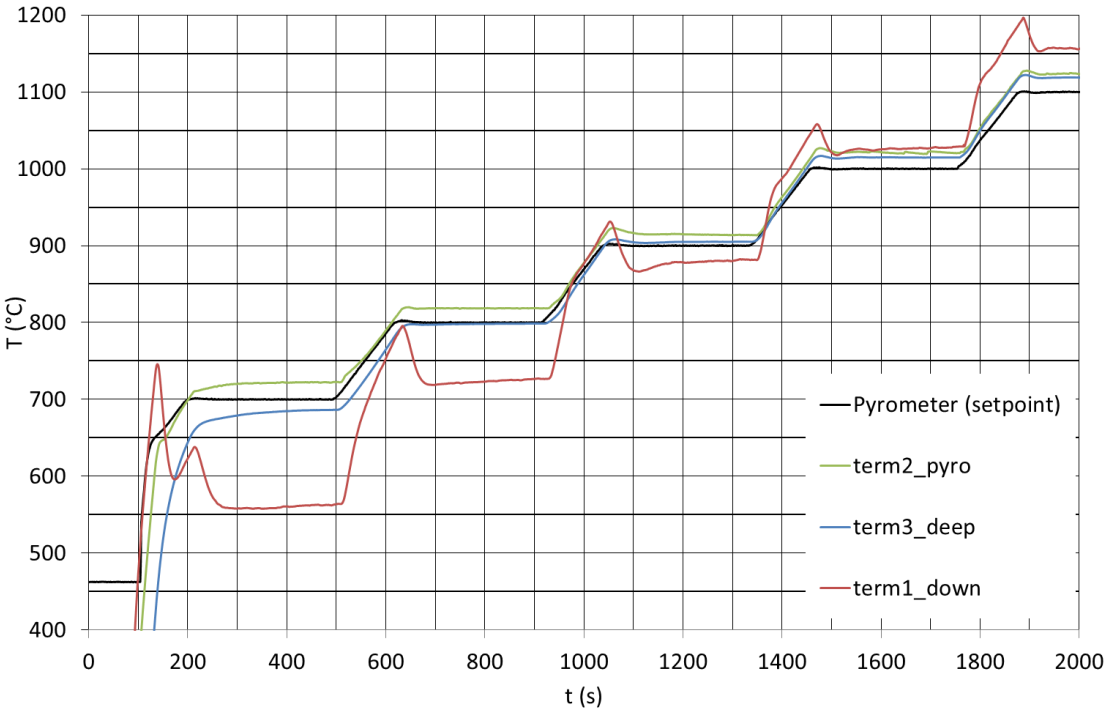

Figure 4-4 Temperature distribution in die and punches during the sintering of a non-conductive sample with the heating rate of 50 °C/min

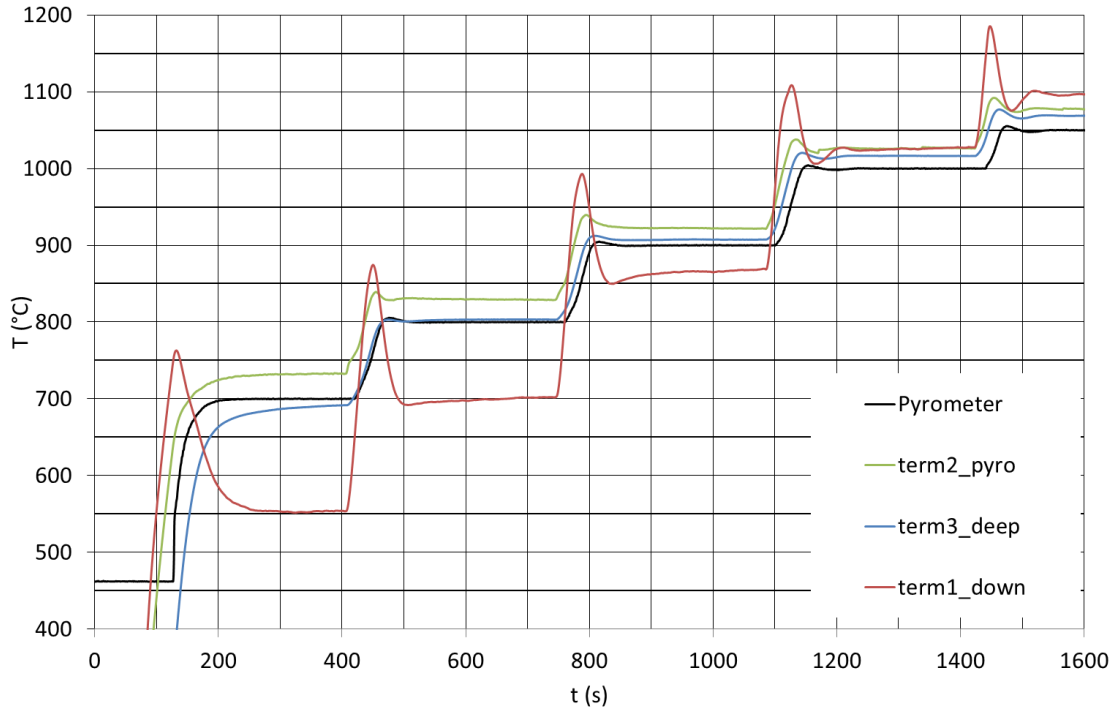

Figure 4-5 Temperature distribution in die and punches during the sintering of a non-conductive sample with the heating rate of 150 °C/min

Both temperature evolutions for nonconductive materials are similar. But sintering with the temperature rate of 150 °C/min results in much higher

temperatures overshoots, which are double in comparison with the process with a slower heating rate.

It is obvious that temperature of "*Term2_pyro*" is higher than that of "*Term3_deep*". The temperature gradient between a shallow and deeper place in the die is more significant at lower temperatures, but it is observable during the entire sintering process. This finding is in agreement with the theory that no electrical current flows through the sintering sample (because its resistivity is orderly higher), but the heat is generated near the die surface and the heat is conducted in direction of the die's centre.

The higher value of temperature "*term1_down*" than the value of "pyrometer" (above the temperature of 1000 °C) is probably caused by the die and punches' different dimensions. The part of a punch between the die and the spacer has a lower diameter (compared to the diameter of the part where the punch is inserted inside the die). The generated heat $P = R.\mathrm{I}_{rms}^2$, is inversely proportional to a diameter $R \approx \frac{1}{r^2}$ due to the lower diameter of a punch where most of the heat is generated. From this part the heat is generated in the punches divided into two directions; conducted to the sample and in the direction to the cooled spacer. With increasing temperatures decrease the cooling effect of the cooled spacer and higher ratio of the heat participates to the heating of the sample.

4.3.2 Temperature measurement of conductive materials

The electric current flows directly through a sintered powder in the case of compacting materials if their electrical conductivity is higher or comparable to the electric conductivity of graphite. In this case, the generate is in the inner side of the die and the die is conducted in towards the surface of the die (where the temperature is measured by a pyrometer).

The verification of sintering temperatures of electrically conductive powders was realized by sintering tungsten powder (*Figure 4-3 b)*). All thermocouples were placed directly in the same position (as shown in *Figure 3-2*), in the same way as the measurement of nonconductive materials. 50 °C/min and 150 °C/min were chosen as heating rates. The maximum sintering temperature of 1000 °C was followed by a 5 min dwell time. During the next heating cycle, the process was stopped when the temperature "*Term1_down*" reached 1200 °C.

The temperature evolution for the heating rate of 50 °C/min is in *Figure 4-6*. The temperature exceeding the temperature "*Term1_down*" over "*pyrometer*" grows with increasing set point temperature. The exceeding temperature is around 50 °C (at set point 700 °C) and 100 °C (at set point 1000 °C). Temperature overshoots are around 25 °C higher than the stabilized temperature and they are constant throughout a whole cycle.

The temperature evolution for the heating rate of 150 °C/min is shown in *Figure 4-7*. It is apparent that the stabilized temperature exceeding that of

"*Term1_down*" is higher than "Pyrometer" by about 100 °C and this difference slightly increases with the increasing set point temperature. The temperature overshoots are 50 °C higher that stabilised temperature.

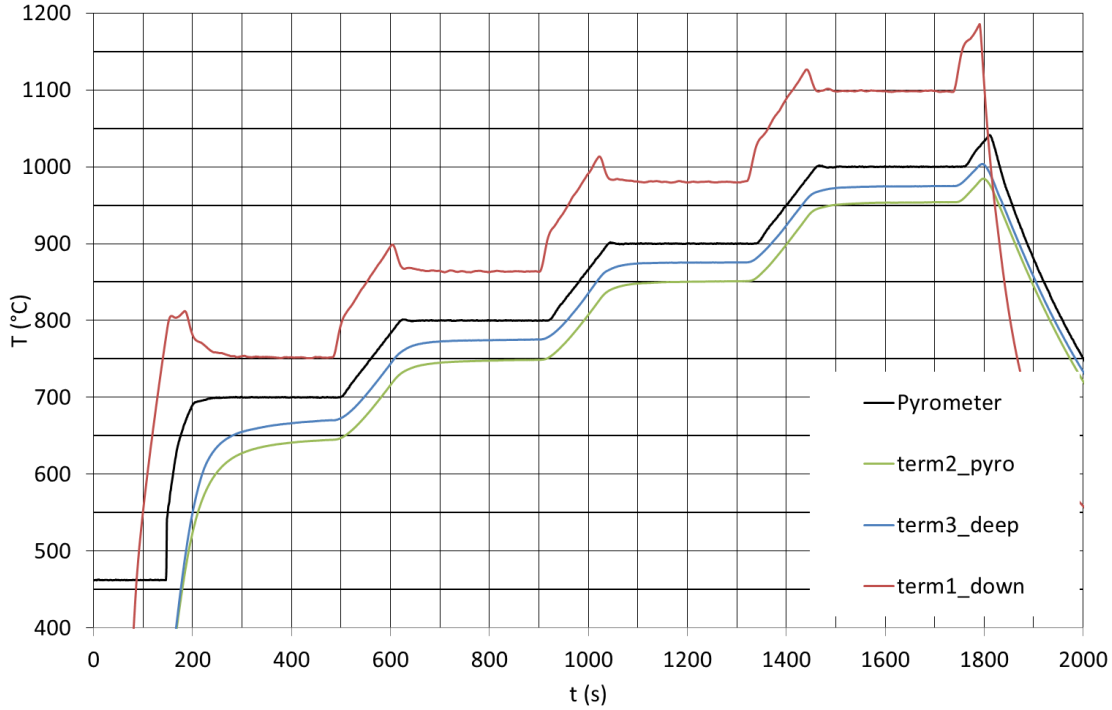

Figure 4-6 Temperature distribution in die and punches during the sintering of conductive samples with heating rate of 50 °C/min

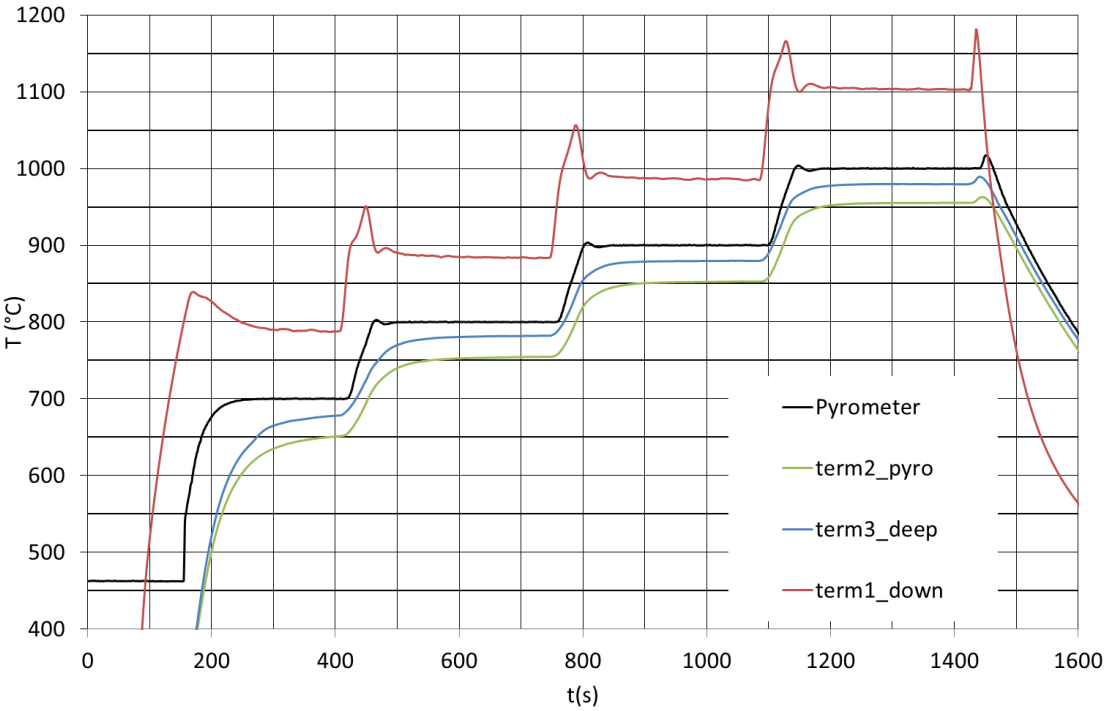

Figure 4-7 Temperature distribution in die and punches during the sintering of conductive samples with heating rate of 150 °C/min

It is noticeable from the measured temperatures that the highest temperature is in the inner side of the die ("term1_down") and the temperature decreases in direction towards the surface of the die ("term3_deep" is higher than "term2_pyro"). It is in accord with the presumption that the heat is mostly generated in the compacted powder and the heat is conducted through the die to its surface where the temperature is measured by a pyrometer.

The difference in temperatures for sintering processes of electrically conductive and nonconductive powders between points "*term1_down*" and "*Pyrometer*" is compared in *Table 4-2*. The temperature exceedings (stabilized temperature difference) and temperature overshoots (temperature in a peak) are compared in the table.

The results can be divided according to the electrical conductivity of the sintered powder.

Concerning the compacting of electrically conductive powder, it was found that temperature overshoots slightly increase with an increasing set point temperature when the powder is compacted with the heating rate of 50 °C/min. However, the value of temperature overshoot is constant if the heating rate is 150 °C/min. In all cases, the temperature exceeding over the set point temperature increases with an increasing set point temperature; at higher temperatures, the value of temperature exceeding is equal for both heating rates.

Temperature overshoots are very significant for the sintering of non-conductive powders. They are strongly dependent on the heating rate; the temperature overshoots are higher for higher heating rates. The temperature exceeding is negative under the temperature of 1000 °C (which means that the temperature of a sintered powder is lower than is the temperature measured by a pyrometer). Above 1000 °C the temperature exceeding is 17 °C and does not depend on the heating rate. But it is obvious that the temperature exceeding grows with a higher set point.

		Set point temperature							
Conductive / non-conductive powder	**Heating rate**	**700 ˚C**		**800 ˚C**		**900 ˚C**		**1000 ˚C**	
		Overshoot (°C)	**exceeding (stabilized)** (°C)	**Overshoot** (°C)	**exceeding (stabilized)** (°C)	**Overshoot** (°C)	**exceeding (stabilized)** (°C)	**Overshoot** (°C)	**exceeding (stabilized)** (°C)
Conductive	**50 ˚C/min**	105	50	100	55	105	80	125	100
	150 ˚C/min	150	90	150	80	152	90	155	100
Non-conductive	**50 ˚C/min**	50	-150	-5	-75	18	-17	25	17
	150 ˚C/min	28	-150	30	-100	75	-20	100	17

Table 4-2 Table of summarised exceeding temperatures over the set point temperature for electrically conductive and nonconductive samples

4.4 Optimization of the SPS process regulated by a pyrometer

Based on the temperatures verification measurement, optimised sintering course for electrically conductive materials was established *Figure 4-8*. The pyrometer can only measure temperatures above 490 ˚C. Therefore, the heating rate from the initial (room) temperature to the temperature of 490 ˚C was set to 500 ˚C/min. In order to avoid the first temperature peak, a very slow heating rate (5˚C/min) was applied between temperatures from 490 ˚C to 500 ˚C as seen in *Figure 4-8*. The slow temperature rate leads to a lower temperature overshoot and the difference between pyrometer and thermocouple is also minimised. Dwell time was held from 2-10 minutes (depending on the type of powder), which should lead to removing of residual gas from the sintered powder and to improve the homogeneous distribution of temperatures (the residual atmosphere was continuously pumped out to keep the atmosphere pressure lower than 10 Pa). The heating rate of 150 ˚C / min was held up to a temperature that was 50 ˚C lower than the maximum temperature and the heating rate of 50 °C/min was used to achieve the maximal temperature. Thus, the temperature overshoot of the reference temperature was minimised.

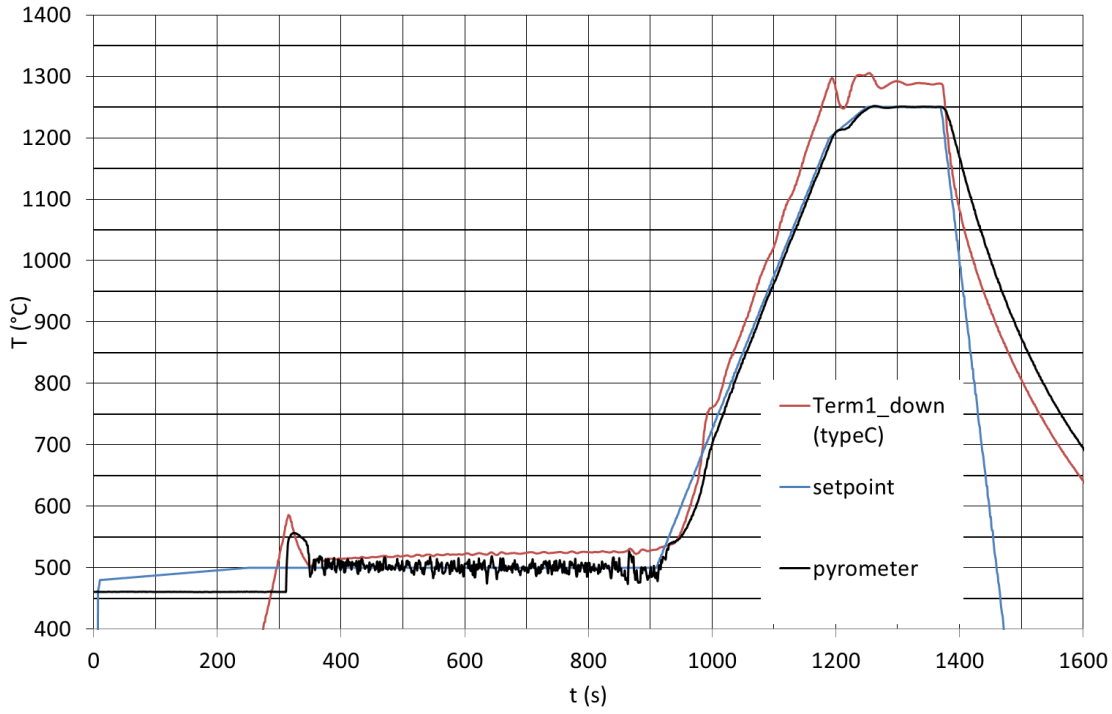

Figure 4-8 Optimised SPS cycle for electrically conductive powder with minimised temperatures overshoot and exceeding

4.5 Determination of sintering temperatures

Material	SPS process is regulated by	5 % of porosity / full dense
Micro Nickel (uNi)	thermocouple	5 %
Nano Nickel (nNi)	thermocouple	5 %
Nano Molybdenum (nMo)	pyrometer	5 %
Al7075	thermocouple	full dense
AlNi	pyrometer	5 %
Al_2O_3	pyrometer	full dense

Table 4-3 Schema of determination of sintering temperatures

All powders were compacted at several different temperatures in the order to determine the optimal temperature where another sintering parameter might be verified at a constant temperature. The range of sintered temperatures was chosen with regard to published papers dealt with sintering of same powders as are used in this work. An impact of pulse current of SPSed samples will be investigated by measuring their material properties. Since no improvement in porosity can be observed on fully dense samples, the reference temperature will be chosen where a sample is sintered around 95 % of its density. However, powders Al7075 and Al_2O_3 will be fully dense sintered.

4.5.1 Micron-sized Nickel

The plasma plasma spheroidised uNi powder with distribution of $D_V(10)$=88,3 μm, $D_V(50)$=123 μm and $D_V(90)$=173 μm was used in this work (*Figure 4-9*).

The SPS process was regulated by a K-type thermocouple. 10g of nickel powder were pressed between graphite punches in a graphite mould under a load of 5 MPa as in *Figure 4-11*. The powder was heated at the temperature of 100 °C and then the temperature was held for 4mins. During this time period any humidity evaporated and the air pressure in the SPS chamber decreased under 10 Pa. The SPS uniaxial pressure was increased to 100 MPa with the rate of 95 MPa/min and when the pressure was reached, the sample was heated with the heating rate of 150 °C/min, respective of 50 °C/min (last 50 °C) as described in *Chapter 4.4*.

Density measurements were performed by the Archimedes method; the obtained results are in *Figure 4-10*. As seen from the graph, the densities of the SPSed pure nickel samples decrease almost linearly with increasing processing temperature up to 950 ˚C, after which, the rate of porosity decrease is slower.

850 ˚C was selected as the reference temperature for studying the influence of pulse current at 850 ˚C (*Figure 4-11*).

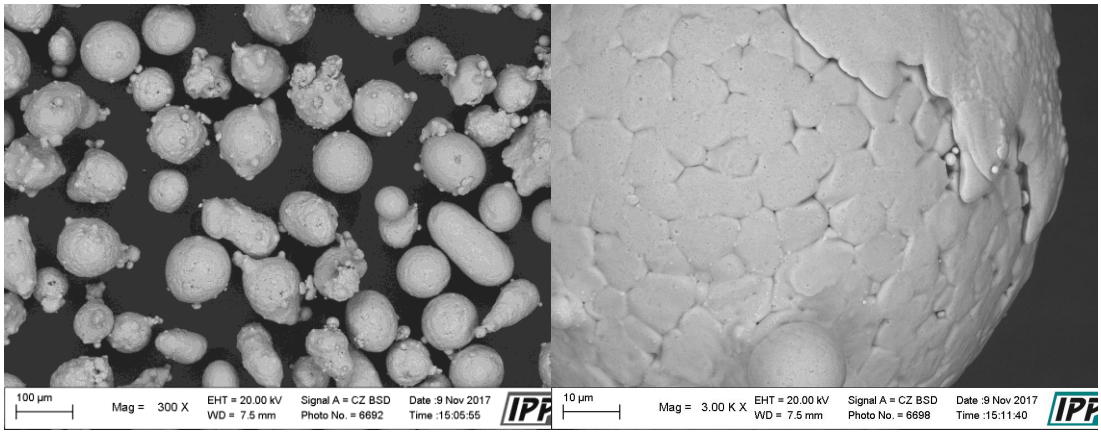

Figure 4-9 uNi powder

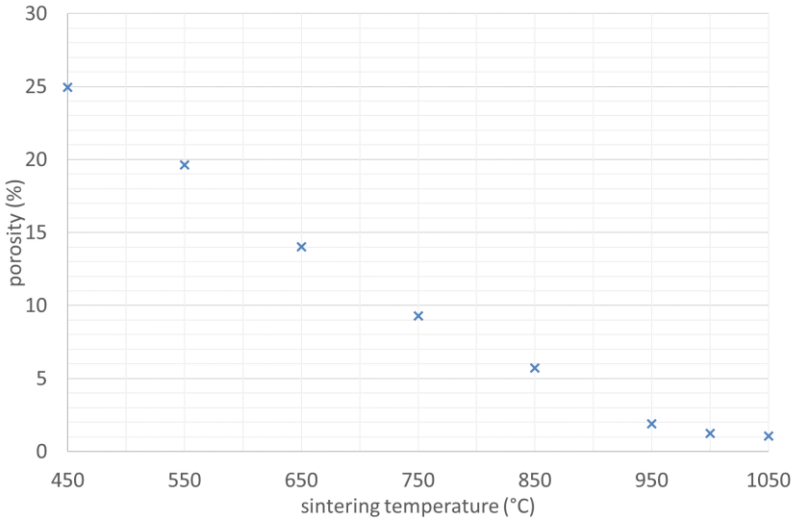

Figure 4-10 Porosity of uNi samples sintered at various temperatures

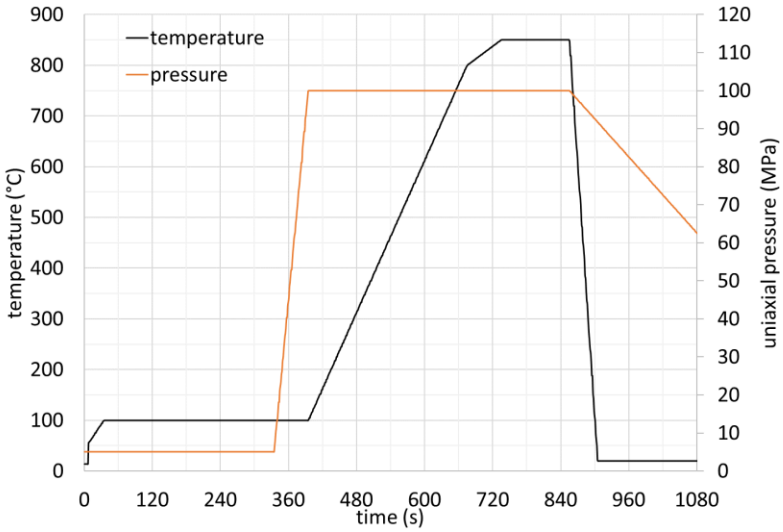

Figure 4-11 Optimised SPS course for uNi at the temperature of 850°C

4.5.2 Nano-sized Nickel

Spherical nNi powder 180 nm (*Figure 4-12*) was used as a comparison to uNi powder.

The sintering temperature of nNi (*Figure 4-13*) was determined within the temperature range from 300 °C to 1050 °C. It is obvious from *Figure 4-13* that the porosity of SPSed samples is steeply falling until 450 ˚C and then the porosity is almost constant above this temperature. There is not any significant difference between porosity obtained by the Archimedes method and the SEM imaging method.

425 °C was chosen as the reference temperature, which is approximately 25 °C below the temperature where the porosity stays constant. The reference sintering process is shown in *Figure 4-14*. There are only two differences compared to uNi sintering. Dwell time at 100 °C is shorter (2 min) due to possible oxidation of nNi under the residual atmosphere (>10 Pa) and the lowering heating rate of 25 °C is set between 400 °C and 425 °C. The reason is that a lower temperature overshoot is expected at this low temperature.

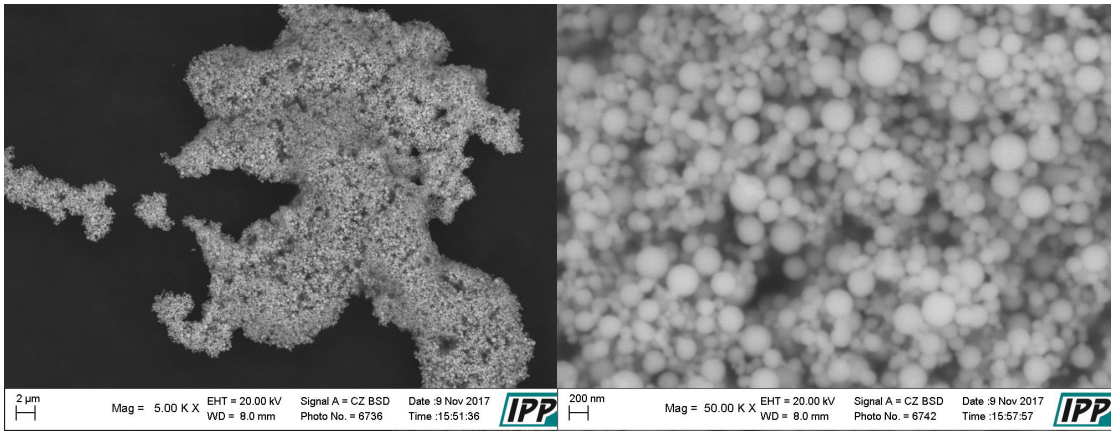

Figure 4-12 Nano Nickel powder

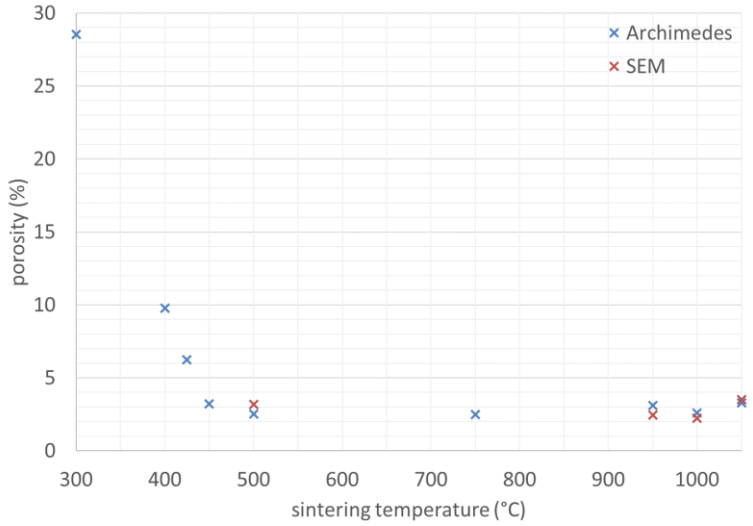

Figure 4-13 Porosity of nano Nickel samples sintered at various temperatures

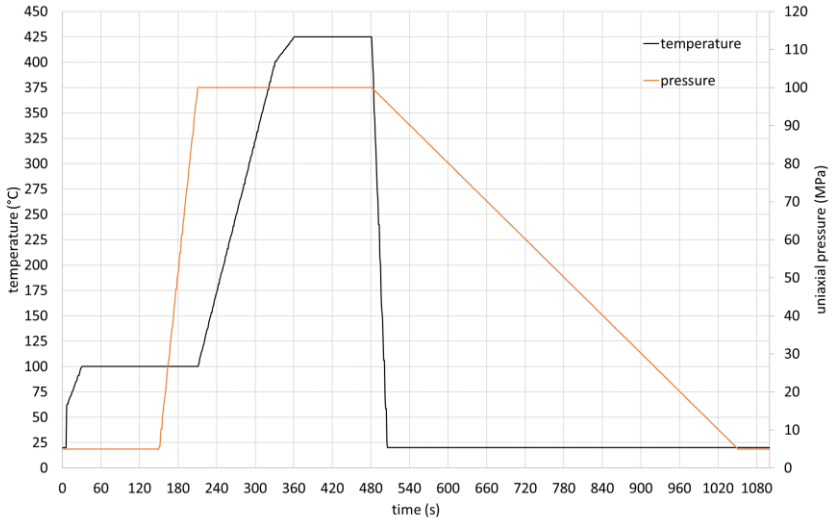

Figure 4-14 Optimised SPS course for nNi at the temperature of 425 °C

4.5.3 Nano-sized Molybdenum

Figure 4-15 shows the nMo spongy particles of 500-800 nm with inner porosity. The nMo powder was sintered in the temperature range from 1000 ˚C to 1600 °C as seen in *Figure 4-16*. It is obvious that the dependence of porosity on sintering temperatures can be divided into three parts. The porosity logarithmically increases below the temperature of 1100 °C; an only small decrease in porosity is observable between temperatures 1100 °C and 1200 °C. The porosity of 4.5 % and lower was reached if the sintering temperature exceeded 1200 °C. Any additional increase in sintering temperature has little impact on the SPSed samples' density. This porosity course is very similar to the results of [76] where 3-5 μm Molybdenum powder was used. However, the sintering temperature of nMo with comparable porosity is about 500 °C lower than in the case of sintering of micron sized Mo powder.

The reference temperatures was chosen 1200 °C with the porosity of of 4-5 % (*Figure 4-17*). The compaction of all samples starts with heating up to the temperature of 500 °C (from 490 °C, as the pyrometer cannot measure lower temperatures) with the heating rate of 5 °C/min followed by a 2 min dwell time. This dwell time was shortened in comparison with other sintering processes due to avoiding of nanoparticles oxidation (in the residual atmosphere lower than 10 Pa). After this dwell time, the punches pressure was raised up to 100 MPa. When the maximal pressure was applied, samples were heating up to temperatures 1030 °C respectively to 1150 °C (for samples sintered at 1200 °C) by a heating rate of 150 °C/min. Slower heating rate of 50 °C/min was applied to reach the maximum sintering temperatures.

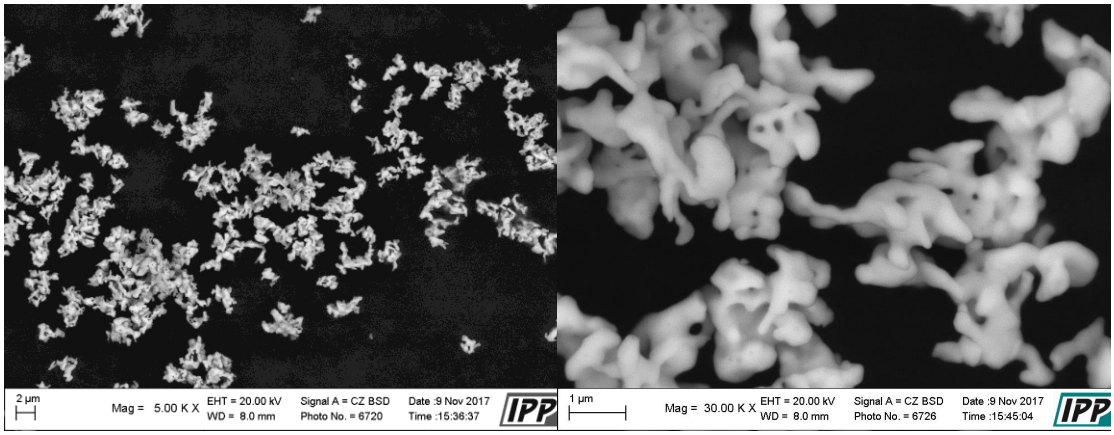

Figure 4-15 nMo powder

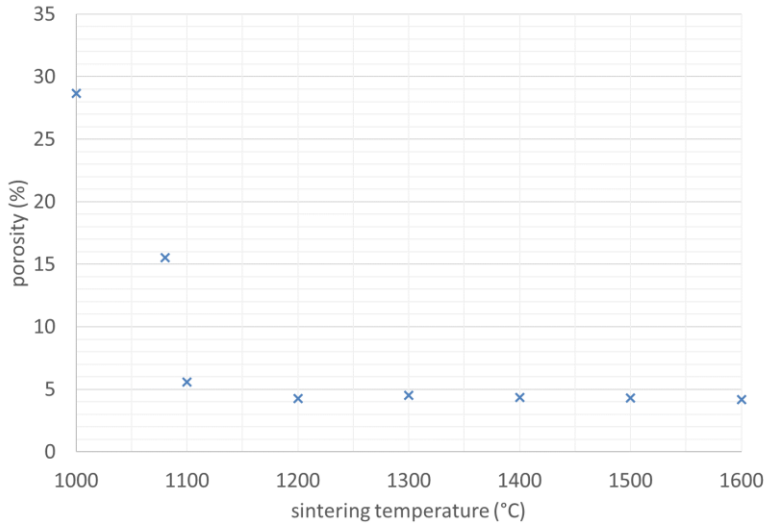

Figure 4-16 Porosity of nMo samples sintered at various temperatures

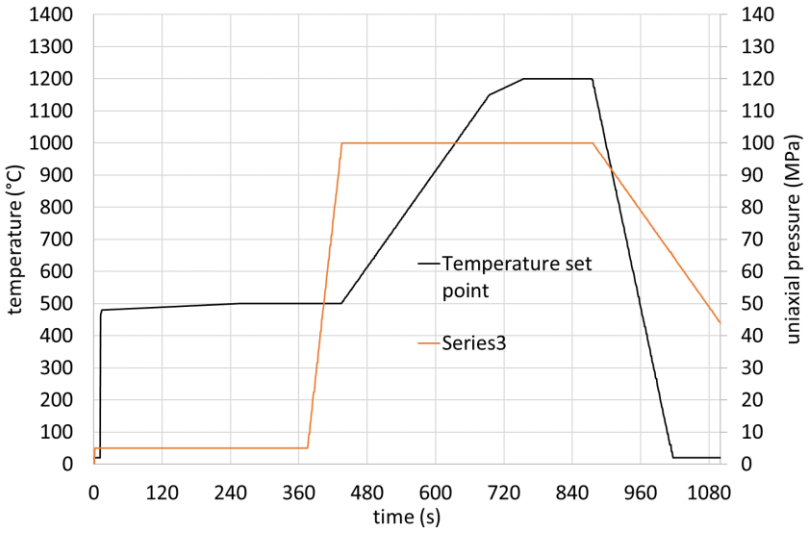

Figure 4-17 Optimised SPS courses for nMo at the temperature of 1200 °C

4.5.4 Al-Ni

A milled Aluminum-nickel powder with particle size (Dv50) 80 μm is in the sintering process regulated by a pyrometer (*Figure 4-18*).

The sintering of Aluminum-nickel has not been described yet in any publication. In view of the fact that the phase of AlNi 50/50 atm% is stable up to 1638 °C (*Figure 3-8*) the highest temperature of sintering was 1400 °C and the lowest 1100 °C. The density of AlNi powder was measured by the Archimedes method and the SPSed samples porosity is given as a ratio of the density of the AlNi powder and samples density obtained from the Archimedes measurement. The density is decreasing from 11.9 % at 1100 °C to approximately 4 % at 1400 °C. The temperature 1250 °C where the porosity is around 5 % was selected as the reference temperature (*Figure 4-19*).

The reference sintering process of AlNi powder is shown in *Figure 4-20*. It is very similar to the nMo, but where the dwell time at 500 °C was 10 minutes and the maximal temperature was 1250 °C.

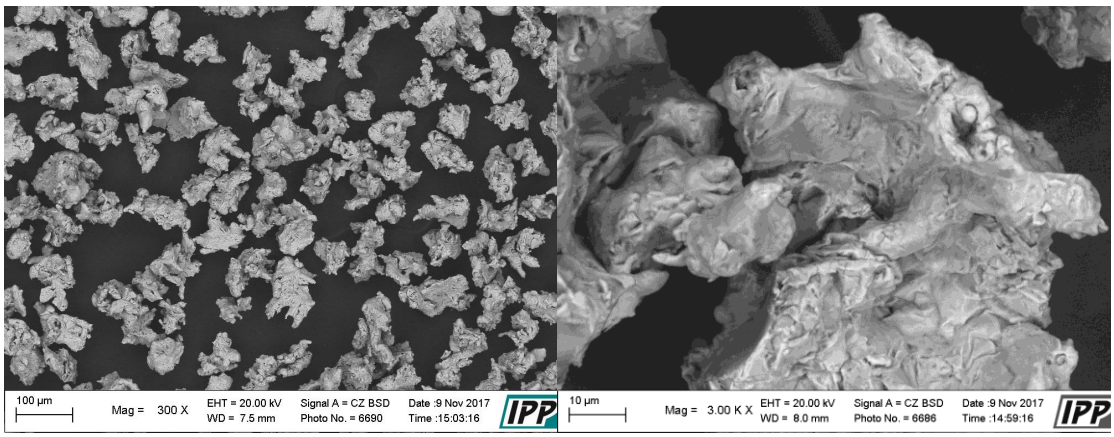

Figure 4-18 AlNi powder

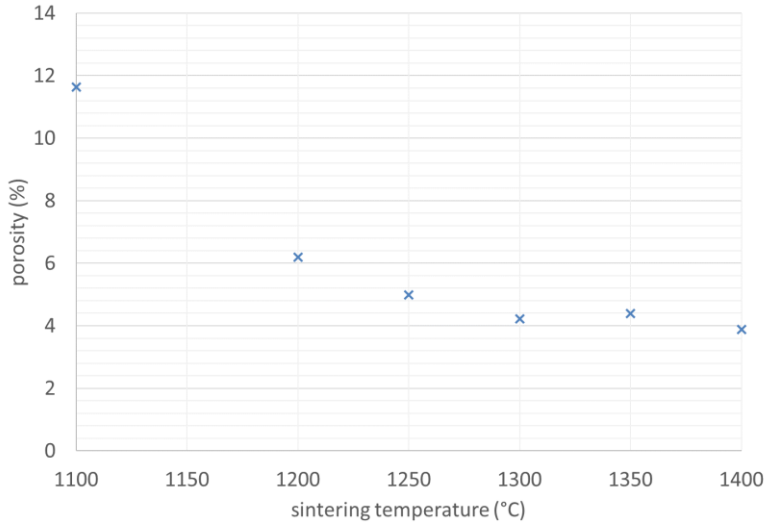

Figure 4-19 Porosity of AlNi samples sintered at various temperatures

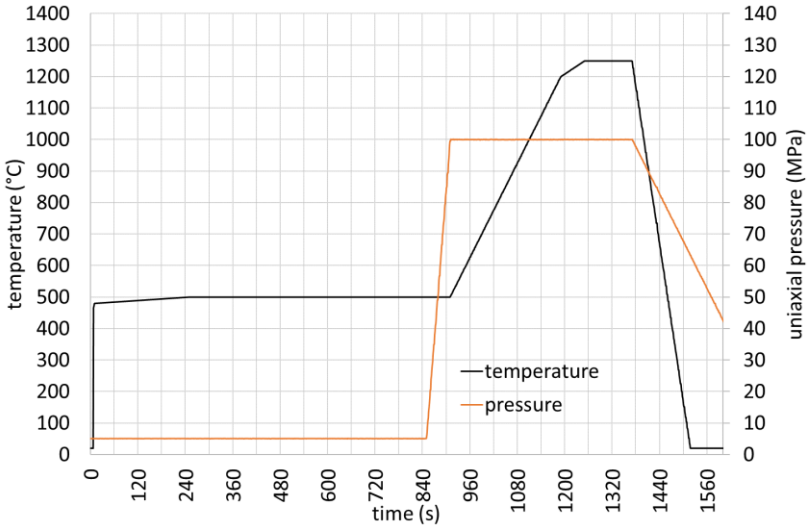

Figure 4-20 Optimised SPS course for AlNi at the temperature of 1250°C

4.5.5 Al7075

The atomised 7075 aluminium alloy powder with particle size of (Dv50) 31µm (*Figure 4-21*) was chosen for studying the impact of pulse current on material properties, because as is supposed, the pulse current might locally increase temperature and to have an influence on distribution of precipitates. The distribution of precipitates has a significant impact on the hardness and yield strength. If the pulse current results in a localized heating sintered particles are heated mostly locally, the precipitates should be small and more dispersed in the matrix and the hardness and yield strength will be high.

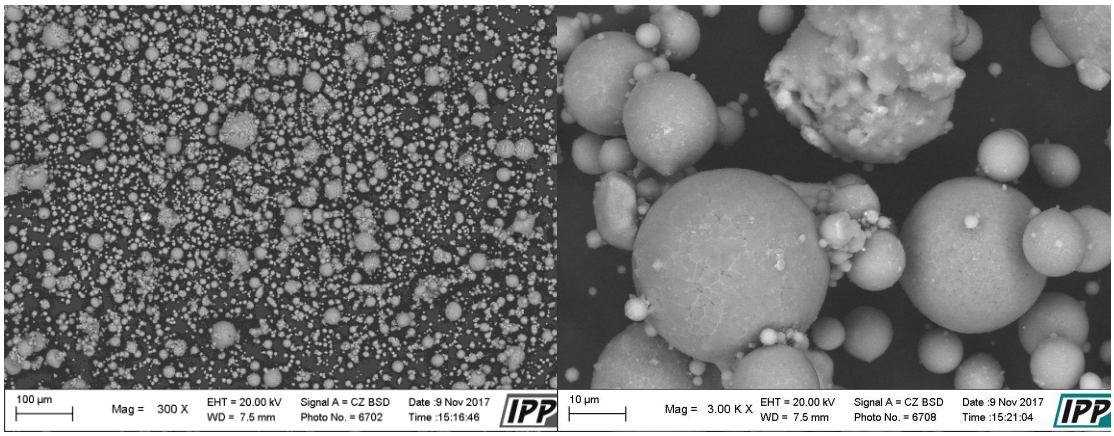

Figure 4-21 Al7075 powder

As materials properties should be influenced only by the precipitates size and their distribution, some fully-dense samples were prepared. The powder was compacted in the temperature range of 275 °C to 425 °C (*Figure 4-22*).

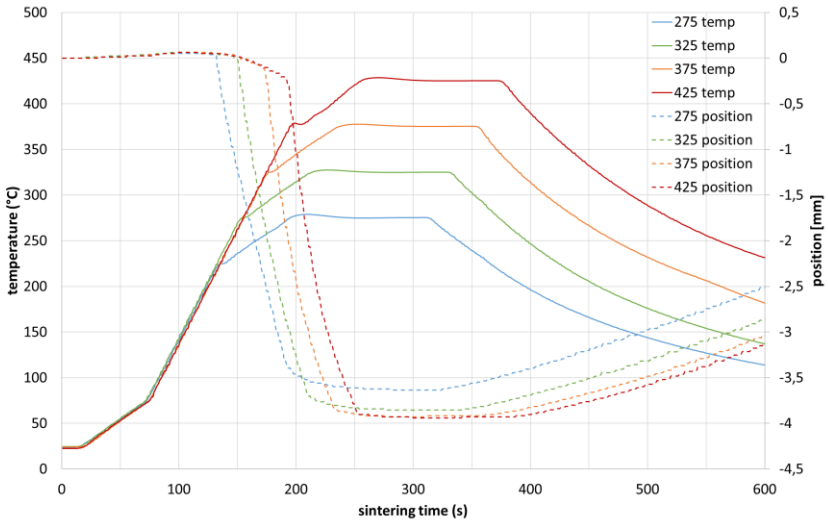

Figure 4-22 SPS courses for Al7075 at the temperatures range from 275 °C to 425 °C

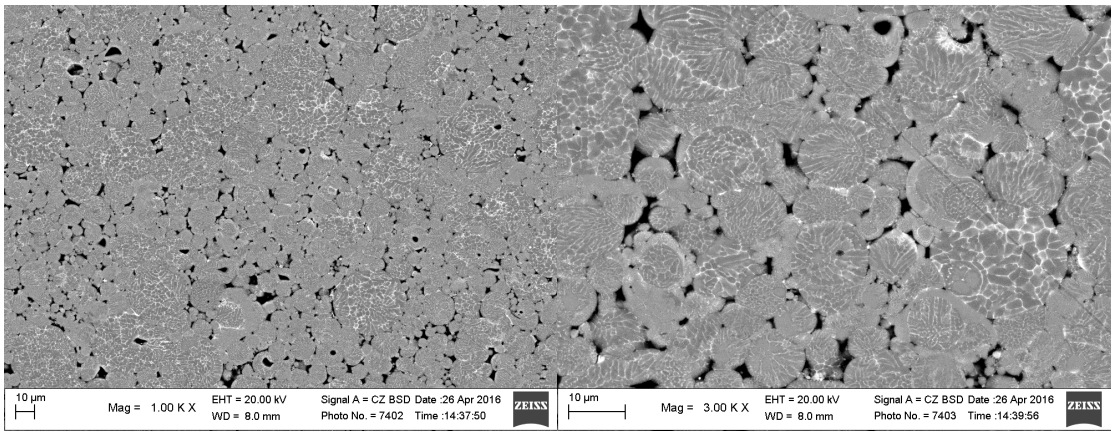

Figure 4-23 Al7075 sintered at the temperature of 275 °C, SEM backscattered electron image

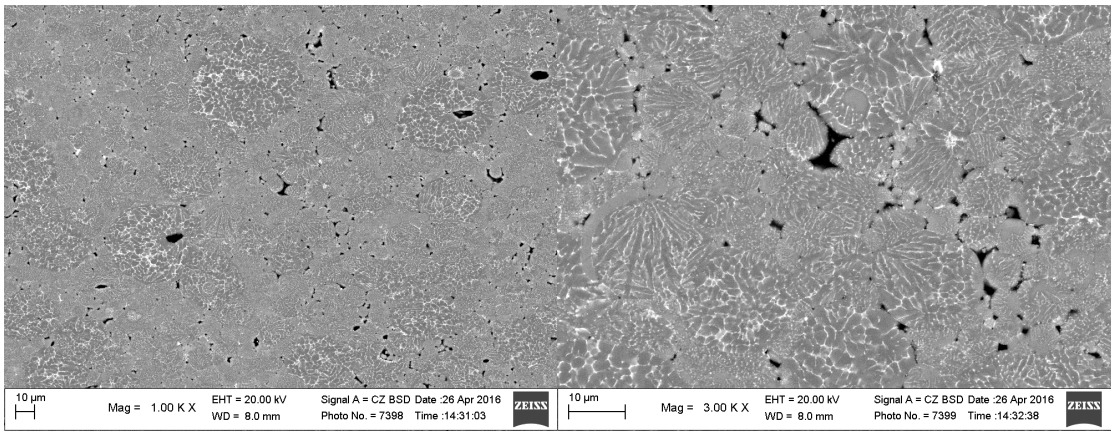

Figure 4-24 Al7075 sintered at the temperature of 325 °C, SEM backscattered electron image

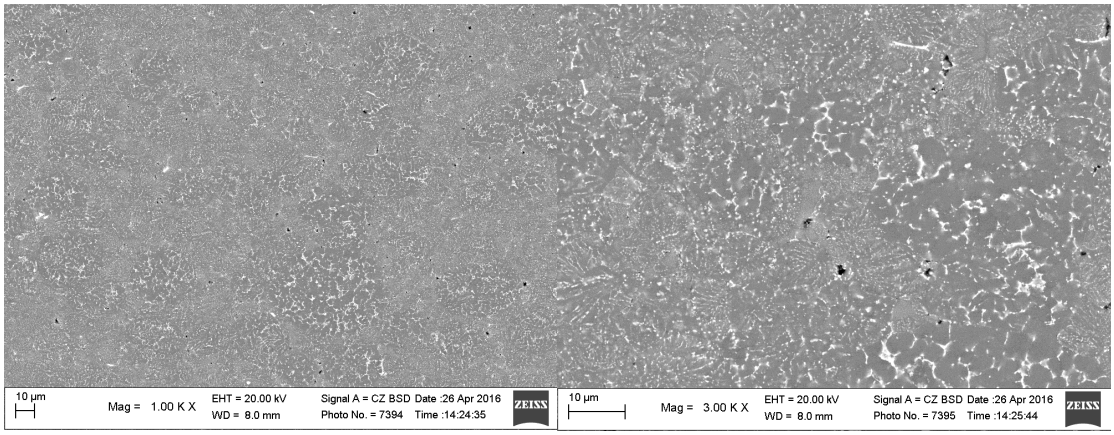

Figure 4-25 Al7075 sintered at the temperature of 375 °C, SEM backscattered electron image

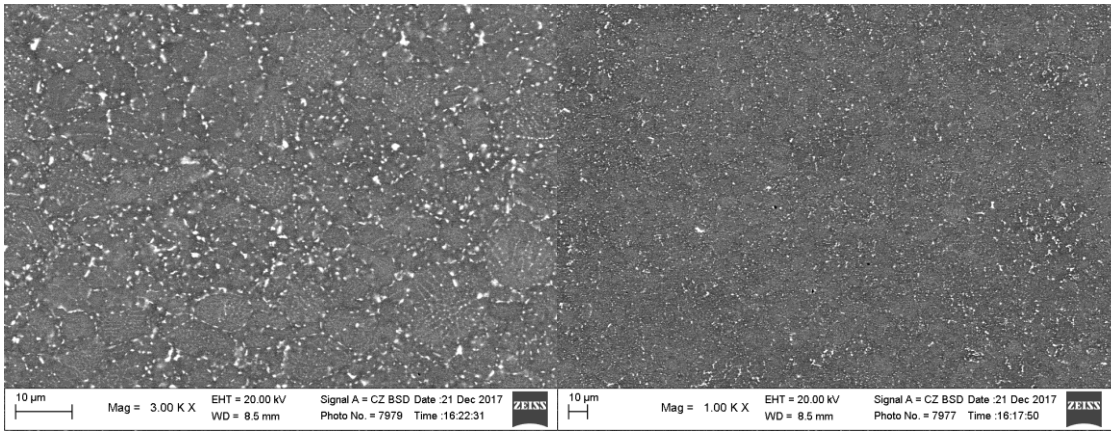

Figure 4-26 Al7075 sintered at the temperature of 425 °C, SEM backscattered electron image

The porosity of SPSed samples was calculated from the SEM images above (*Figure 4-23* to *Figure 4-26*). It decreases from 4.3 % at 275 °C to 0 at 425 °C in *Figure 4-27*. The precipitates grow in size, but decrease in number with higher sintering temperature and as seen from the SEM images above, they are distributed more around the grain borders. The XRD analysis of all samples did not show any difference in phase compounds.

Two beams (for the three point test) of each sample - as seen in *Figure 3-5* - were prepared for the three-point bending flexural test. For the purpose of clarity, the measured data is divided into two graphs in *Figure 4-28* and *Figure 4-29.* It is obvious that the different SPSed samples have different characteristics in how they respond to and resist fracture. The samples of materials with a little porosity (up to 0.15 % at 375 °C) have near to linear hardening behaviour.

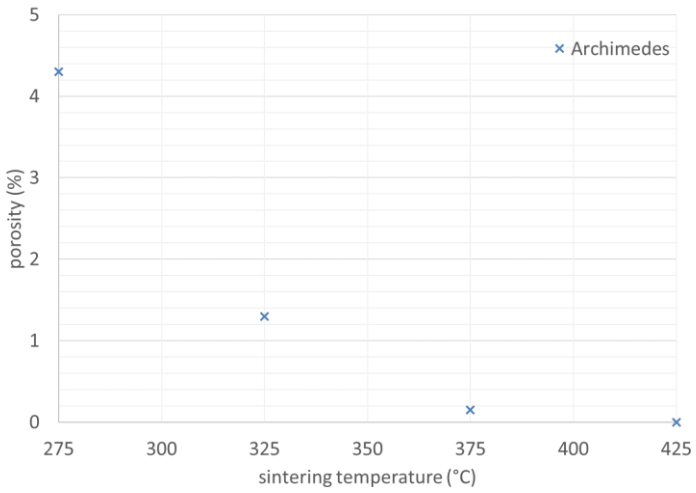

Figure 4-27 Porosity of Al7075 samples sintered at various temperatures

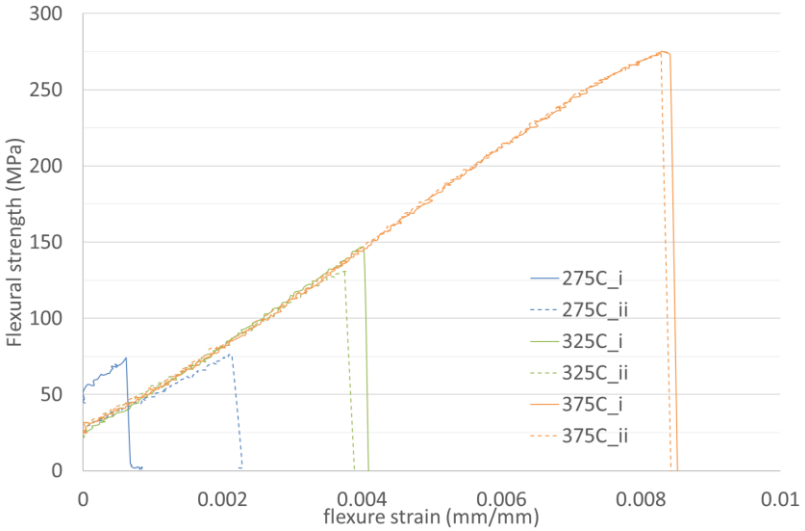

Figure 4-28 3-point bend strength test of Al7075 samples sintered at the temperature range from 275 °C to 375 °C

The sample compacted at 425 °C shows a ductile fracture which has a large amount of plasticity that precedes a final fracture. This plastic deformation absorbs energy and thus increases the energy required for a crack growing. Compared to other samples, it shows a double value for the fracture toughness.

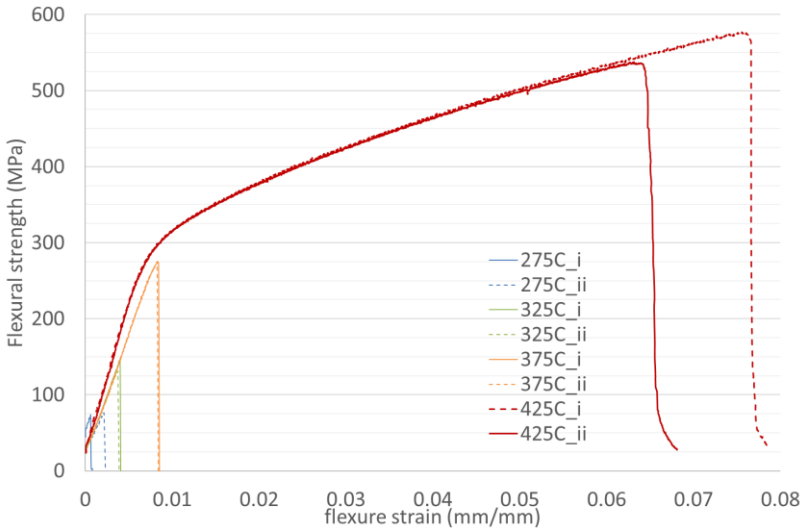

Figure 4-29 3-point bend strength test of Al7075samples sintered at the temperature range from 275 °C to 425 °C

4.5.6 Nano-sized Al_2O_3

The SEM images of Al_2O_3 powder materials with powder size of (Dv50) 40 nm are shown in *Figure 4-20*. This value was hardly verifiable; the Mastersizer 3000 laser diffraction particle size analysis did not correctly measure the particles size due to particle agglomeration.

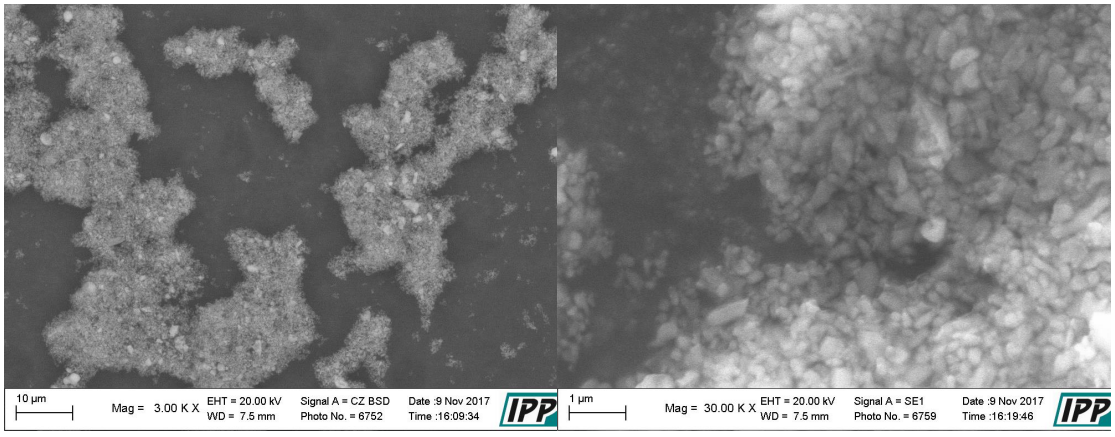

Figure 4-30 Al_2O_3 powder

The Al_2O_3 powder was sintered at various temperatures and it was found that 99 % of its density was achieved at a sintering temperature higher than 1200 °C. The biggest advantage of using a nano-sized powder is a higher flexural strength when compared to a sample compacted from micro sized powder. Thus this crystallite size was estimated from XRD analysis, shown below in *Table 4-4*.

The compacting of Al_2O_3 powder carried out by the SPS machine was regulated by a pyrometer. However, the sintering temperature was not verified by the thermocouple type C, since it was not available (*Figure 4-31*).

Sintering temperature (°C)	Crystallite size (nm)
1300	158
1400	280
1600	332

Table 4-4 Crystallite size of Al2O3 samples estimated from XRD analysis

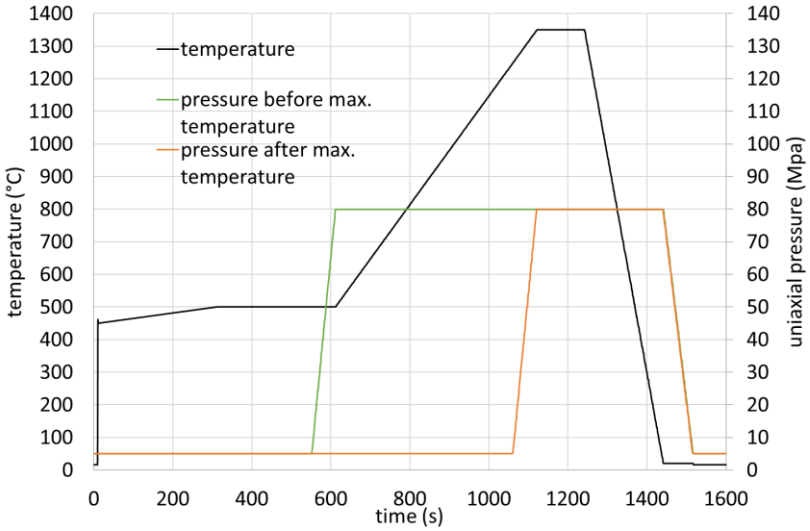

Figure 4-31 The SPS sintering process for Al_2O_3 at the temperature of 1350 °C. Pressure applied after max temperature (orange) is in Chapter 4.9

4.6 Evaluation of measured hardness

4.6.1 Hardness mapping

The samples described in *Chapter 4.5* were cut and materialographic samples were prepared according to the description in *Chapter 3.6*.

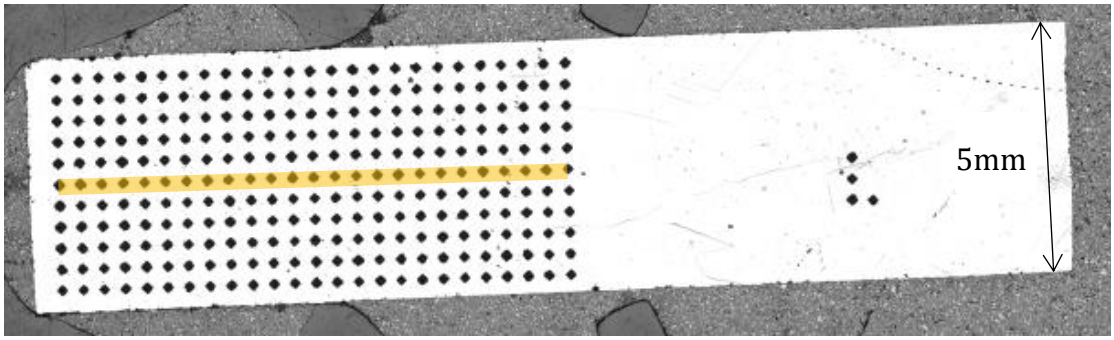

Figure 4-32 Vickers indentations in the samples' cross-section

All samples had dimension sizes of 20 mm in length and their thickness is related to their compactness and the final grindding - however, the thickness is usually about 4 to 5 mm *Figure 4-32*. The Vickers hardness mapping was

performed on one half of the samples, because the samples are supposed to have an axially symmetric hardness distribution. As the sintered samples were removed from the die after sintering, an orientation of the samples was not marked, therefore the samples' upper side in *Figure 4-32* cannot correspond with the samples' orientation during sintering. For that reason, the influence of current flow direction cannot be verified.

As hardness mapping is a time-consuming measurement, not every sample was mapped. Two SPSed samples of nMO, nNi and AlNi compacted at different temperatures were mapped and an appropriate method of hardness testing will be evaluated based on the obtained results. All axis on the hardness map are in mm and the hardness units are in HV2. The hardness obtained from mapping was compared with the hardness measured on the horizontal axis (yellow line on the sample *Figure 4-32*). If these values are in common, this method of hardness measurement (on the horizontal axis of the sample) will be used for are hardness measurement.

4.6.2 nMo

The hardness of nMo samples compacted at temperatures of 1200 °C and 1600 °C are compared in *Figure 4-33*. It is obvious that both samples are non-homogenous. The hardness of the sample compacted at 1200 °C is between 340 HV2 and 430 HV2, and between 226 HV2 and 292 HV2 for the sample compacted at 1600°C. This decrease in sample hardness is caused by the dependence of hardness on the grain size according to the Hall-Petch relation.

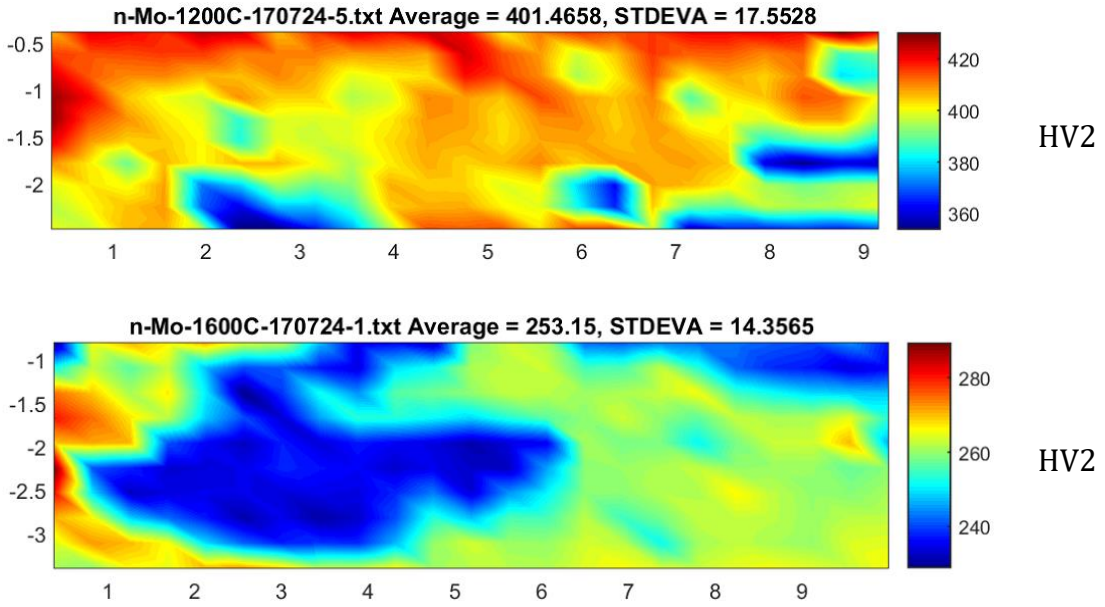

Figure 4-33 Hardness mapping of the nMo samples sintered at the temperatures of 1200 °C and 1600 °C

The increase in sintering temperature from 1200 °C to 1600 °C does not result in more homogenous samples, therefore the mapped hardness from one half of the sample was compared to the values of hardness measured in the horizontal axis of the sample marked by the yellow line in *Figure 4-32*.

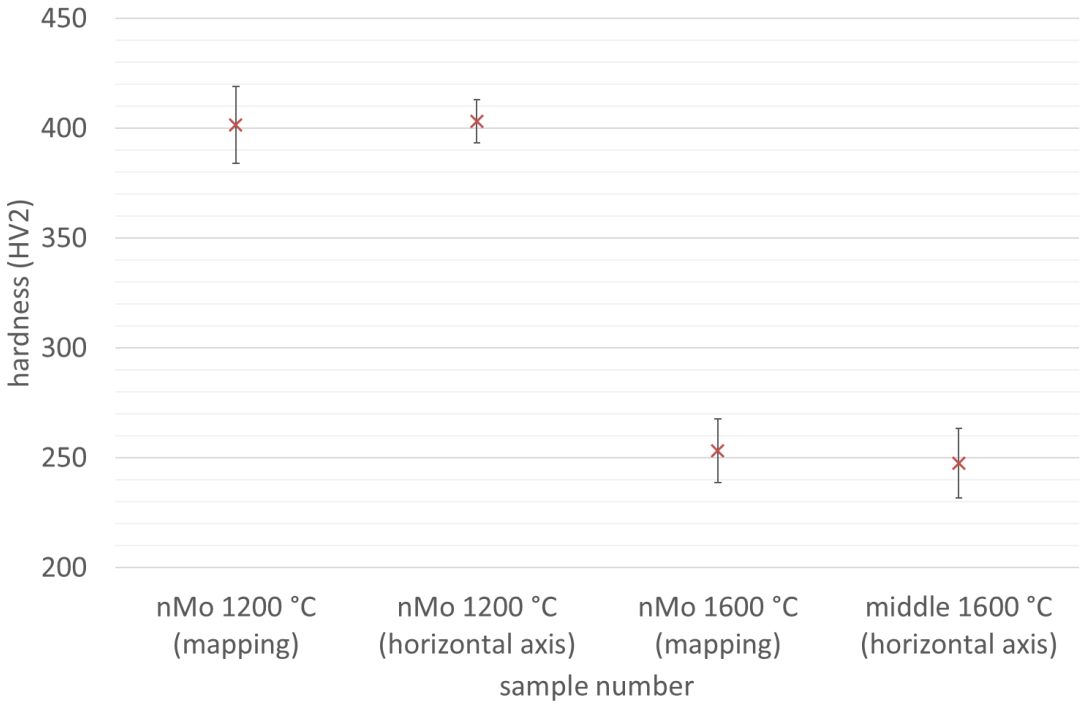

Figure 4-34 Hardness: comparison of methods of its evaluation (nMo)

4.6.3 uNi

The map of hardness was measured for two uNi samples, sintered at 950 °C and 1150 °C (*Figure 4-35*). The hardness slightly decreases with increasing sintering temperature, however, the difference between maximum and minimum value is nearly constant.

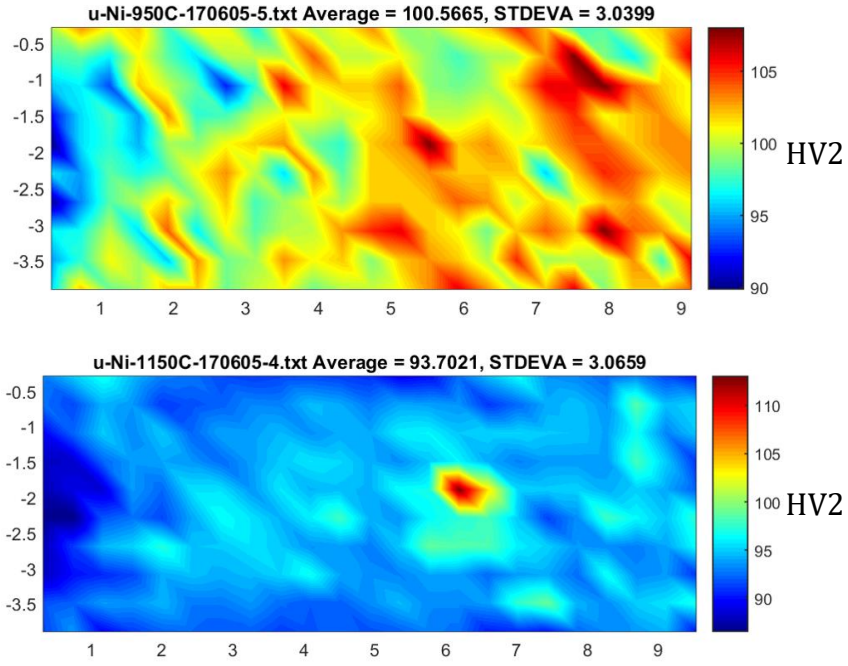

Figure 4-35 Hardness mapping of the uNi samples sintered at the temperatures of 950 °C and 1150 °C

The comparison of the hardness obtained from the mapping and from the middle of the samples is in *Figure 4-36*. The difference in their average hardness value is around 2 HV2, thus both measured methods are comparable.

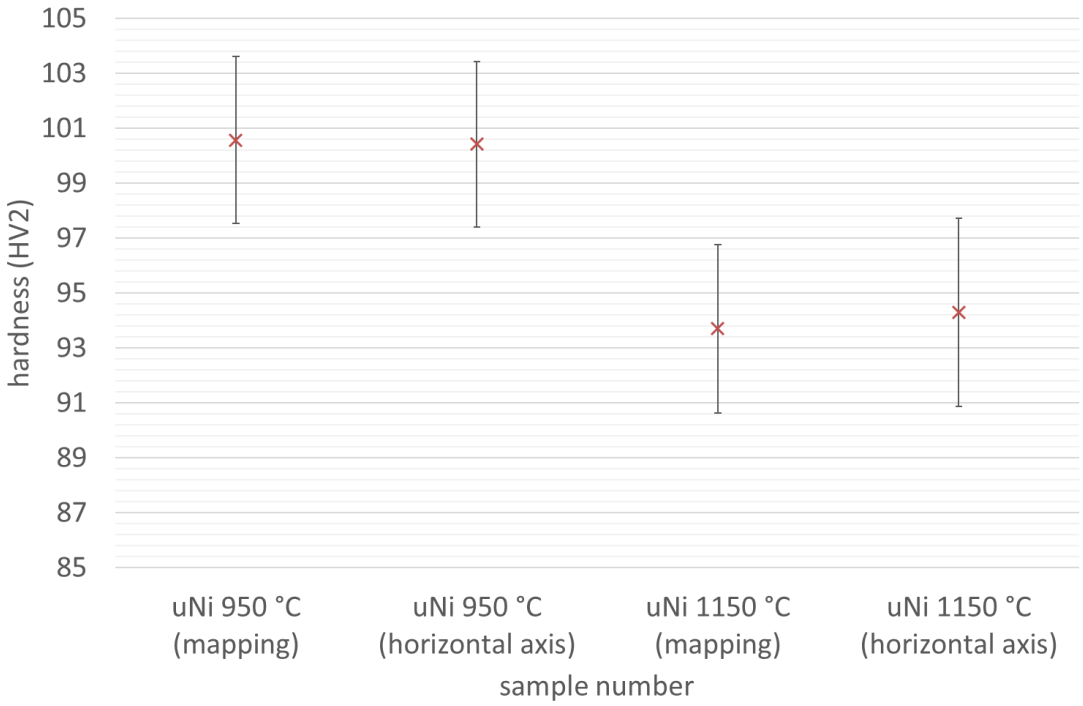

Figure 4-36 Hardness: comparison of methods of its evaluation (micro Nickel)

4.6.4 nNi

The hardness of two nNi samples is shown in *Figure 4-37*. The hardness of the sample compacted at 450 °C is between 421 HV2 and 364 HV2. The increase in sintering temperature results in a much homogenous sample, but its hardness significantly decreases up to values between 138 HV2 and 153 HV2. This is caused by grain growth, similar to that of nMo powder sintering.

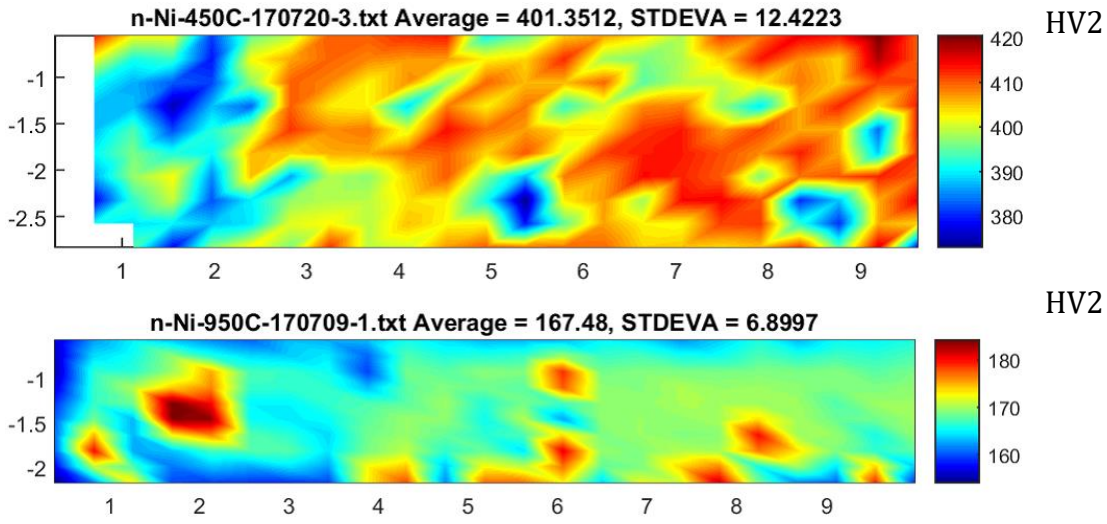

Figure 4-37 Hardness mapping of the nNi samples sintered at the temperatures of 450 °C and 950 °C

The measured hardness values are compared in *Figure 4-38*. It is obvious that the hardness measured by both methods is in agreement and both methods are well comparable.

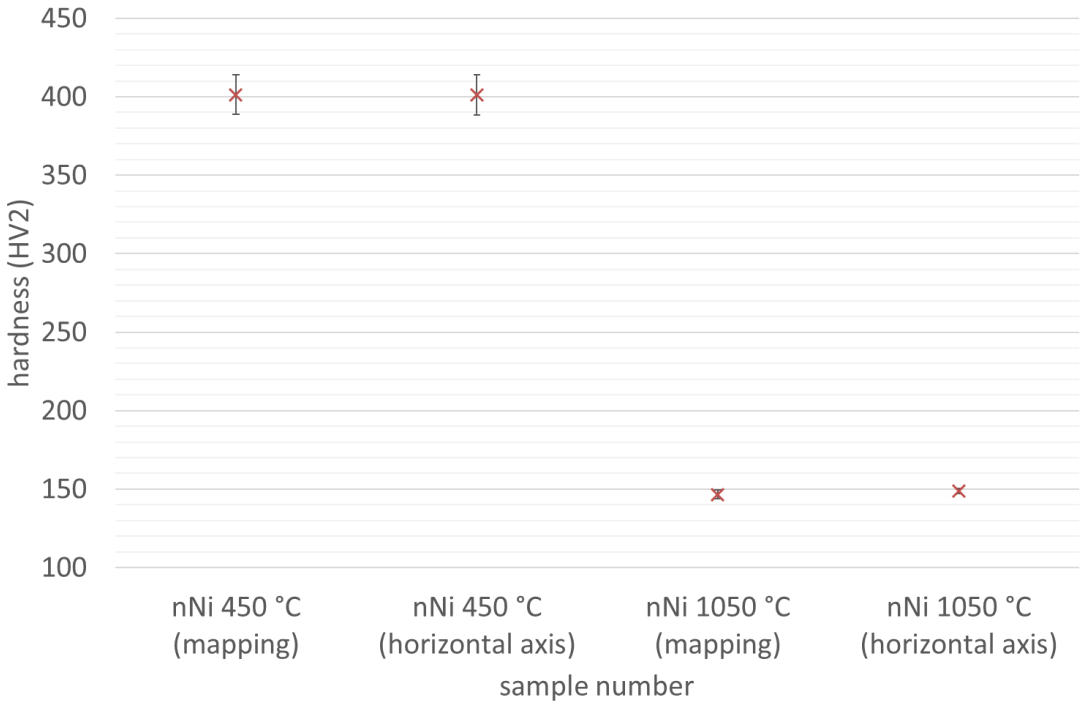

Figure 4-38 Hardness: comparison of methods of its evaluation (nano Nickel)

4.7 Reproducibility of the sintering process

In order to investigate reproducibility of the sintering process three samples of AlNi and nMo were sintered and the process parameters (temperature and punches position) of each process were compared. The SPS processes were regulated by pyrometer and temperature was verified by thermocouple type C, located in lower punch (position Term1_down).

4.7.1 Reproducibility of the sintering process – AlNi samples

AlNi samples were compacted at the temperature of 1250 °C in accordance with the optimized sintering evolution in *Figure 4-20*.

Samples were heated by a non-pulsing DC current and prepared by using different sets of dies and punches, but their size was identical. The SPS process was regulated by a pyrometer. However, the temperature was measured by the thermocouple "Term1_down" and a thrice-repeated sintering experiments (AlNi ref1, AlNi ref2 and AlNi ref3) are compared in *Figure 4-39*. Temperature courses "ref2" and "ref3" are nearly identical only with a little temperature difference during the first stage of sintering at 500°C. Nevertheless, as this difference is present only at the initial sintering stage, it does not have any impact on the sintering result. The maximum temperature of the "ref1" experiment exceeds the "ref2" and "ref3" experiments by approximately 10°C. Similar exceeding

temperatures might be a significant issue for sintering materials near their melting point temperature of a phase transformation.

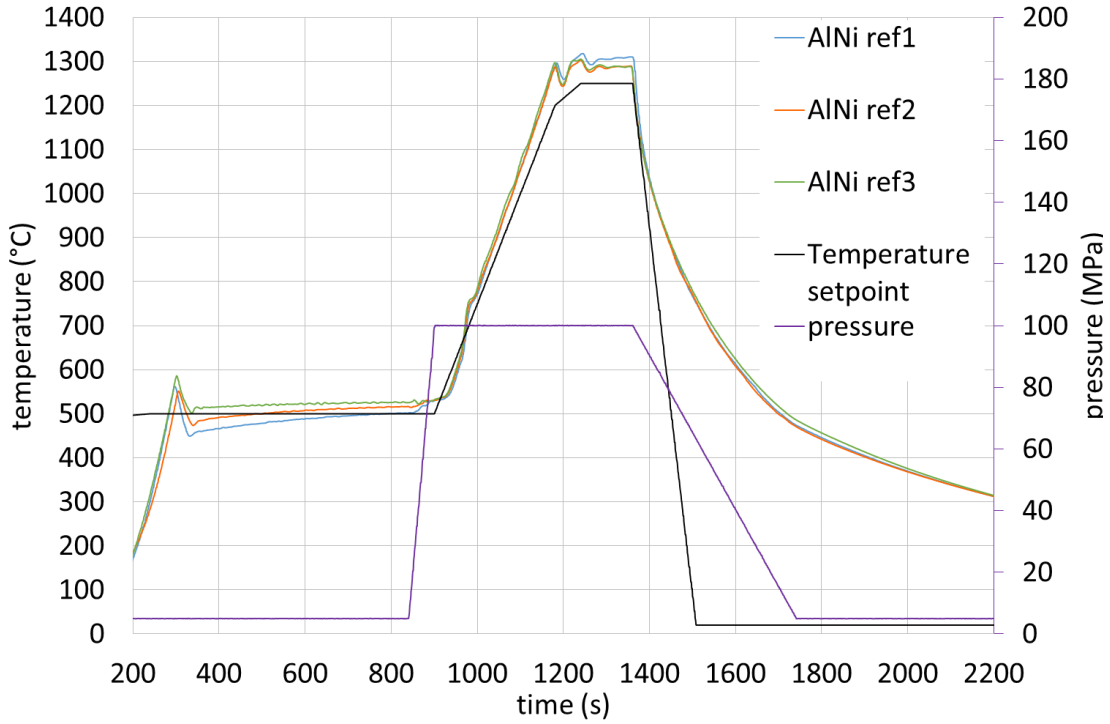

Figure 4-39 Verification of SPS repeatability - sintering of AlNi with a non-pulsed DC current

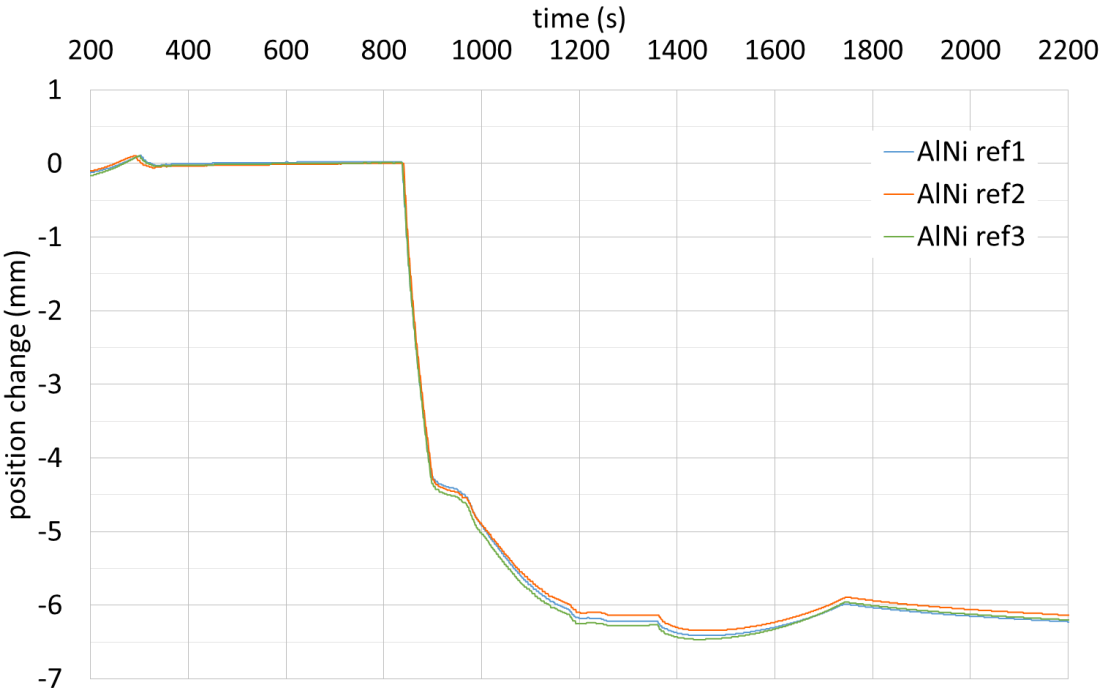

Figure 4-40 Verification of SPS repeatability - sintering of AlNi with non-pulsed DC current, punches positions (shrinking of sample volume)

Punches positions of three repeated sintering processes are in *Figure 4-40*. This value is related to the distance of the SPS electrodes, its change is

equal of the powder compaction. The evolutions of all three positions are very similar. Therefore, the sintering of AlNi by a non-pulsed DC current is a repeatable process (from the point of view of temperature and position evolutions).

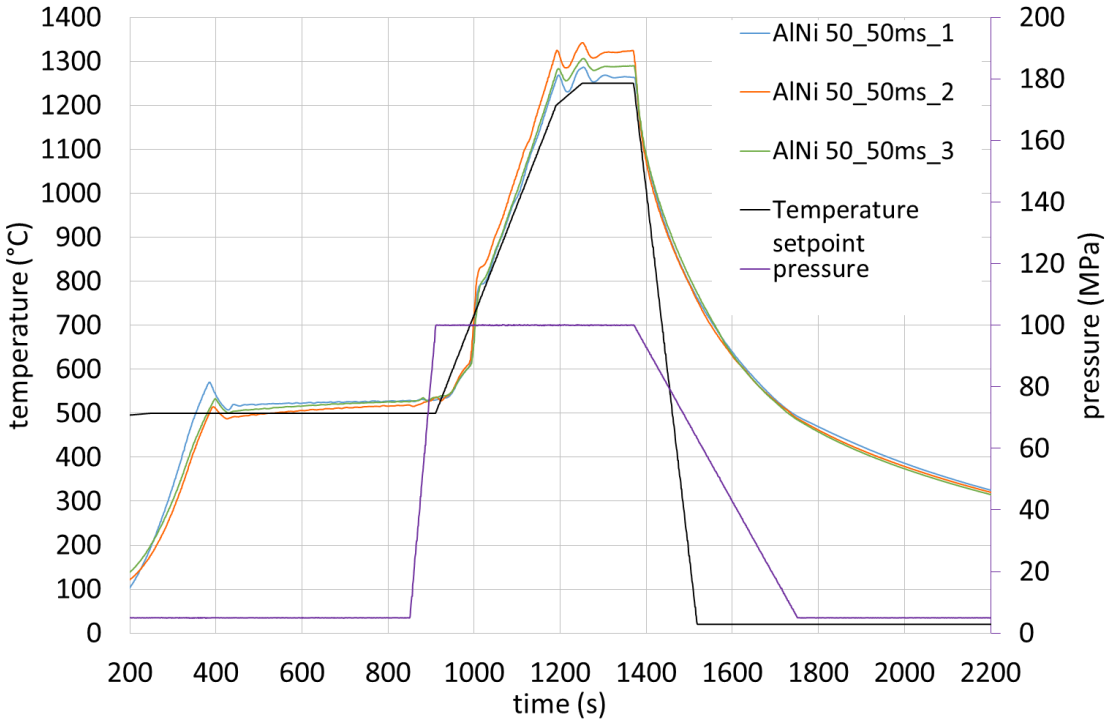

Figure 4-41 Verification of SPS repeatability - sintering of AlNi with current patterns of 50-50 ms

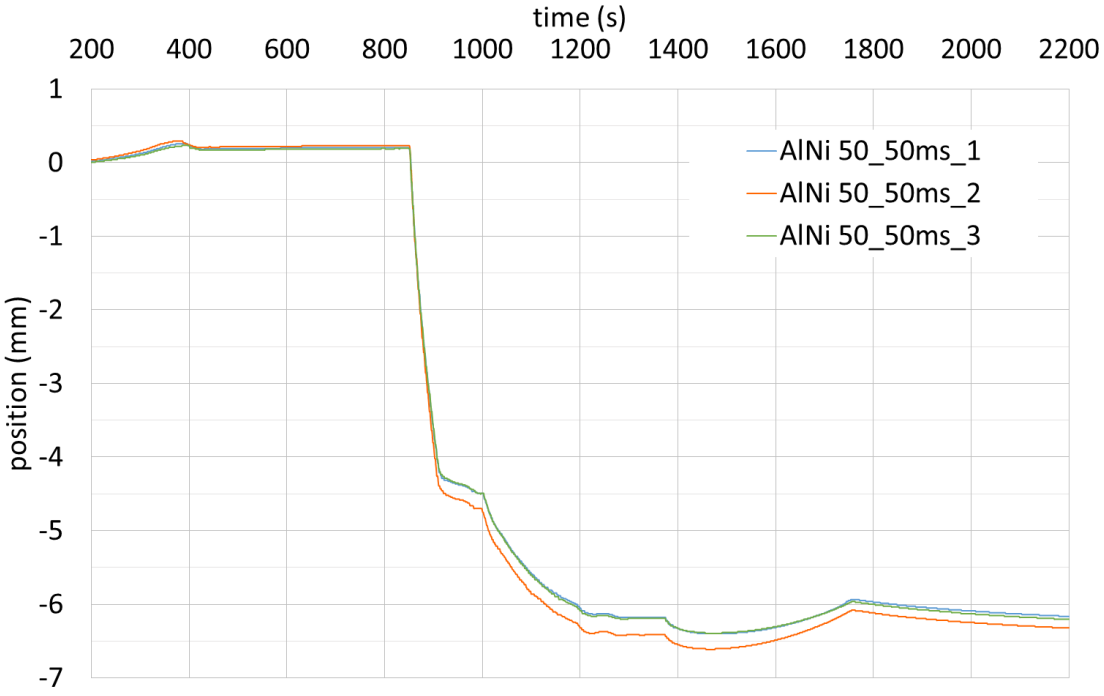

Figure 4-42 Verification of SPS repeatability - sintering of AlNi with current patterns of 50-50 ms, punches positions (shrinking of sample volume)

The same sintering process was repeated using DC pulsed current. The pulse current was applied from the start of a SPS process to its finish. Temperature evolutions for samples heated by pulse patterns of Ton=50ms and Toff = 50ms is shown in *Figure 4-41*. There are significant differences in temperature evolutions. The difference between the maximum and minimum temperatures (when the temperatures are stabilised) is 55 °C. Such temperature differences have an impact on the sintering position in *Figure 4-42*. "*50_50ms_1*" and "*50_50ms_3*" are almost identical whereas the position "*50_50ms_2*" is about 0.25 mm lower.

It was shown that using of pulsed current has a crucial impact on the temperature evolution. The temperature difference between the three identical sintering setups was 55 °C. When non pulsed current was used, the temperature difference was only 10 °C.

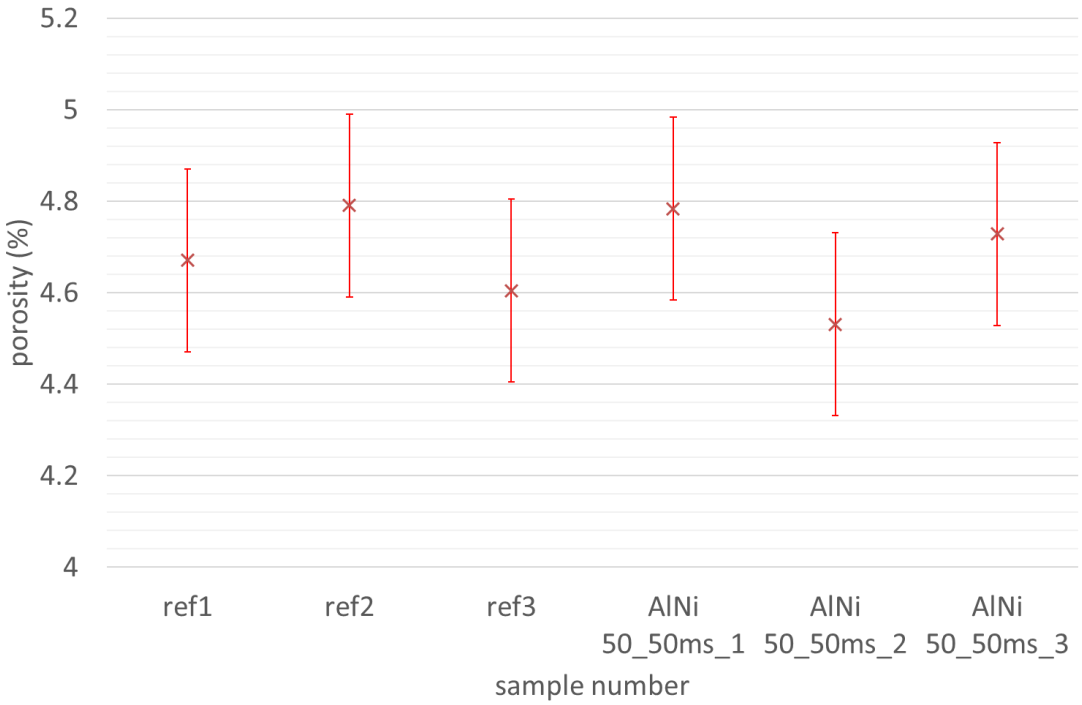

Figure 4-43 Verification of SPS repeatability – measured porosity of the AlNi samples sintered under the same conditions (three samples by non-pulsed DC current and three samples by pulsed current)

4.7.2 Reproducibility of the sintering process – nMo samples

Reproducibility measurement of the sintering process was repeated with the nMo powder sintered at 1200°C. The initial dwell time was shorter (to avoid nMo oxidation in residual atmosphere of <10 Pa) and the maximal temperature was 50°C lover compared to the sintering of AlNi.

As seen in *Figure 4-44*, all temperatures measured by the thermocouple "Term1_down" seem to be more oscilating, but it is given by shorter dwell time at 500 °C due to the fact that these temperatures are not stabilised. The temperature "ref1" is approximately 10 °C higher than the temperatures "ref1"and "ref3".

The punches positions are shown in *Figure 4-45*. Although the position of the consolidated samples decreased by around 11 mm, the maximum difference between the evolutions is only around 0.1 mm and no significant difference in position is evident.

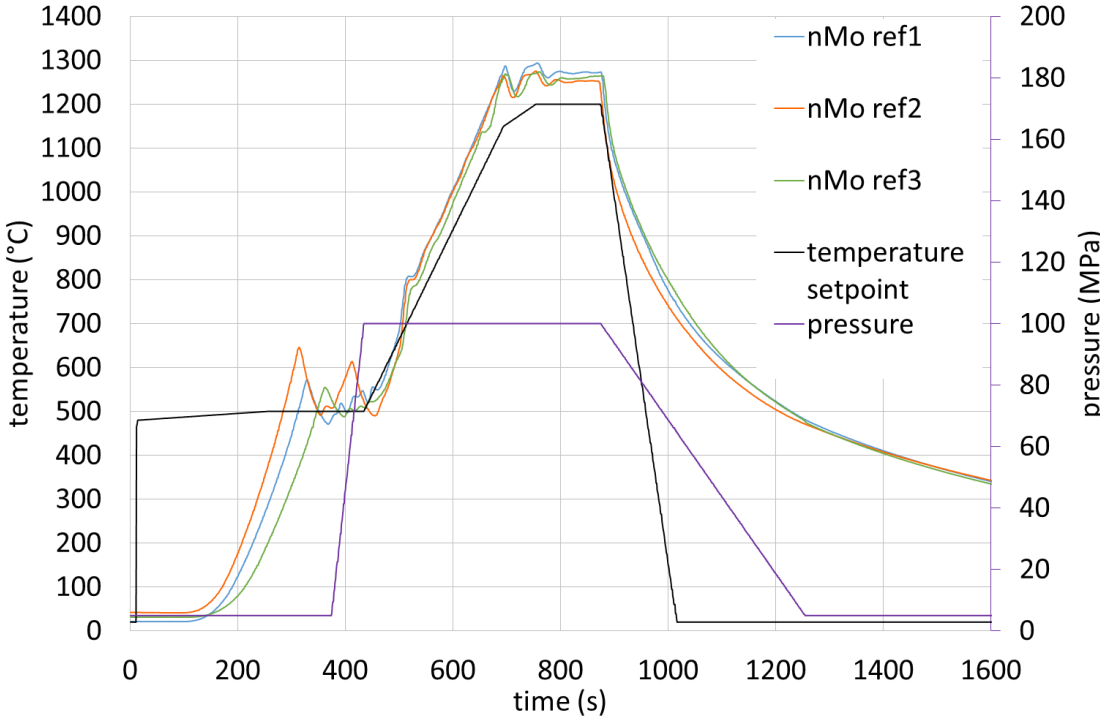

Figure 4-44 Verification of SPS repeatability - sintering of nMo with non-pulsed DC current

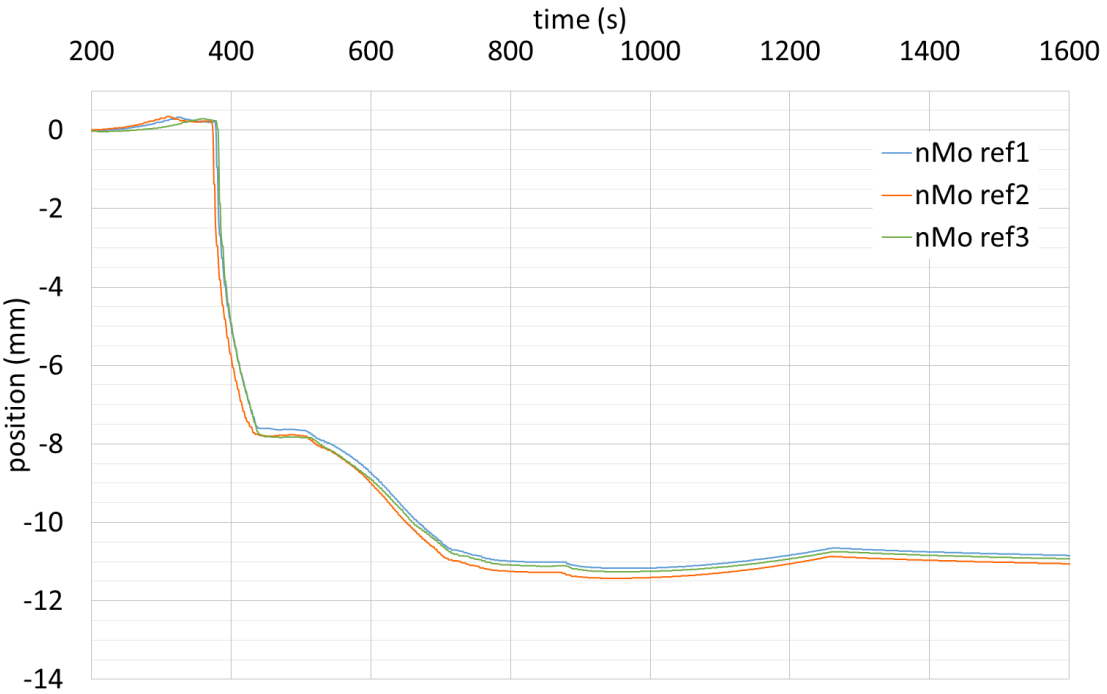

Figure 4-45 Verification of SPS repeatability - sintering of nMo with non-pulsed DC current, punches positions (shrinking of sample volume)

The same process was repeated using a pulsing current with T_{on} and T_{off} 5 ms as seen in *Figure 4-46*.

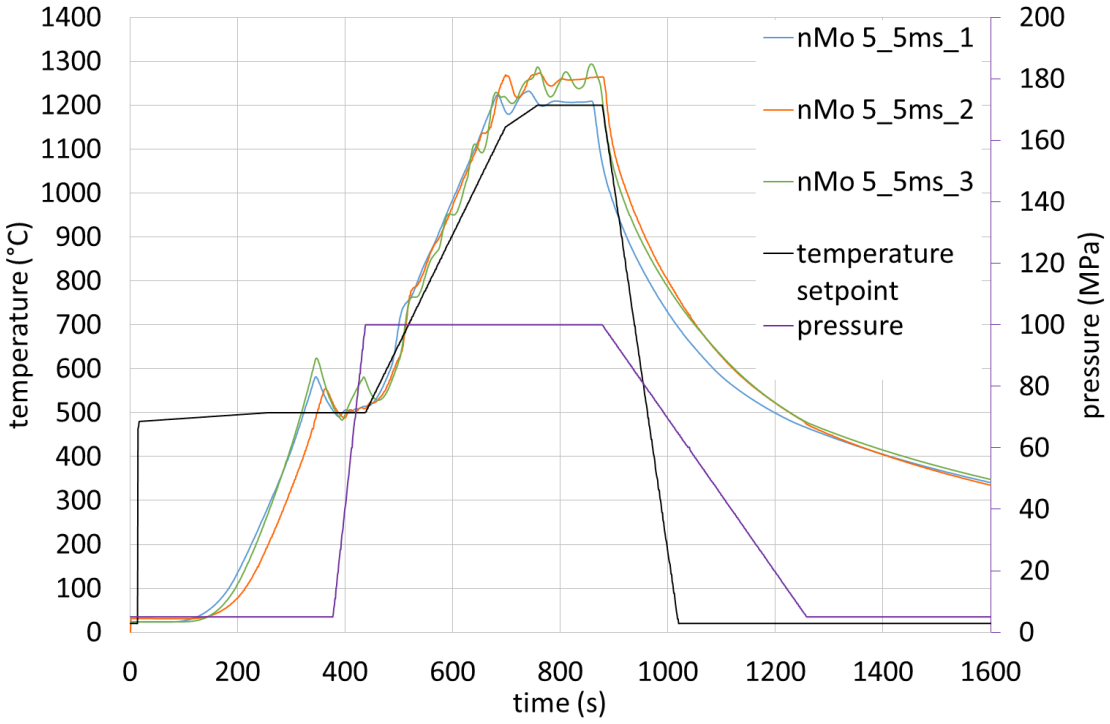

Figure 4-46 Verification of SPS repeatability - sintering of nMo with current patterns of 5-5 ms

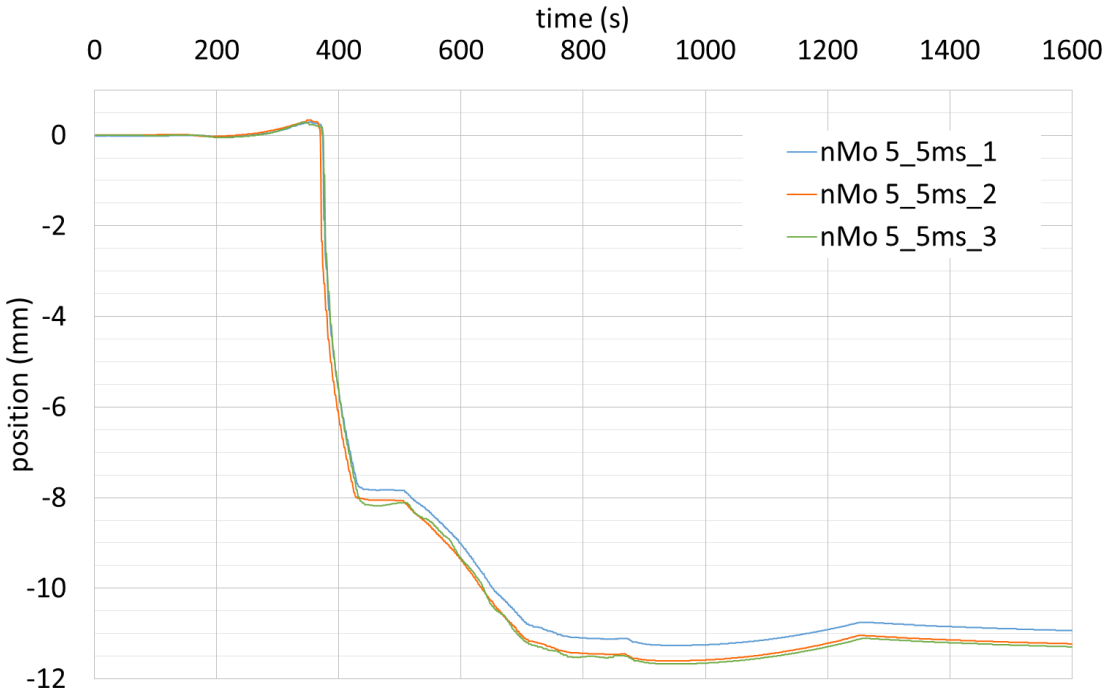

Figure 4-47 Verification of SPS repeatability - sintering of nMo with current patterns of 5-5 ms, punches positions (shrinking of sample volume)

The obtained data from this measurement show a noticeable difference in temperatures during each of three SPS processes. The maximum temperature of "*5_5ms_1*" is about 70 °C lower than the maximum temperature of "*5_5ms_2*" and 100 °C lower than the maximum temperature of the "*5_5ms_3*" experiment. The SPS process "*5_5ms_3*" is improperly regulated as it is oscillating between temperatures of 1300 °C and 1250 °C.

The temperatures overcome the result in different samples consolidation, which is evident in *Figure 4-47*. The sample "*5_5ms_1*" is not consolidated as well as the samples "*5_5ms_2*" and "*5_5ms_3*", where the shrinkage is about 2.5 mm lower, which means that its volume (and porosity) is higher than in the other samples as seen in *Figure 4-48*.

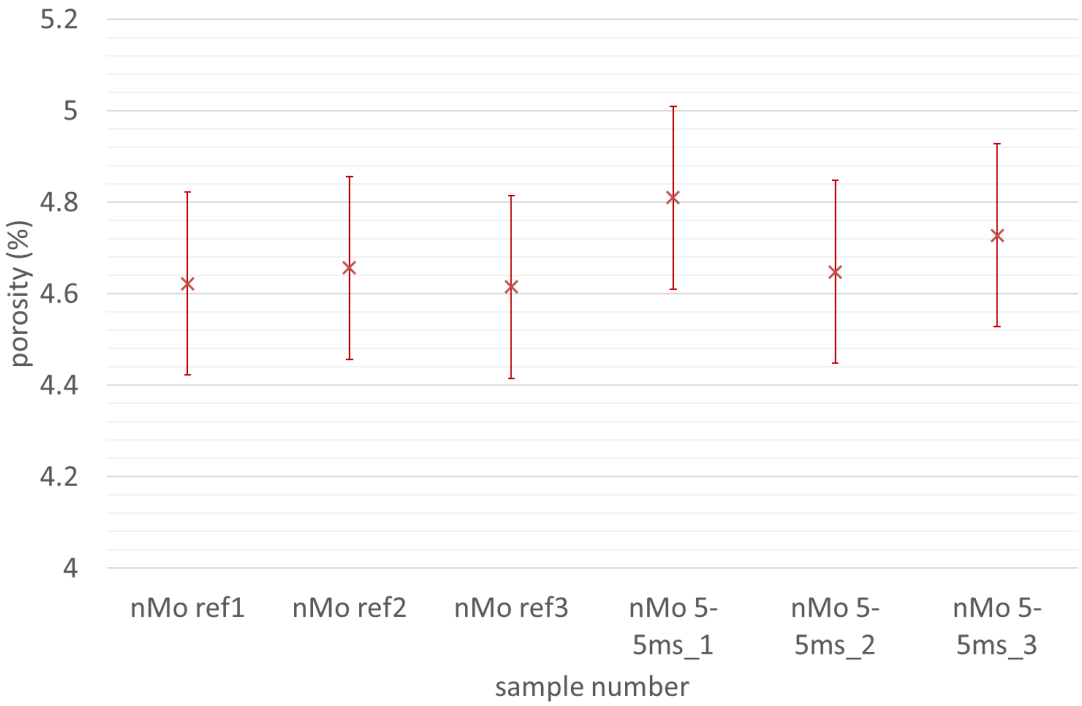

Figure 4-48 Verification of SPS repeatability – measured porosity of the nMo samples sintered under the same conditions (three samples by non-pulsed DC current and three samples by pulsed current)

4.7.3 Verification of the repeatability of sintering - hardness

The hardness of the samples compacted and described in *Chapter 4.6* was measured in order to investigate if the maximum temperature reached on the sample has a measurable influence on the material properties. The hardness of the samples was measured only in the horizontal axis of the samples, since this method provides reliable results as was proved in *Chapter 4.6.1*.

4.7.3.1 nMo

The hardness of three nMo samples compacted under the same conditions in *Chapter 4.7.2* by using non pulsed and pulsed DC current was investigated in order to determine the reproducibility of sintering. The hardness was measured on the horizontal axis of the metallographic samples.

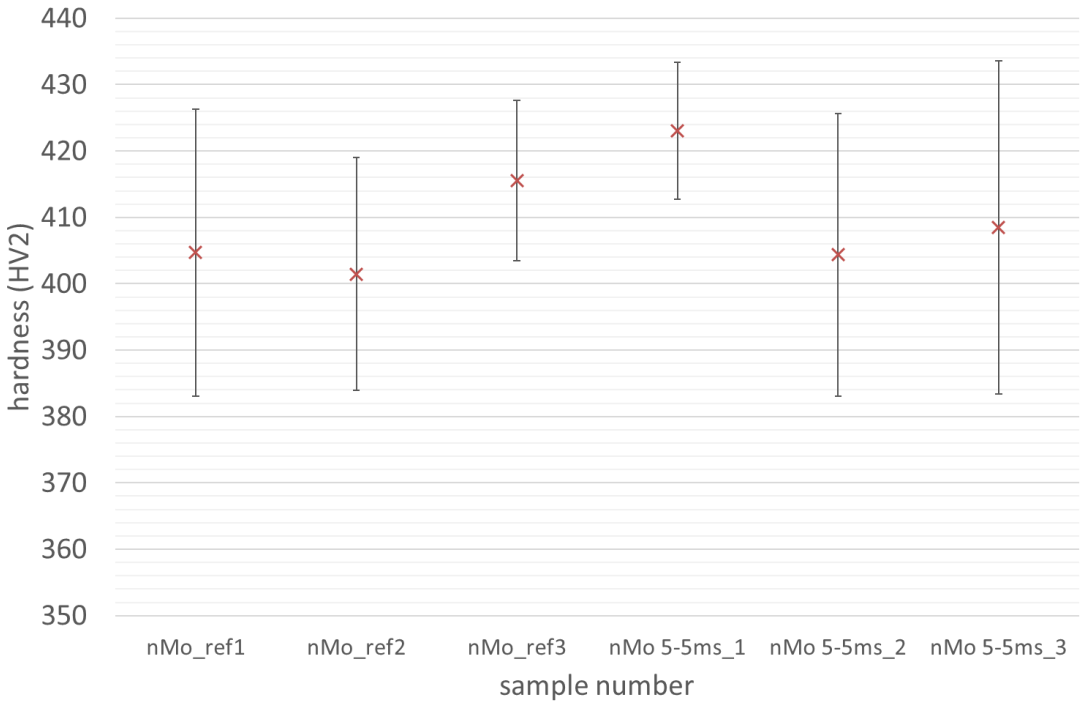

Figure 4-49 Hardness of nMo samples sintered under the same conditions by a non-pulsed (Figure 4-44) and pulsed DC current (Figure 4-46)

The results of measured hardness are summarised in *Table 4-5*. The hardness values of samples *ref1* and *ref2* compacted with no pulsed current are comparable and there is no observable difference (after the standard of measured hardness is calculated), but the average value of hardness of sample *ref3* is a bit higher and its variance of measured values is lower. However, as seen in *Figure 4-44*, there is no significant difference in sintering temperatures.

Samples *5-5ms_2* and *5-5ms_3* sintered with a pulsing current (5 ms on and 5 ms off) have comparable hardness to the samples sintered by a non-pulsed current. The hardness of the sample *nMo5-5ms_1* is higher, even if the standard deviation of measured values is taken into account. It corresponds to the finding that this sample was compacted at a lower temperature *Figure 4-46* since it was shown that hardness decreases with increasing sintering temperature.

nMo samples	**ref1**	**ref2**	**ref3**	**5-5ms_1**	**5-5ms_2**	**5-5ms_3**
Hardness (HV2)	404±21	401±17	415±12	423±10	404±22	408±25
Max. temperature (°C)	1294	1275	1273	1232	1273	1294

Table 4-5 Reproducibility of nMo samples - hardness comparison

4.7.4 AlNi

The same measurement was repeated with AlNi samples compacted in *Chapter 4.7.1*. The hardness of three reference samples sintered under the same

conditions is evaluated in *Figure 4-50* and it is obvious that the hardness of the sample "AlNi ref1" is higher than the others, despite the fact that the variance of measured values is double. However, as seen in *Figure 4-39*, this sample was, in comparison to the other samples, compacted at the highest temperature (even though the temperature difference was about 25 °C).

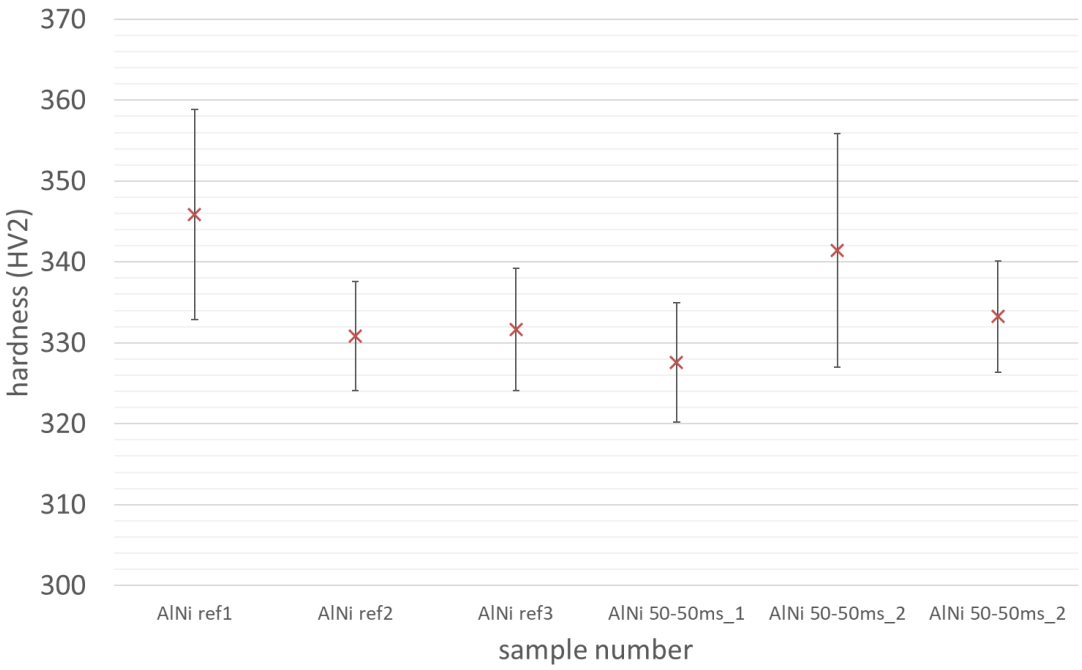

Figure 4-50 Hardness of AlNi samples sintered by non-pulsed DC current (Figure 4-39) and by current patterns of 50-50 ms (Figure 4-41)

The hardness of AlNi samples compacted with a pulsed current with pulse pattern 50 ms on and 50 ms off is also in *Figure 4-50*. It is noticeable that the measured hardness corresponds to the sintering temperatures. Sample *50-50ms_2*, which has the highest temperature during the sintering process, has also the highest hardness from all samples. On the other hand, the hardness of sample *50-50ms_1* is the lowest, even when compared with samples compacted with a non-pulsed current. The lowest hardness value is related to the fact that its sintering temperature was the lowest of all samples.

AlNi Samples	**ref1**	**ref2**	**ref3**	**50-50ms_1**	**50-50ms_2**	**50-50ms_3**
Hardness (HV2)	346±13	331±7	332±8	328±7	341±14	333±7
Max. temperature (°C)	1318	1303	1305	1287	1342	1308

Table 4-6 Reproducibility of AlNi samples - hardness comparison of samples compacted under the same conditions

4.8 Influence of DC pulses current

Material	SPS process regulated by	Evaluated material properties				
		porosity	hardness	3PB	XRD	SEM
Nano Nickel	Thermocouple	X	X	-	-	X
Micro Nickel	Thermocouple	X	X	-	-	X
Nano Molybdenum	Pyrometer	X	X	-	-	X
AlNi	Pyrometer	X	X	-	X	X
Al7075	Thermocouple	-(*)	X	X	X	X
Al_2O_3	Pyrometer	-(*)	-(**)	X	-	X

Table 4-7 Influence of pulsed current on mechanical properties of SPS samples - summarised measurements

The SPS processes for lower sintering temperature were regulated by thermocouple type K (placed in "term1_down"). These processes included the compacting of powders nNi, uNi and Al7075. Other powders – nMo, AlNi and Al_2O_3 – were compacted by using a pyrometer, respectively the SPS process was regulated by a pyrometer and temperature in the place "term1_down" was verified by a type C thermocouple except for the sintering of Al_2O_3, where the thermocouple C was not available.

All temperature courses were studied in detail, especially the maximum peak temperature and the average difference between the stable temperature and the set point temperature. As shown previously the degree of compaction of sintered material is related to the sintering temperature. Therefore the change in punches positions and its dependence on temperature maximum peak temperature was studied. Once reference position was chosen, the distance between punches, where the powder was compressed, is loaded by full pressure (100 MPa, respectively 80 MPa for Al_2O_3). The volume of a compacted powder decreases with increasing sintering temperature, therefore the distance between punches also decreases. The change in volume of a sintered sample is calculable from the change in distance of punches and of the punch radius (10 mm). For that reason, the porosity of compacted samples was measured and thus the influence of porosity and the punch position might be investigated.

A SEM morphological analysis of samples with the biggest difference in hardness and porosity compared to reference samples was performed in order to investigate if the changes are observable.

All alloys will be analysed by an XRD. As the spark or plasma presence between particles should locally increase the temperature, it should have an impact on their phase composition. Therefore the XRD phase identification will distinguish the major and minor phases, and it will trace differences between the initial powders and the samples sintered with a non-pulsed and pulsed current.

(*) Porosity will not be investigated on the Al7075 and Al_2O_3 samples. As the samples were sintered at nearly 100 % of their density, no change in the porosity can be observed.

(**) Hardness measurement was not performed on Al_2O_3 samples. The hardness meter was not able to determinate edges of the indents since Al_2O_3 is a very brittle material and the samples' surface is shiny thus the hardness tester cannot evaluate edges of the indents.

4.8.1 Nano Nickel

The temperature evolutions for various pulse conditions are investigated in *Figure 4-51*. It is evident, from the temperatures overshoots that the peak temperature (above the set point temperature) depends on the current's duty cycle. Samples sintered with the current of duty cycle of 25 % (pulses 5-15ms and 25-75ms) have the highest temperature overshoots in comparison to the reference course (non-pulsed current). The shape of the temperature courses for the current duty cycle of 75 % (5-15ms and 75-25ms) is nearly identical to the reference course.

The samples compaction in *Figure 4-52* corresponds to the temperature courses. Sample 25-75ms, which has the highest temperature overshoot over the set point temperature, has the biggest change in its volume and sample 15-5ms is less compacted than other samples. However, this change is not very significant.

The measured porosity of nNi samples in *Figure 4-53* corresponds to sample compaction: sample 15-5ms has the lowest overshoot in temperature and the lowest change in punch position, which results in the highest porosity of all samples (7.4±0.3 %). The lowest porosity – 5.1±0.2 % - was measured for the sample 25-75ms, which has the highest overcome in temperature during sintering and also its compaction is highest from all samples. The porosity of other samples is similar in regard to the deviation of measurement.

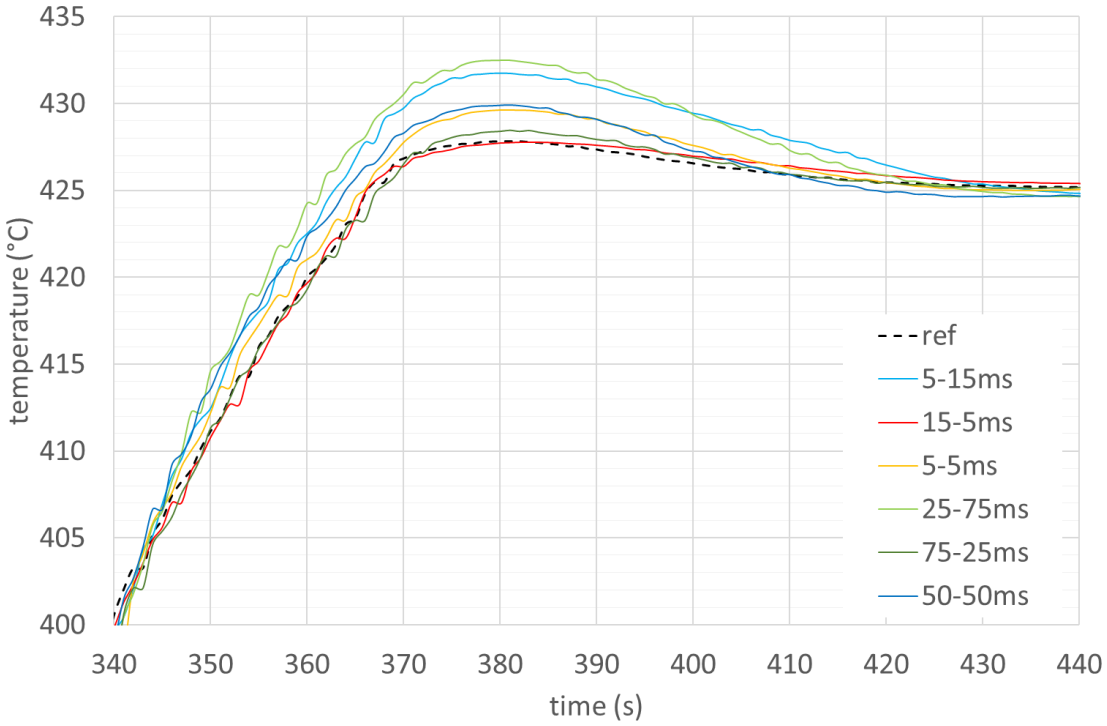

Figure 4-51 Temperature courses (thermocouple K) of nNi sintering cycles - various pulsed pattern conditions (reference process course is in Figure 4-13)

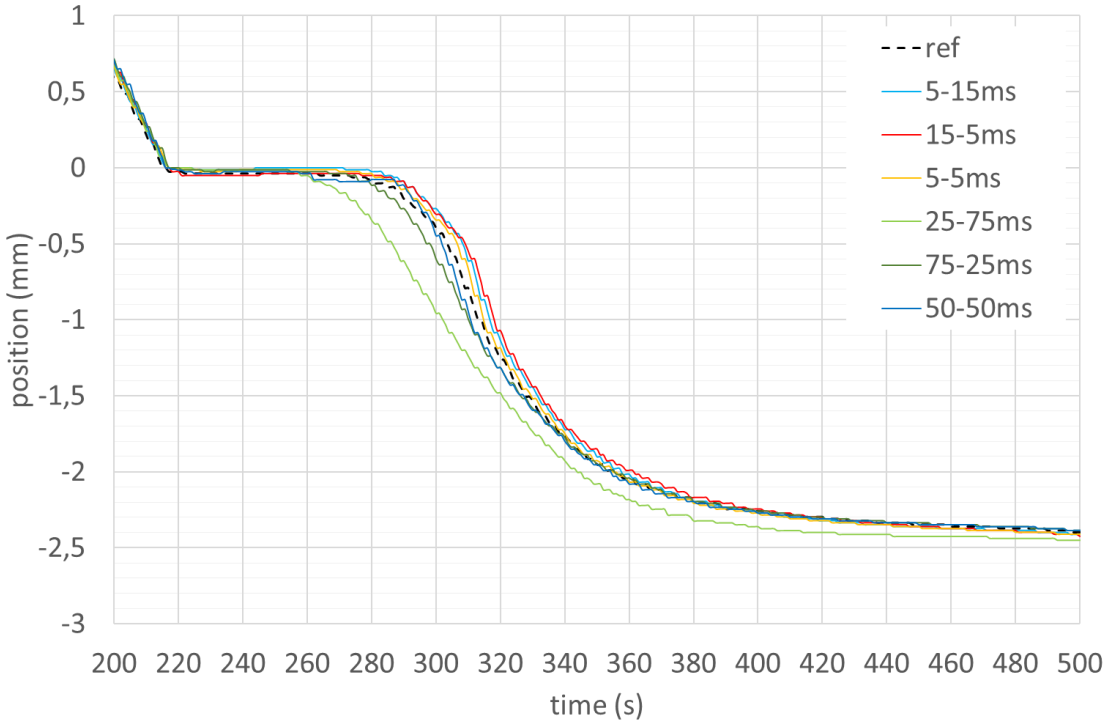

Figure 4-52 nNi compaction – change in punches position for various pulsed pattern conditions

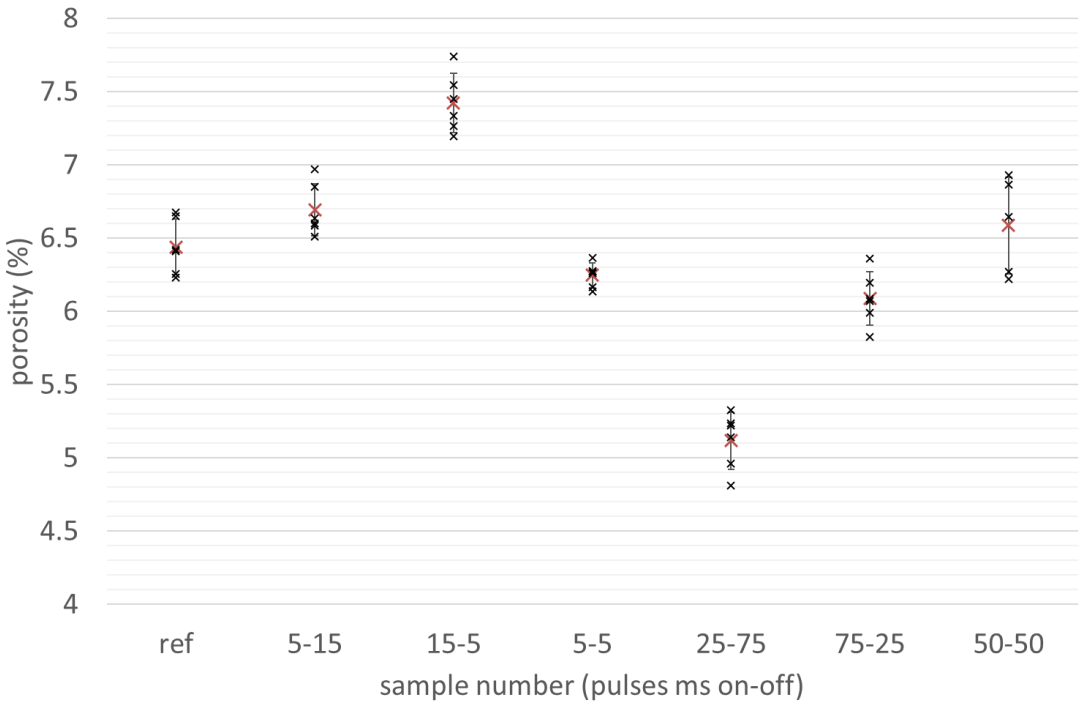

Figure 4-53 Porosity of nNi samples compacted by various pulse pattern conditions

Hardness is evaluated in *Figure 4-54.* The hardness of the reference sample is 324±7 HV2 and there is no any observable difference between all of the samples.

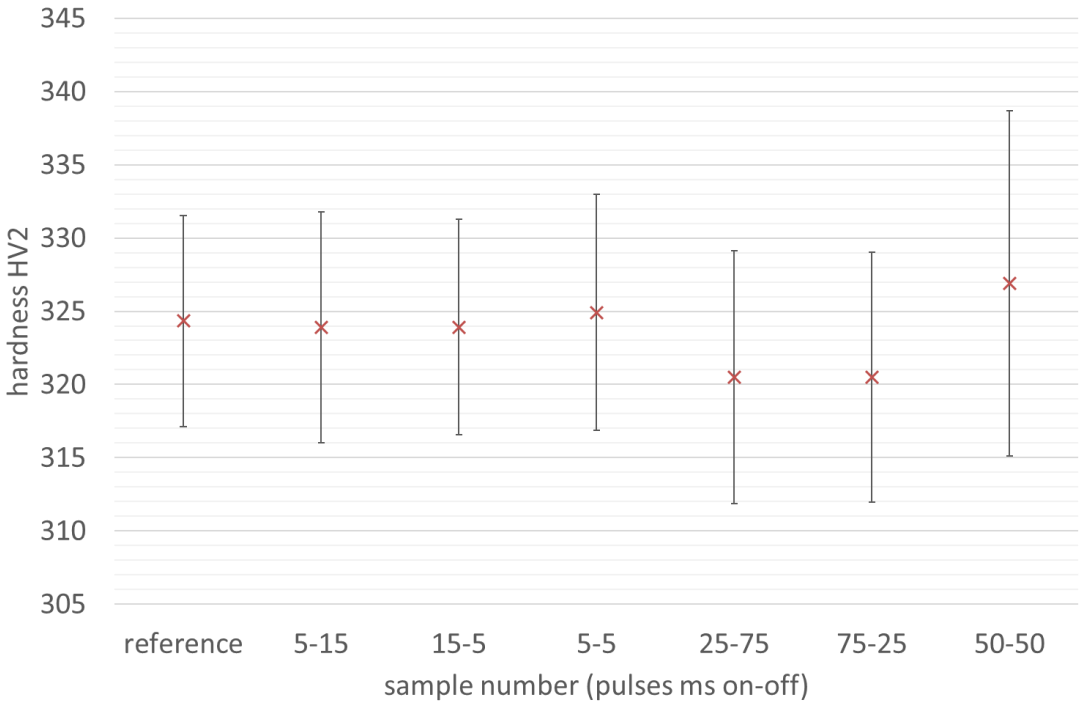

Figure 4-54 Hardness of nNi samples compacted by various current pulse patterns conditions

Backscattered SEM images of the SPSed nNi samples sintered at the temperature of 425 °C by using different pulsed conditions are shown in *Figure 4-55 to Figure 4-57*. The microstructure for these samples appear to be very similar and responds to the results observed in *Figure 4-53*. It is obvious that when compared to other samples, the microstructure of samples for 15-5ms shows room for further densification improvement and the sample 25-75ms has the lowest porosity which was proved by the porosity measurement in *Figure 4-53*. The grain sizes of all samples are similar to that of the initial powder.

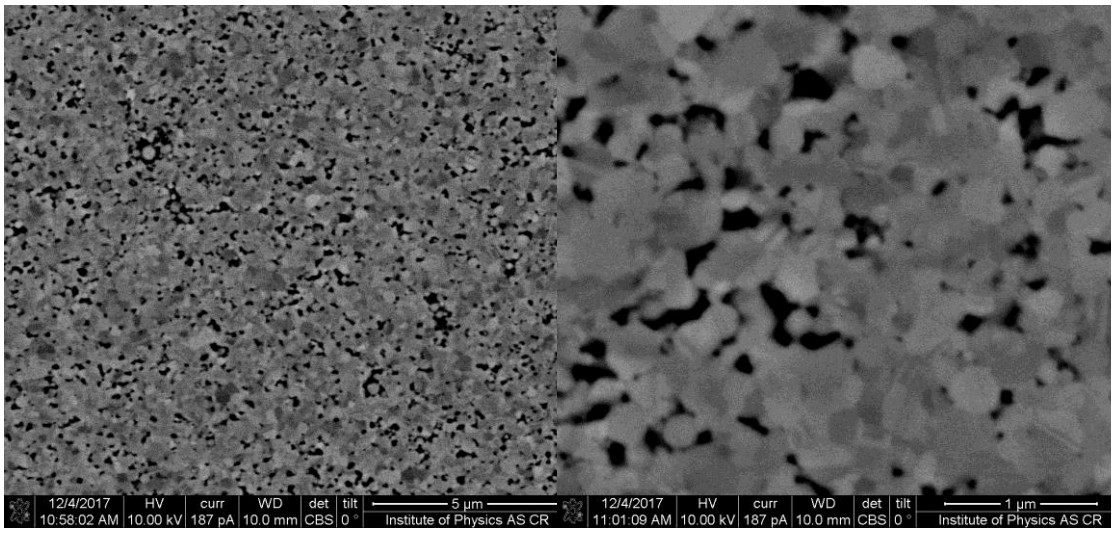

Figure 4-55 Backscattered SEM image of nNi sintered at the temperature of 425 °C with non-pulsed current

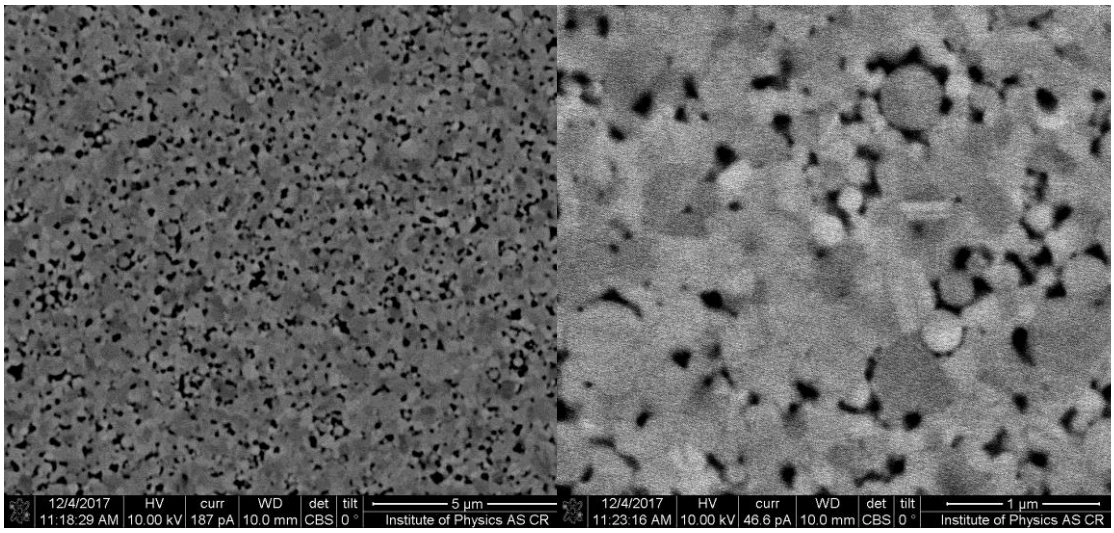

Figure 4-56 Backscattered SEM image of nNi sintered at the temperature of 425 °C with DPC 15-5 ms

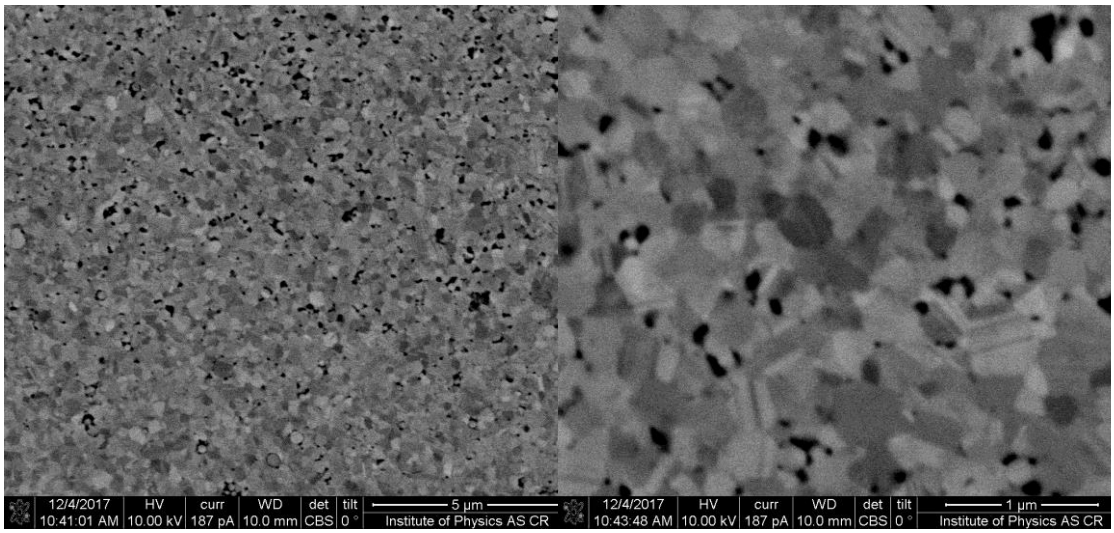

Figure 4-57 Backscattered SEM image of nNi sintered at the temperature of 425 °C with DCP 25-75 ms

4.8.2 uNi

Details of of temperature evolition for uNi sintering with temperature overshoots are in *Figure 4-58*. It is significant that the temperatures overshoots are not so high when compared to nNi sintering. It is possibly due to the longer dwell time (as seen in *Figure 4-11*) at the temperature of 100 °C, therefore all temperatures courses were more stabilised. The highest overshoots are for pulse current of the 25 % duty cycle (pulses 5-15ms and 25-75ms); other temperatures shapes are similar, but still a little bit higher than the reference course. Courses of temperature for samples 50-50ms and 25-75ms are "undulated", which might mean that the "off time" is long enough to slightly decrease the sample temperature. Nevertheless, all temperature differences are <3 °C.

The changing punches positions during the compacting of uNi samples are shown in *Figure 4-59*. The biggest difference in position is for the sample heated by pulse patterns 25-75ms, which is in agreement with the higher sintering temperature. On the other hand, the position is lower only by about 0.1 mm in comparison to the other samples.

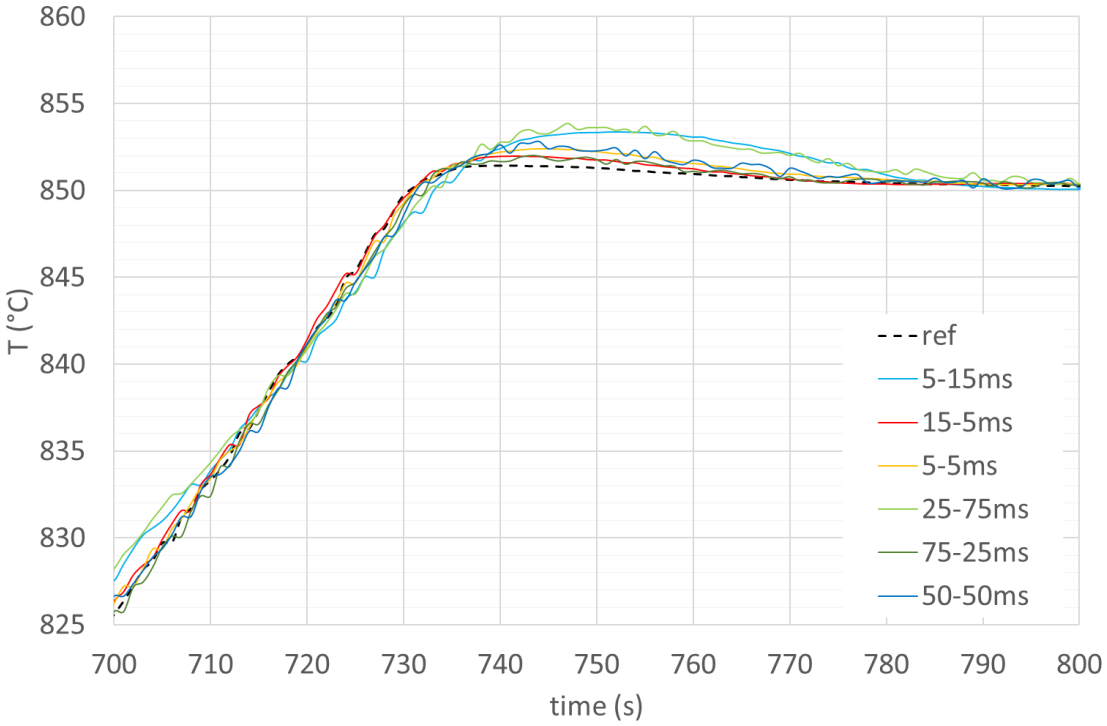

Figure 4-58 Temperature courses (thermocouple K) of uNi sintering cycles - various pulsed pattern conditions (the reference process course is in the Figure 4-11)

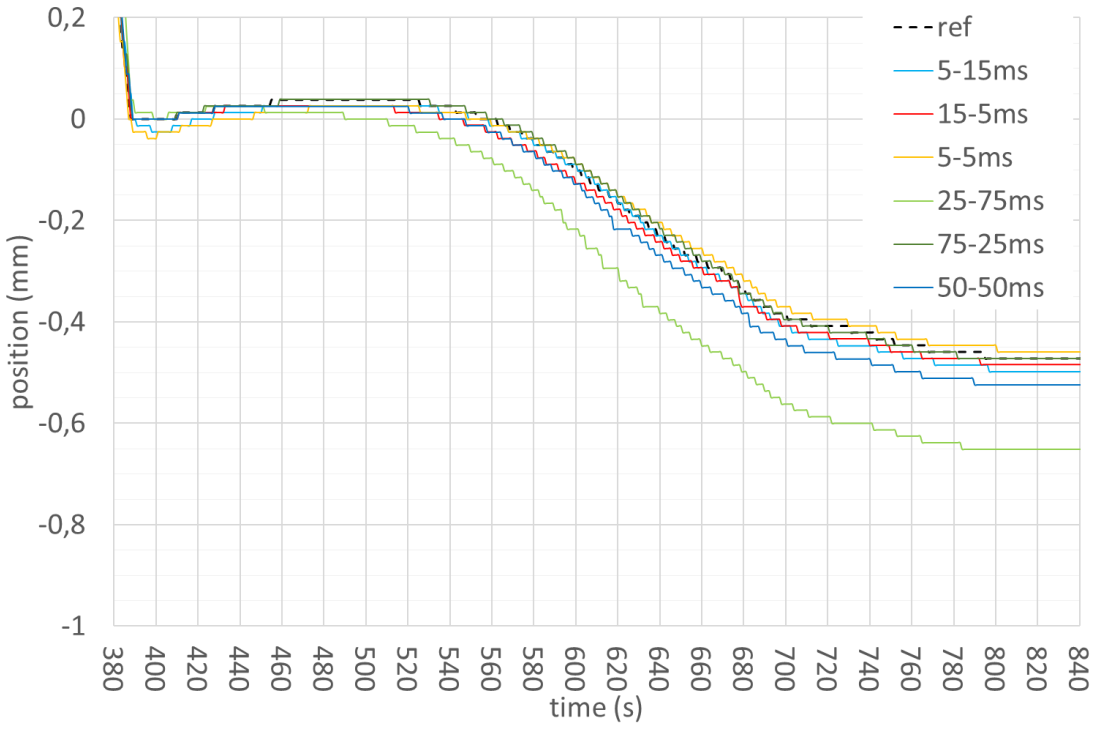

Figure 4-59 uNi compaction – change in punches position for various pulsed pattern conditions

The porosity of uNi samples presented in *Figure 4-60*. Although the porosity of samples was measured only two times, it is possible to observe, that the highest porosity was measured for samples sintered by the pulse current

with duty cycle of 75 % (samples 75-25ms and 15-5ms) and the lowest porosity has the sample sintered by pulse current with duty cycle of 25 % (sample 5-15ms).

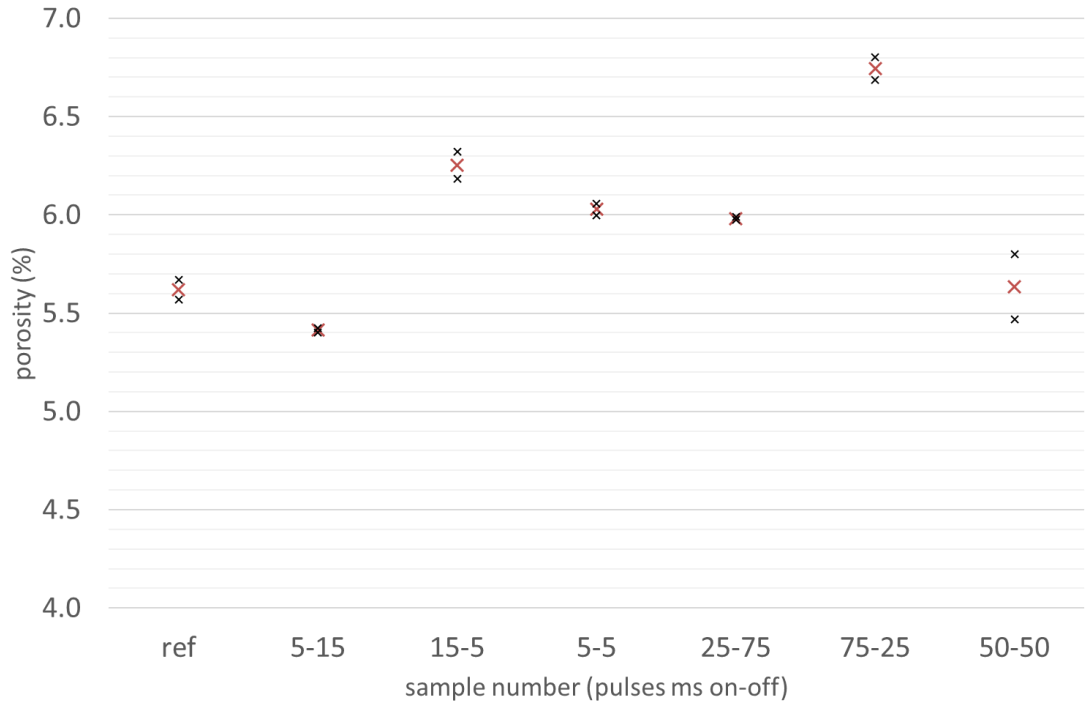

Figure 4-60 Porosity of micro Nickel samples compacted by various pulse patterns condition

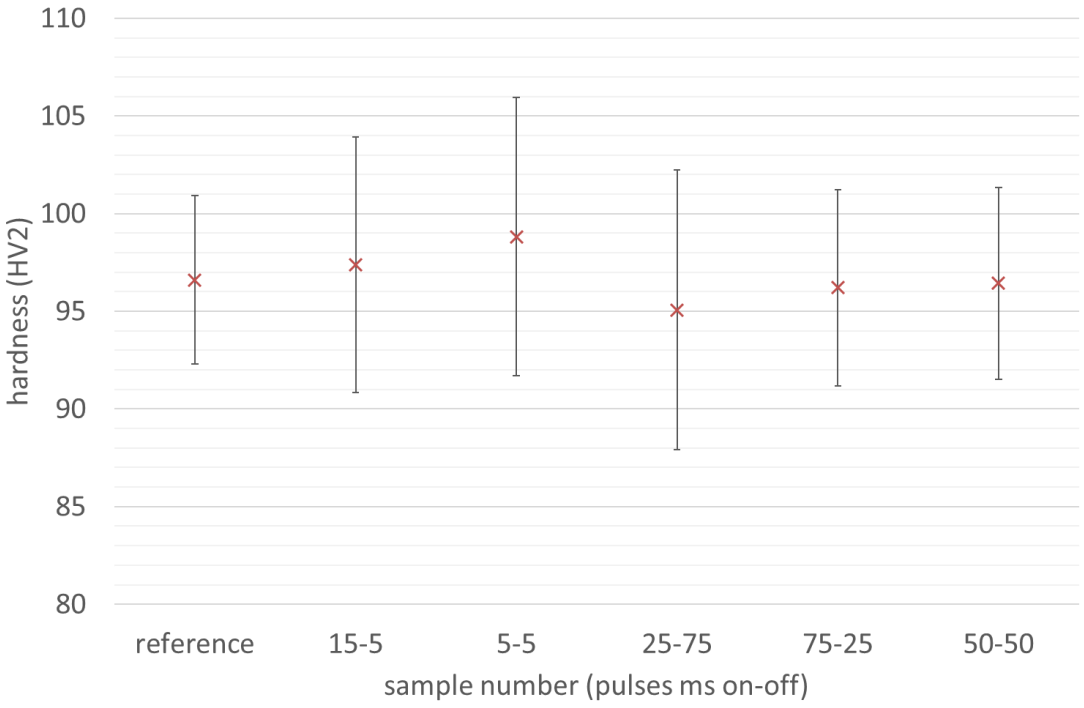

Figure 4-61 Hardness of uNi samples compacted by various current pulse patterns conditions

The Hardness of uNi samples is compared in *Figure 4-61*. It is evident, that no significant differences in hardness are measurable between all samples. The average value is in the range of 95-100 HV2.

The SEM backscatter images of three samples cross-sections are shown in *Figure 4-62* to *Figure 4-64*. Samples were chosen based on hardness and porosity measurements; sample 75-25ms has the highest porosity and sample 5-5ms has the highest average hardness (even though standard deviation indicates that the data points are similar in all samples). It is noticeable that the porosity between sub-grains is present even in the initial powder in *Figure 4-9* and these pores are approximately as big as the grains of OP-S used for polishing and which are stacked into the pores. Except for the porosity, which is lowest for the reference (non-pulsed current), no other significant difference in microstructure are observable.

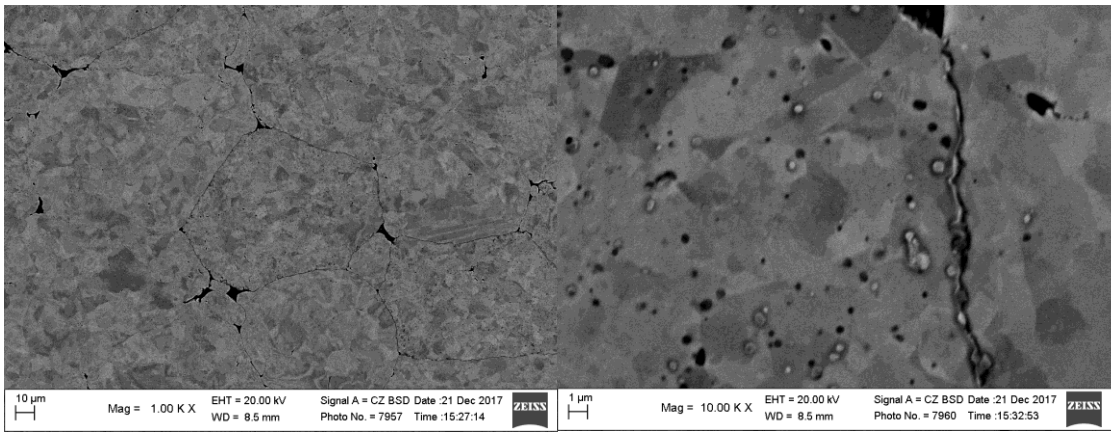

Figure 4-62 Backscatter SEM image of uNi sample sintered at the temperature of 850 °C with non-pulsed DC

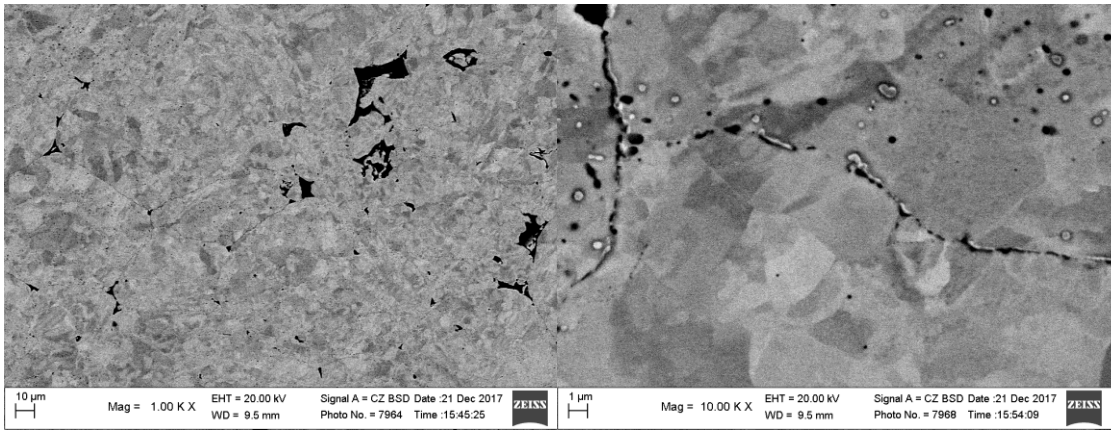

Figure 4-63 Backscatter SEM image of uNi sample sintered at the temperature of 850 °C with DPC of 5-5 ms

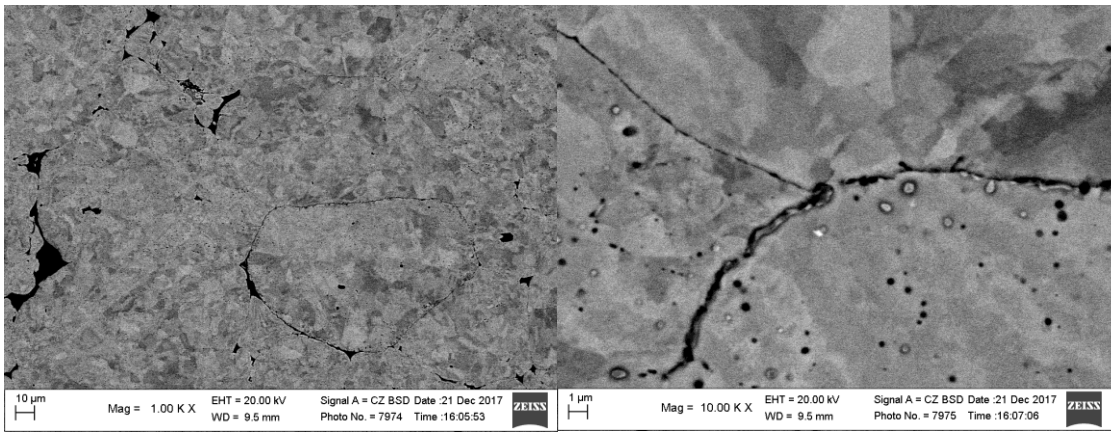

Figure 4-64 Backscatter SEM image of uNi sample sintered at the temperature of 850 °C with DPC of 75-25 ms

4.8.3 Al7075

The temperature courses of sintering cycles of Al7075 powder are in the *Figure 4-65*. Each of these courses has a significant temperature overshoot, especially the courses for the current duty cycle of 25 % (5-15ms and 25-75ms). Another courses are very similar to the reference course. Since all samples were sintered to more than 99 % of their density, no differences in the punches position changes are significant in *Figure 4-66*.

Results of the three-point bending flexural test are presented in *Figure 4-67*. The Flexural stress for the reference sample (compacted by a non-pulsed current) is 410±5 MPa, which is significantly higher than for the other samples (383-395±8) that were compacted by using a pulsed current. Also, even the variance of measured values of the reference samples is lower than in the case of samples compacted by a pulsed current. One interesting trend is observable: the average values of the flexural tests for pulsed current depend on their current duty cycle. It seems that the average value of flexural stress decreases with a lower duty cycle of sintering current. This finding is based on a large quantity of tested samples (testing of 10 samples for each pulse pattern).

The hardness of Al7075 samples was also evaluated, as seen in *Figure 4-67*. The result is similar to the three-point bending flexural test. The highest hardness was measured for the reference sample (100±0.8 HV1). Other samples' hardness is lower (around 98 HV1). Although the difference in hardness is small, the change in hardness is measurable thanks to the small variance of measurement error.

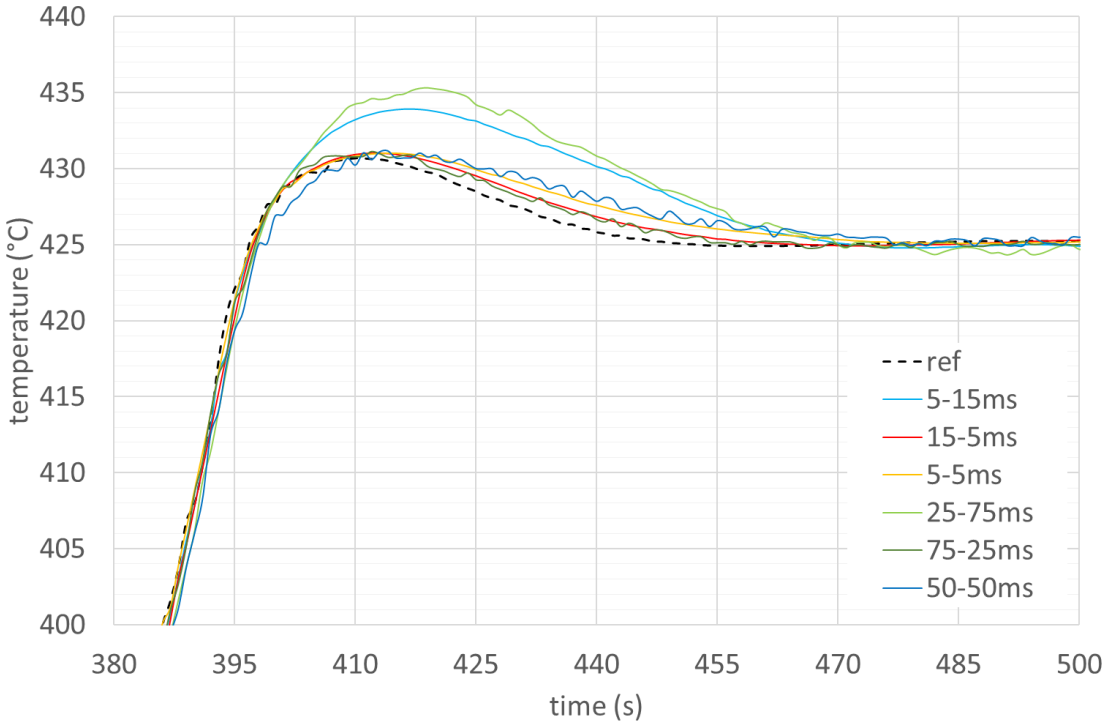

Figure 4-65 Temperature courses (thermocouple K) of Al7075 sintering cycles - various pulsed pattern conditions (reference process course is in the Figure 4-22)

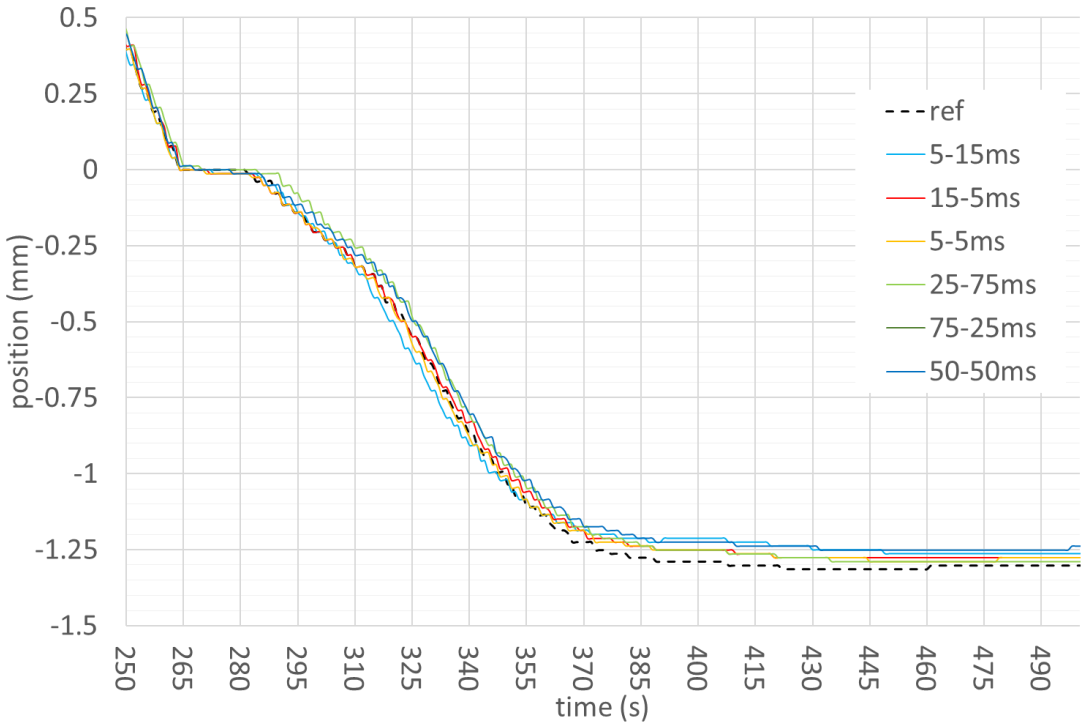

Figure 4-66 Al7075 compaction – change in punches position for various pulsed pattern conditions

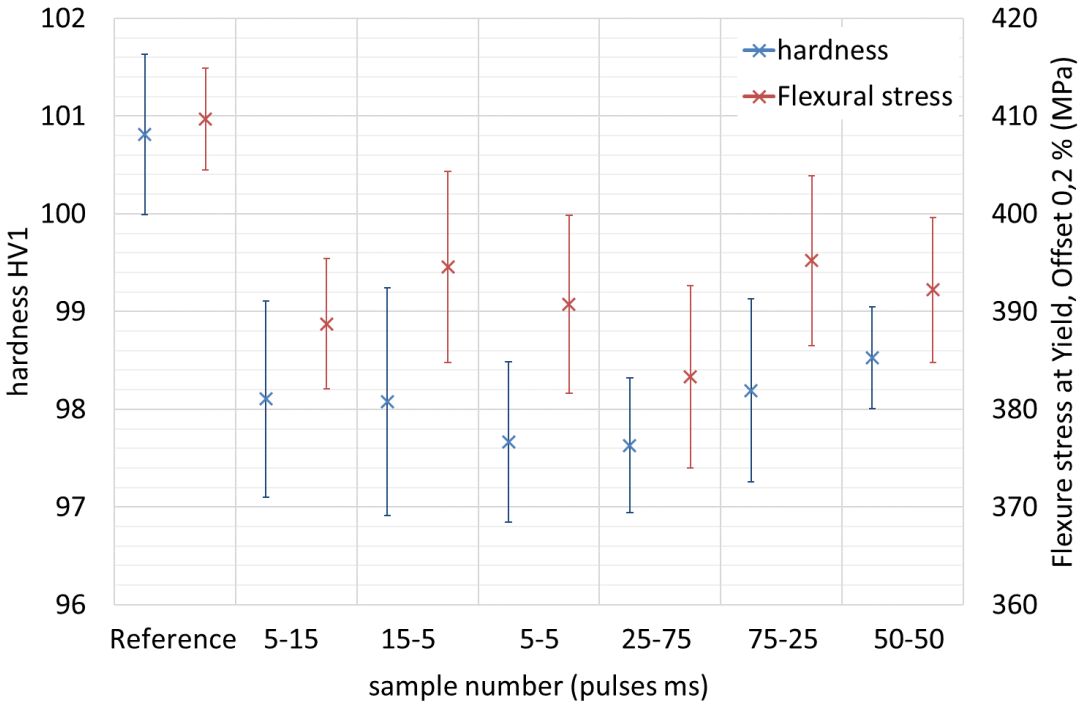

Figure 4-67 Hardness and Flexural stress at yield of Al7075 samples compacted by various current pulse patterns conditions

The SEM backscatter image of Al7075 microstructures are in *Figure 4-68* to *Figure 4-70*. It is noticeable that the sub-grains and grains (dark particles) are surrounded by precipitates (bright particles). The amount of precipitates is higher around the grains of samples 5-5ms and 25-75ms. It was found by image analysis (measured on the SEM images 10k magnification) that the ratio of precipitates is around 10% for the reference sample while it is 12 % for the other samples. This means that the amount of dissolved elements is higher by 2 % in the reference sample, therefore the reference sample has higher Flexural stress and higher hardness.

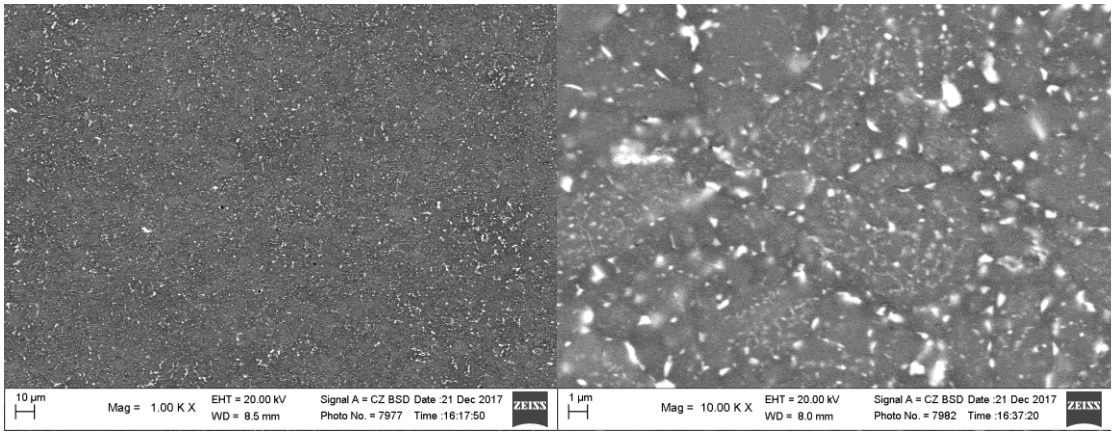

Figure 4-68 Backscatter SEM image of Al7075 sample sintered at the temperature of 425°C with non-pulsed DC

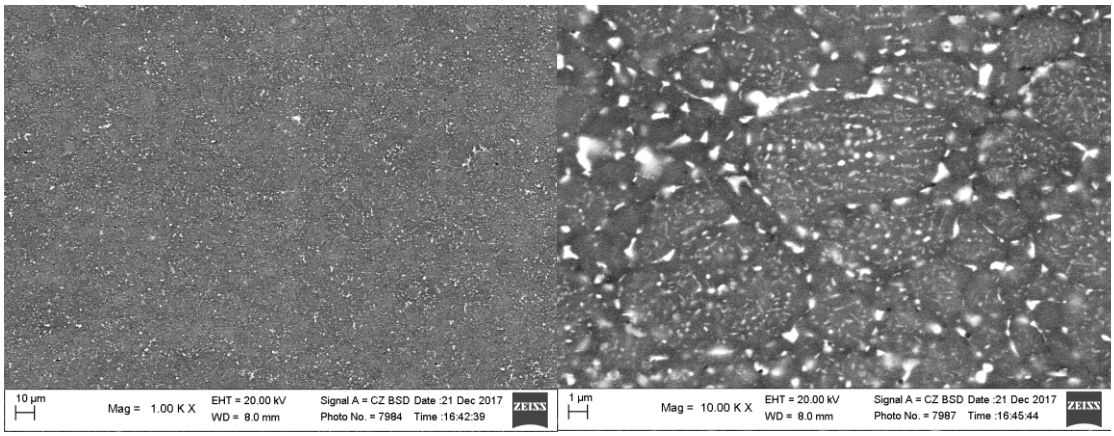

Figure 4-69 Backscatter SEM image of Al7075 sample sintered at the temperature of 425°C with DPC of 5-5 ms

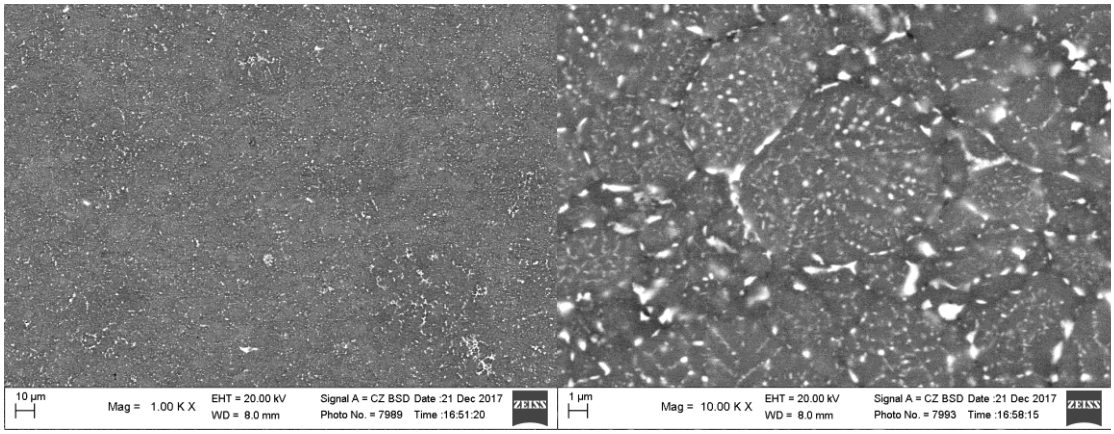

Figure 4-70 Backscatter SEM image of Al7075 sample sintered at the temperature of 425°C with DPC of 25-75 ms

The samples of aluminium alloy 7075 exhibited the following phases: 1. Al matrix of face centered cubic phase with the space group Fm-3m; 2. hexagonal phase of MgZn2 precipitates with the space group P63/mmc; 3. orthorhombic phase of Al2CuMg precipitates with the space group Cmcm.

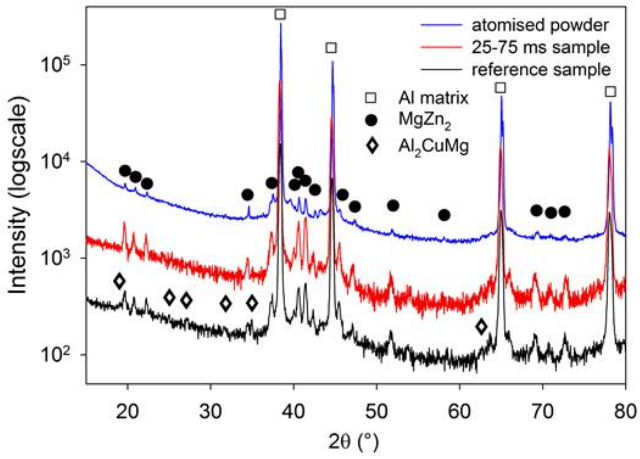

Figure 4-71 comparison of XRD Al7075 powder, samples sintered wit pulsed and non-pulsed current

4.8.4 AlNi

AlNi powder was compacted at the temperature of 1250 °C, and the detailed temperature evolutions are in *Figure 4-72*. It is significant that higher in temperature overshoots appear for pulse patterns of 15-5ms, 5-15ms and 5-5ms. The resulting temperature for courses with amplitude of 100 ms are either similar (25-75ms) or lower (50-50ms and 75-25ms) than the reference temperature. It is probably caused by a poor reproducibility of the sintering process regulated by a pyrometer as shown in *Chapter 4.7.1*.

The SPS process regulator causes nonlinearity in position evolution around 980 seconds where the temperature was not optimally regulated, as seen in *Figure 4-73*. Since it took place at the temperature of 750 °C, it did not have any impact on the result of sintering. All measured changes in punches position (powder compaction) correspond with the measurement of temperatures. The highest decrease in position is observable for sample 15-5ms, which also has the highest peak temperature during sintering.

This finding is in common with measured samples porosities in *Figure 4-74*. Lowest porosities (4.45 %) were measured for samples 15-5ms and 5-5ms, which have also the highest overshoot in sintering temperatures. On the other hand, the porosity of sample 5-15ms, which was sintered at very similar temperature, is a bit higher (4.65 %).

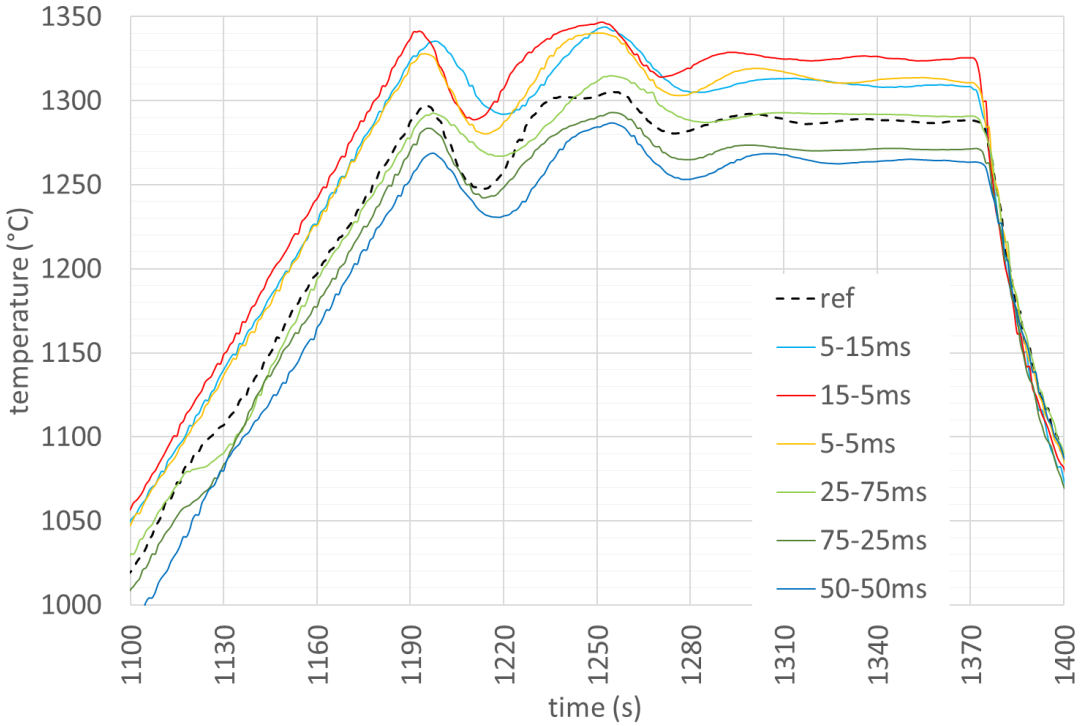

Figure 4-72 Temperature courses (thermocouple C) of AlNi sintering cycles - various pulsed pattern conditions (reference process course is in the Figure 4-20)

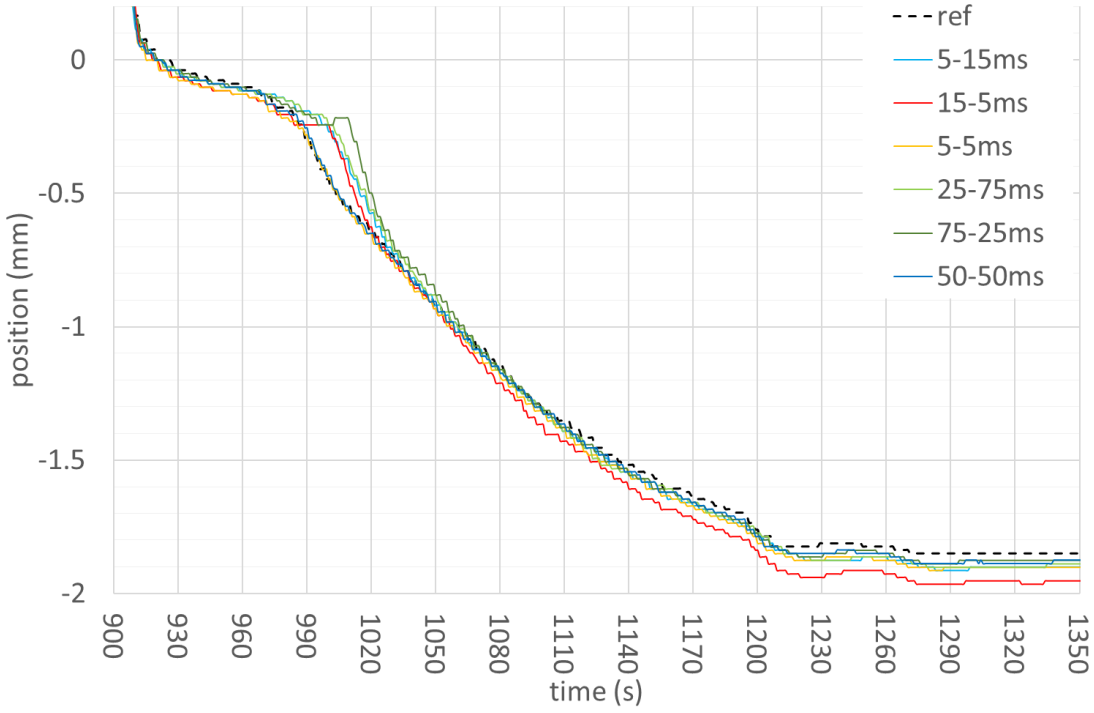

Figure 4-73 AlNi compaction – change in punches position for various pulsed pattern conditions

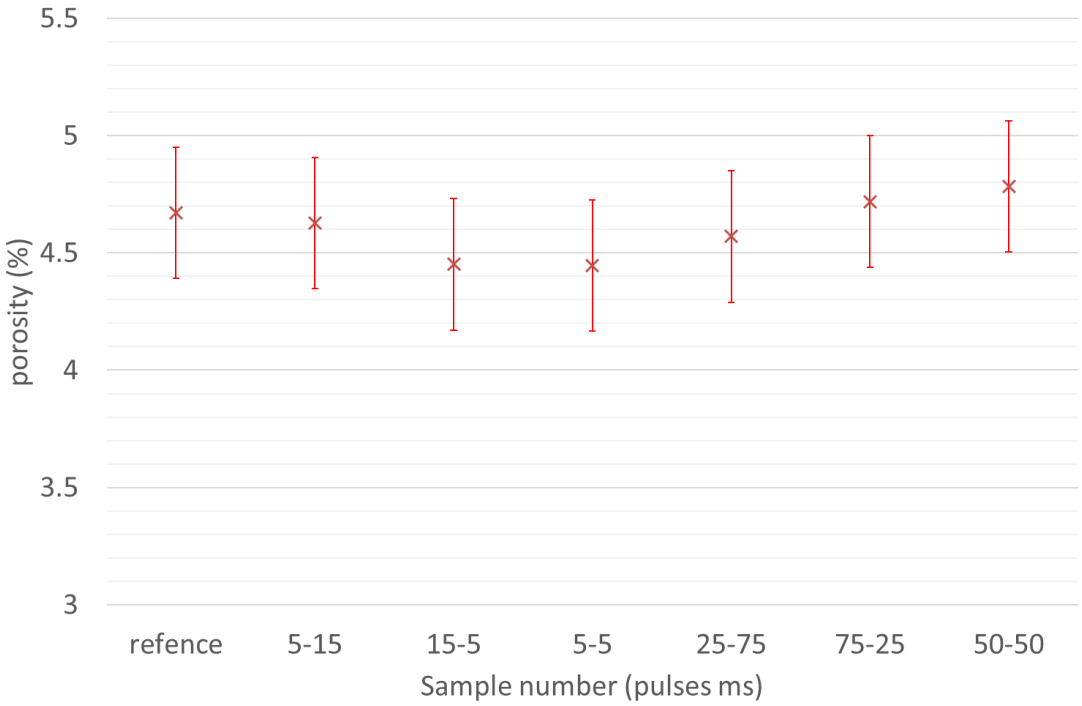

Figure 4-74 Porosity of AlNi samples compacted by various pulse patterns condition

The measured hardness of AlNi samples is shown in *Figure 4-75* and its value is in the range 322±8 HV2 to 330±10 HV2 and there is no observable significant difference in hardness.

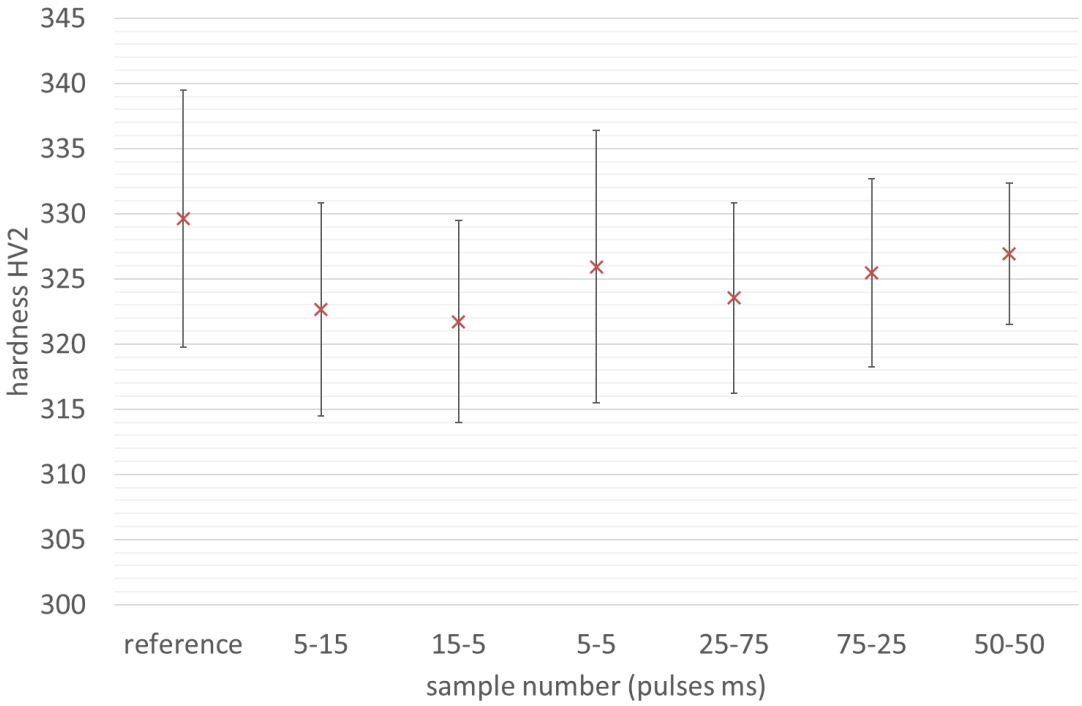

Figure 4-75 Hardness of AlNi samples compacted by various current pulse patterns conditions

The backscatter SEM images in *Figure 4-76* to *Figure 4-78* show AlNi microstructures in cross section. There are no significant difference between samples. The porosity inside the grains is caused by the shape of particles as seen in *Figure 4-18* and the light particles are probably grains of OP-S used for polishing and stacked into the pores.

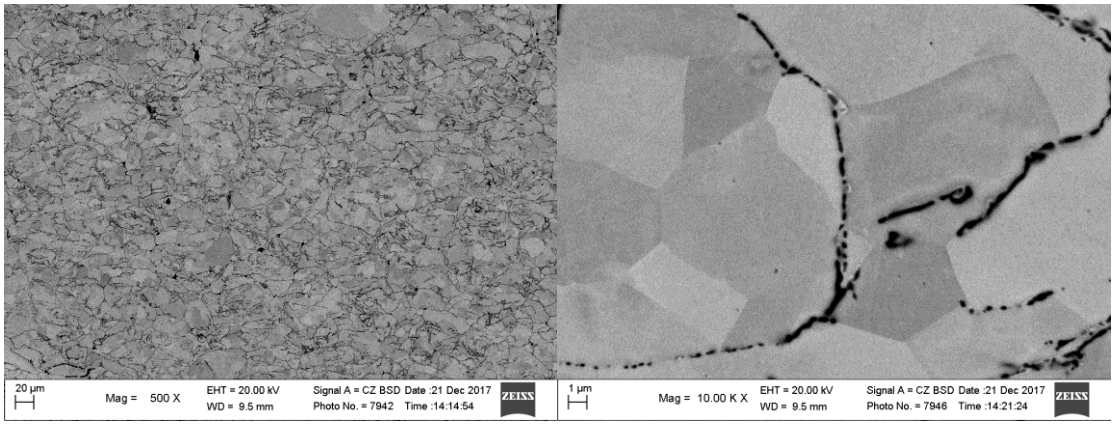

Figure 4-76 Backscatter SEM image of AlNi sample sintered at the temperature of 1250°C with non-pulsed DC

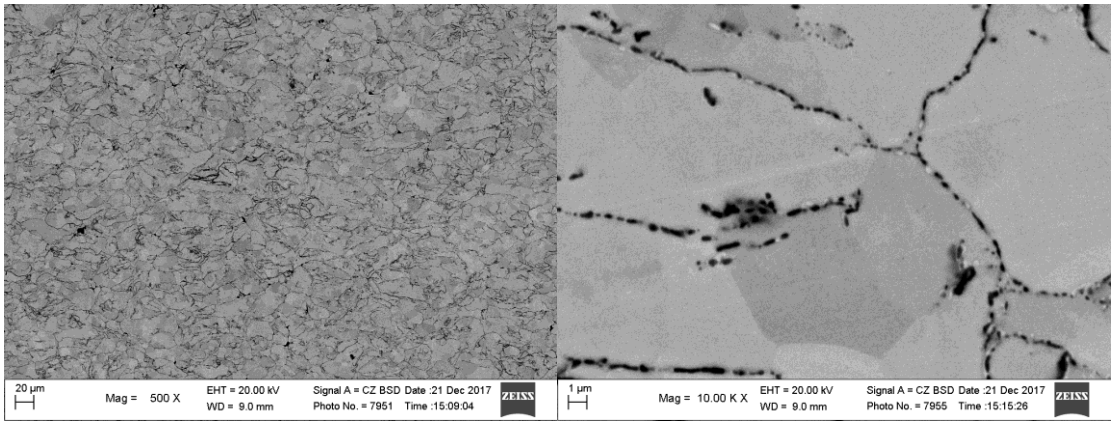

Figure 4-77 Backscatter SEM image of AlNi sample sintered at the temperature of 1250°C with DPC of 15-5 ms

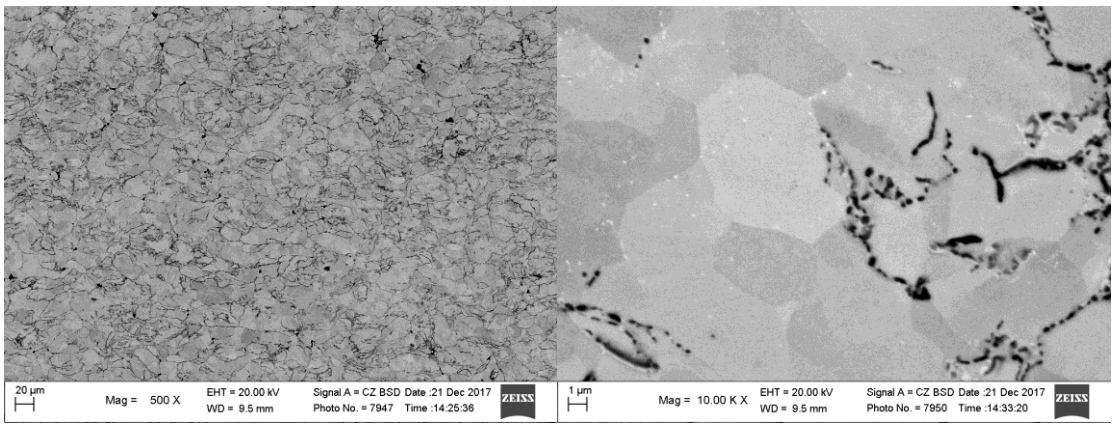

Figure 4-78 Backscatter SEM image of AlNi sample sintered at the temperature of 1250°C with DPC of 75-25 ms

The samples of AlNi alloy exhibited intermetallic phase of the ordered AlNi base centered cubic phase with the space group Pm-3m (*Figure 4-79*). The samples contain aluminium oxide in the form of alpha-Al*2O3* phase (corundum) in the small amount on the limit of sensitivity of the XRD method (~1 wt. %). Since only one phase of AlNi is present, the phase stable temperature of 1638 °C was not exceeded. It shows no presence of plasma or sparking discharges during the sintering process.

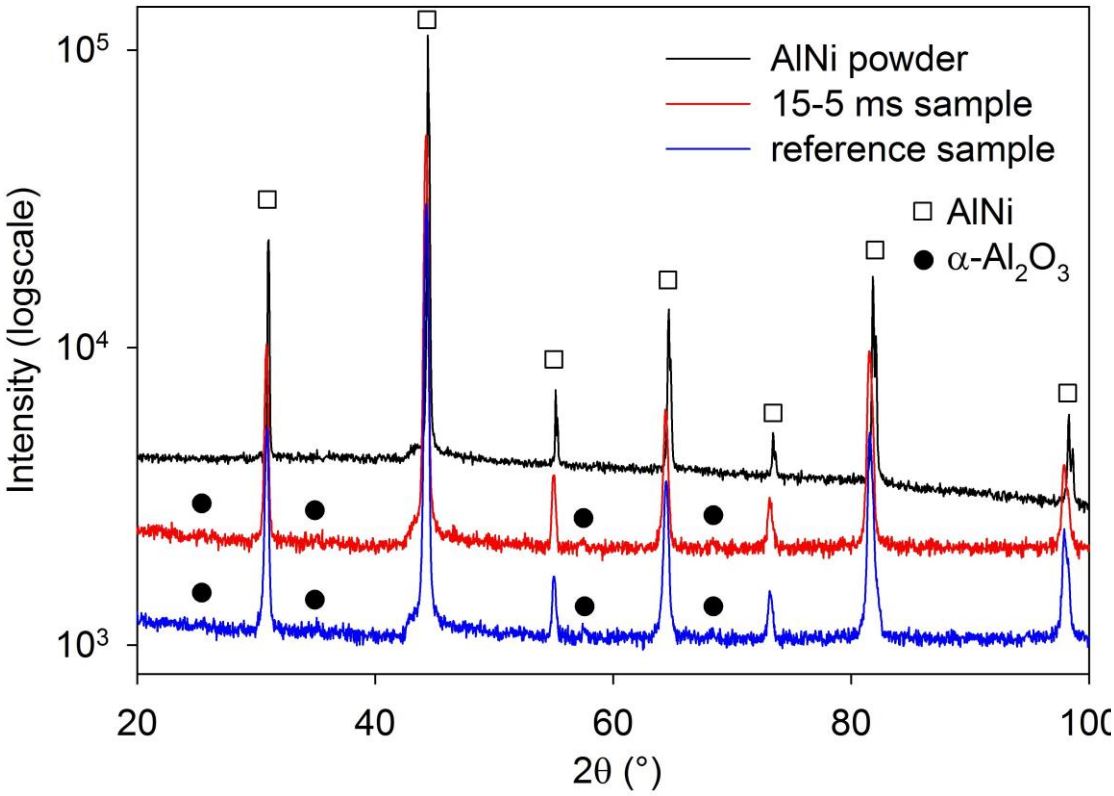

Figure 4-79 comparison of XRD AlNi powder, samples sintered with pulsed and non-pulsed current

4.8.5 nMo

The nMo powder was sintered at temperature of 1200 °C. The temperatures courses of nMo sintered at the temperature at 1200 °C are shown in *Figure 4-80*. The difference between minimum and maximum temperatures is about 100 °C which corresponds to the measurement of AlNi in *Figure 4-72*. It is obvious that the temperature course 75-25ms oscillates around the reference temperature and the temperature controller does not optimally regulate this sintering process.

This non-optimal regulation has an impact on the punches position as seen in *Figure 4-81*. The shape of the 75-25ms course is not straight, because the non-stabilised heating results in change in position due to the thermal expansion of graphite. The punches positions for other samples are comparable without any observable non-linear parts.

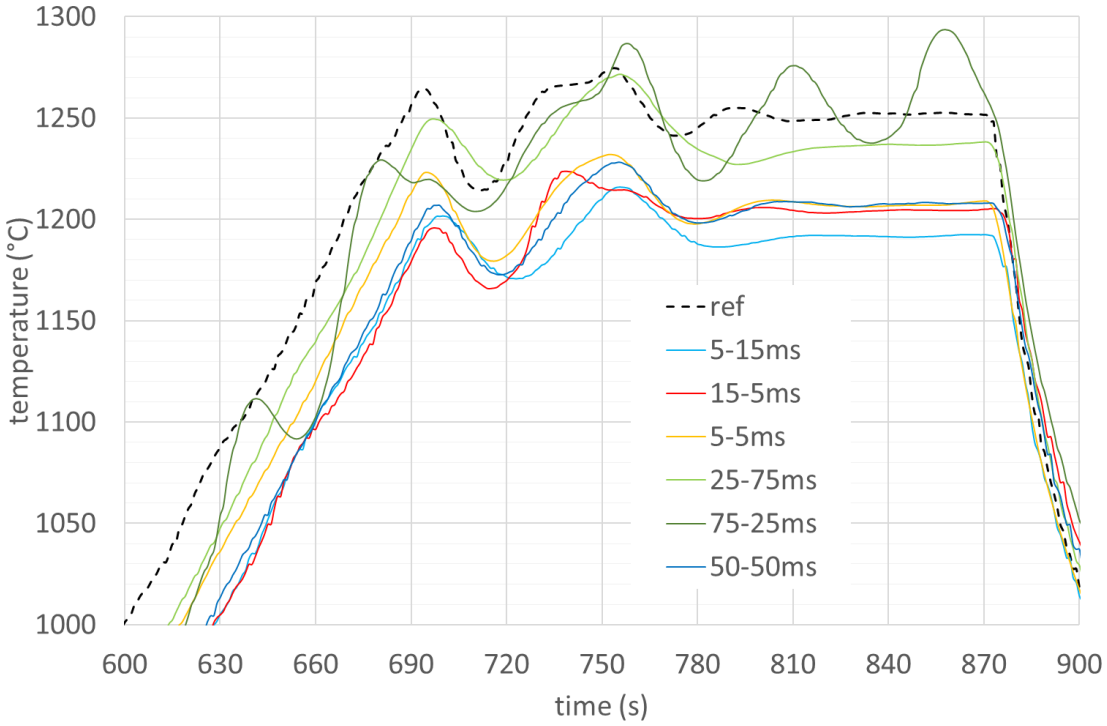

Figure 4-80 Temperature courses (thermocouple C) of nMo sintering cycles (1200 °C) - various pulsed pattern conditions (reference process course is in the Figure 4-17)

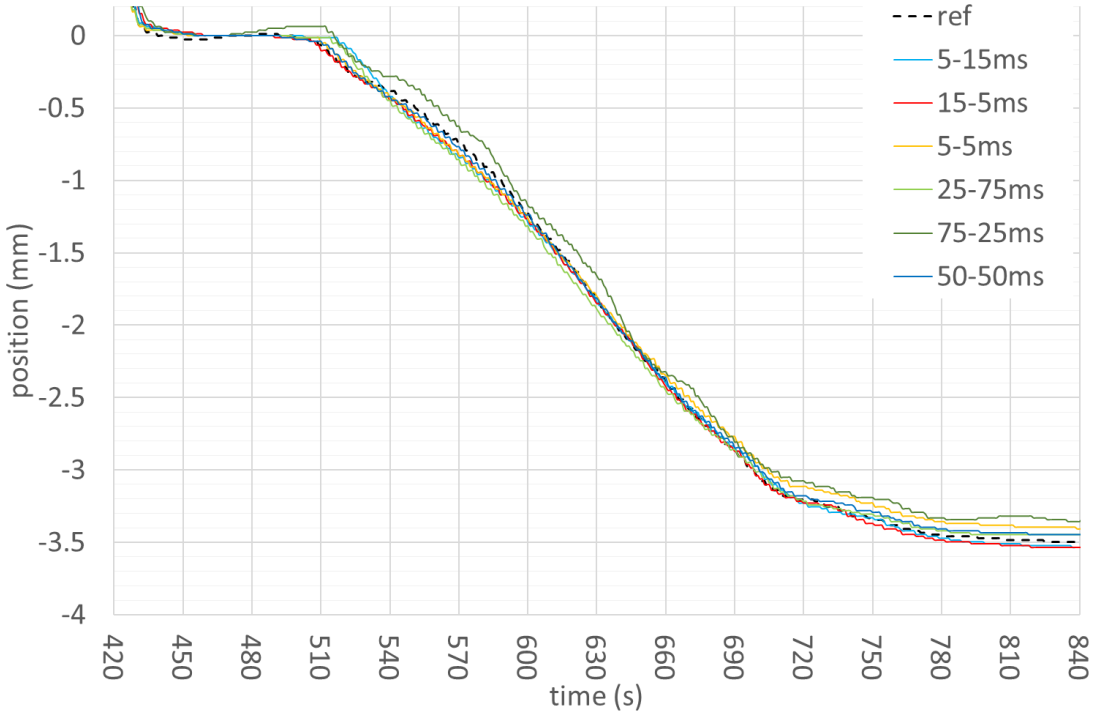

Figure 4-81 nMo (1200 °C) compaction – change in punches position for various pulsed pattern conditions

The higher sintering temperature lower porosity of samples 25-75ms and 75-25ms. On the other hand, the porosity of the reference sample is higher

when compared to the samples 25-75ms and 75-25ms despite the fact that their maximum peak temperatures were similar.

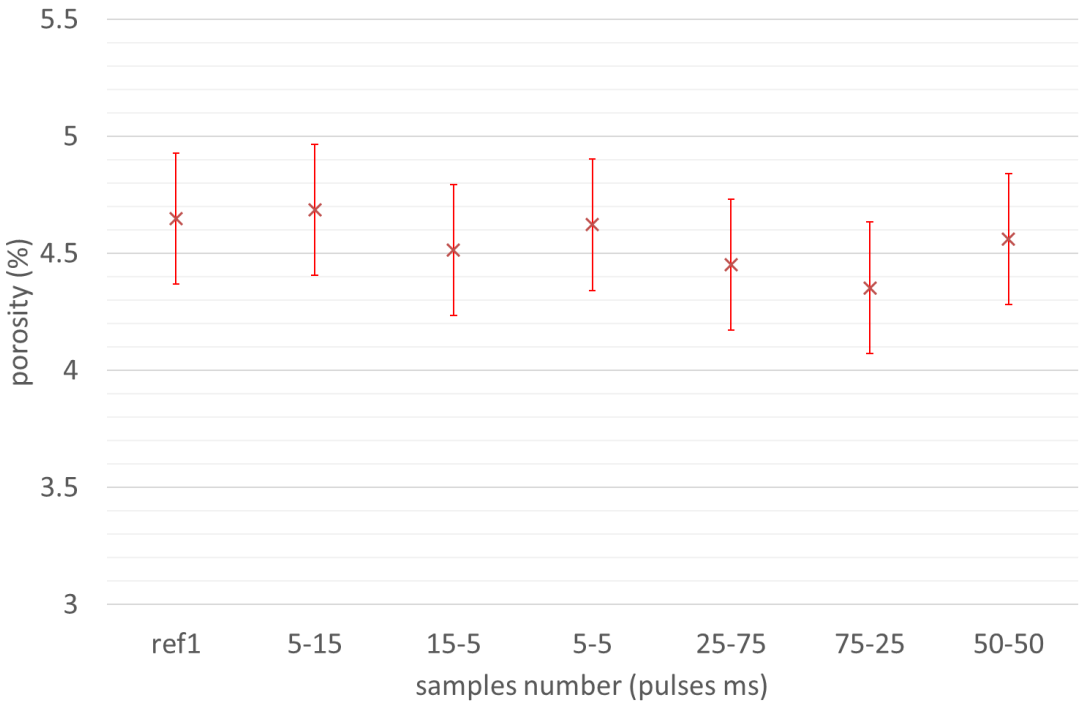

Figure 4-82 Porosity of nMo (1200°C) samples compacted by various pulse patterns condition

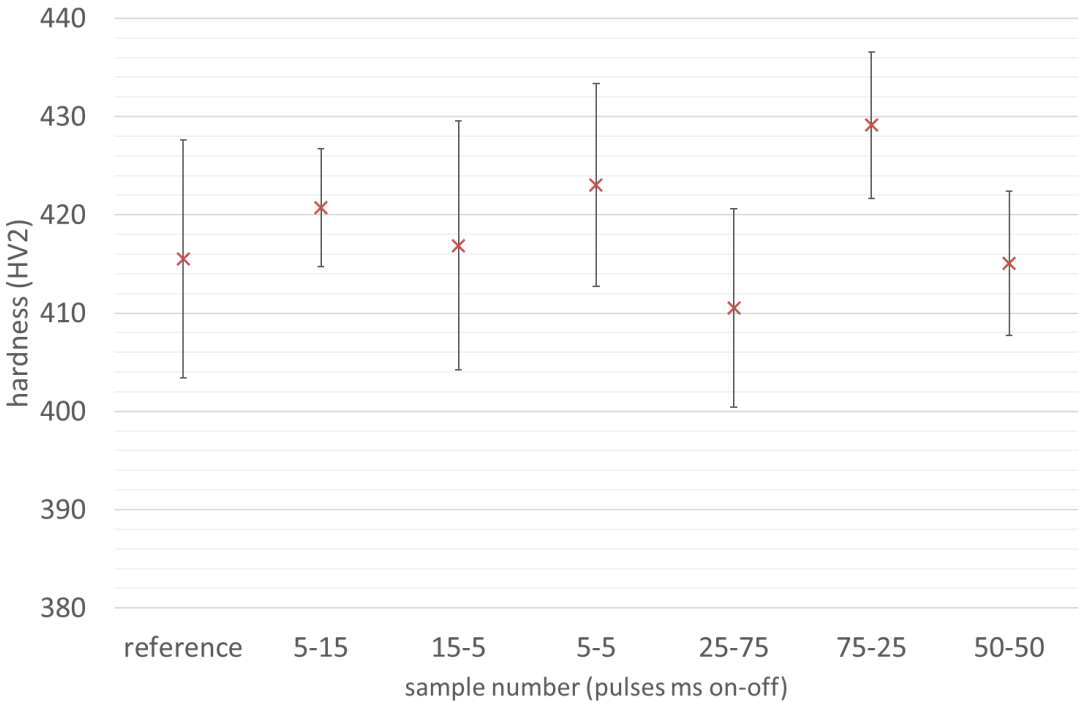

Figure 4-83 Hardness of nMo samples compacted by various current pulse patterns conditions

The hardness of the samples is evaluated in *Figure 4-83*. All hardness values are from the range of 403±12 HV2 (reference sample) to 429±7 HV2 (sample 75-25ms).

The SEM backscatter images of the microstructure of nMo samples sintered at the temperature 1200 °C are shown in *Figure 4-84* to *Figure 4-85*.

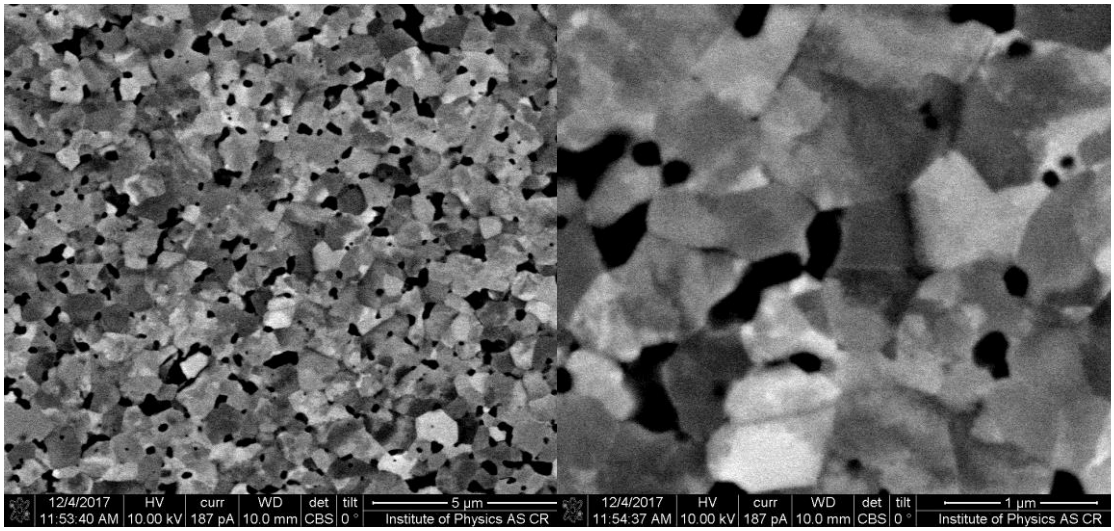

Figure 4-84 Backscatter SEM image of nMo sample sintered at the temperature of 1200°C with non-pulsed DC

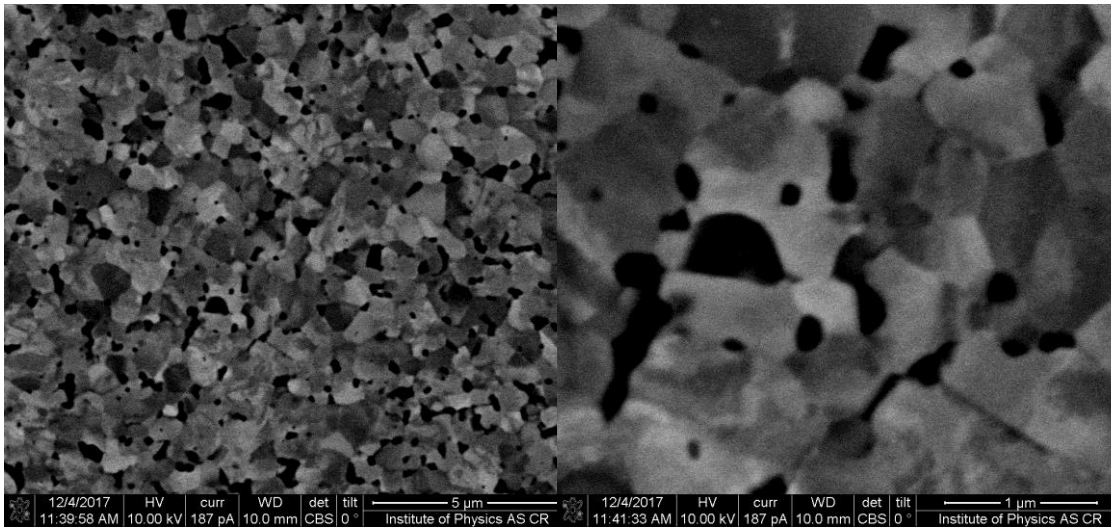

Figure 4-85 Backscatter SEM image of nMo sample sintered at the temperature of 1200°C with DPC of 25-75 ms

4.8.6 Al_2O_3

The flexural stress of corundum samples sintered at the temperature of 1350°C is in the range from 523±16 MPa (reference sample) to 447±56 MPa (25-75ms sample) as shown in *Figure 4-86*. The lower average values of flexural stress and their larger variance are significant for the samples compacted using pulsing current compared to the reference sample.

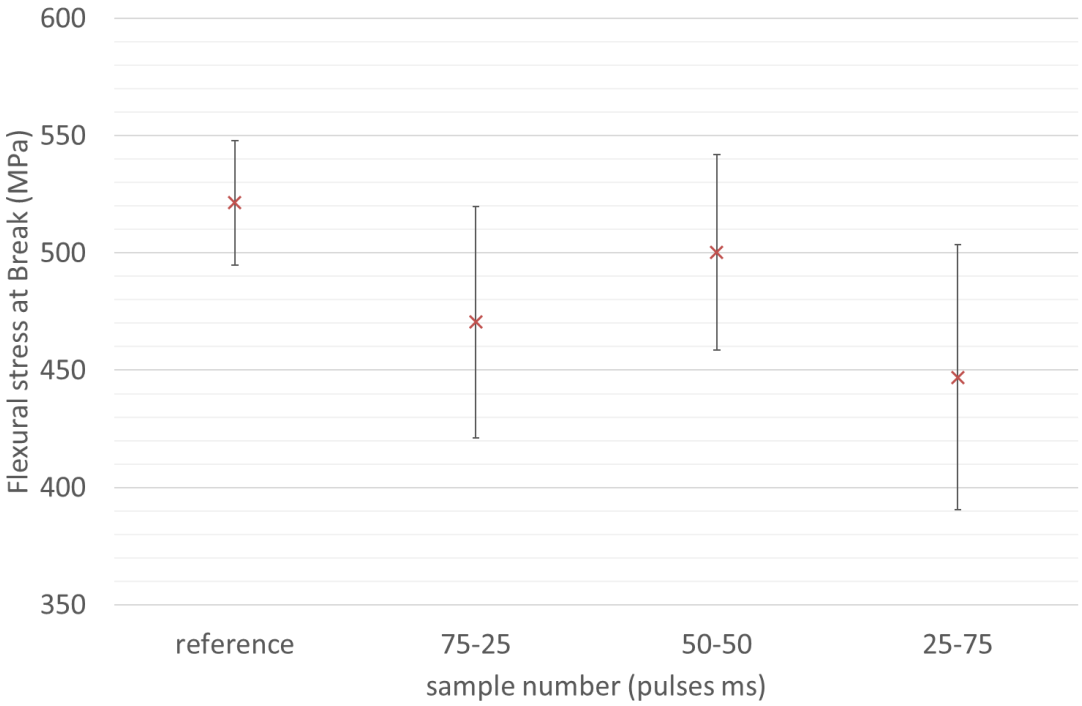

Figure 4-86 Flexural stress at break of Al_2O_3 samples compacted by various current pulse patterns conditions

The fracture surface of corundum samples is seen in *Figure 4-87* and *Figure 4-88* where the samples were coated (sputtered) with a thin conductive layer (gold) to prevent the sample charging during SEM. As seen from the SEM images, there is a number of closed pores, entrapped in Al_2O_3 grains. All pores inside the particles are typical for agglomerated powders, because powders with hard agglomerates usually have poor compaction behaviour and thus the agglomerates are difficult to crash [77] and might contain cavities. Both types of fractures are observable, though transgranular fractures are more common in the case of the reference sample. There are fairly smooth-looking areas with less sharp edges, indicating a presence of strong grain-boundaries which is in common with a measured higher flexural strength. The grains can be easily identified and there are minimum smooth- looking areas in the fracture of the sample 50-50ms, therefore the main type of fracture is intergranular.

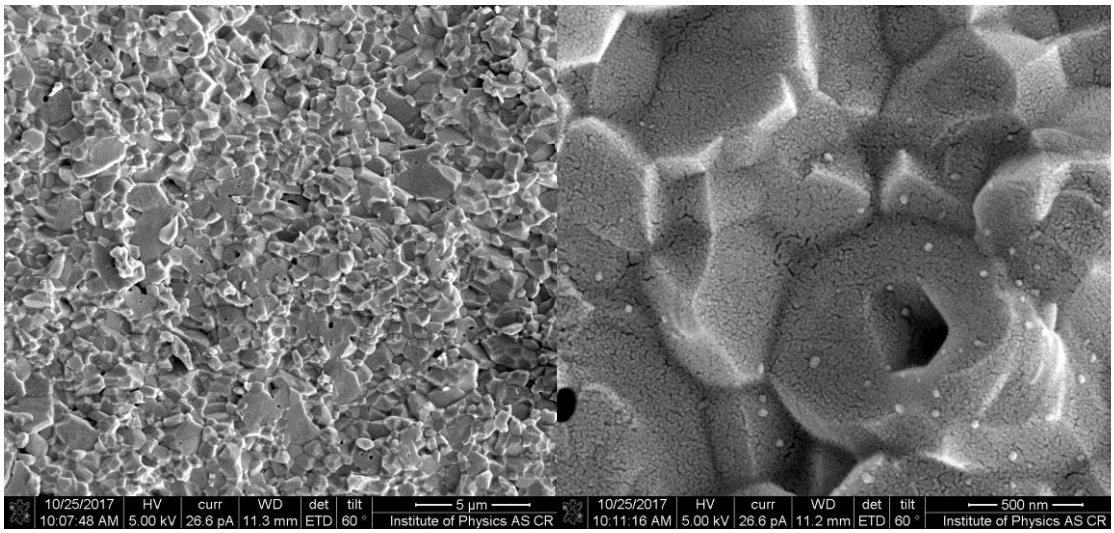

Figure 4-87 SEM image of Al_2O_3 sample sintered at the temperature of 1350 °C with non-pulsed DC

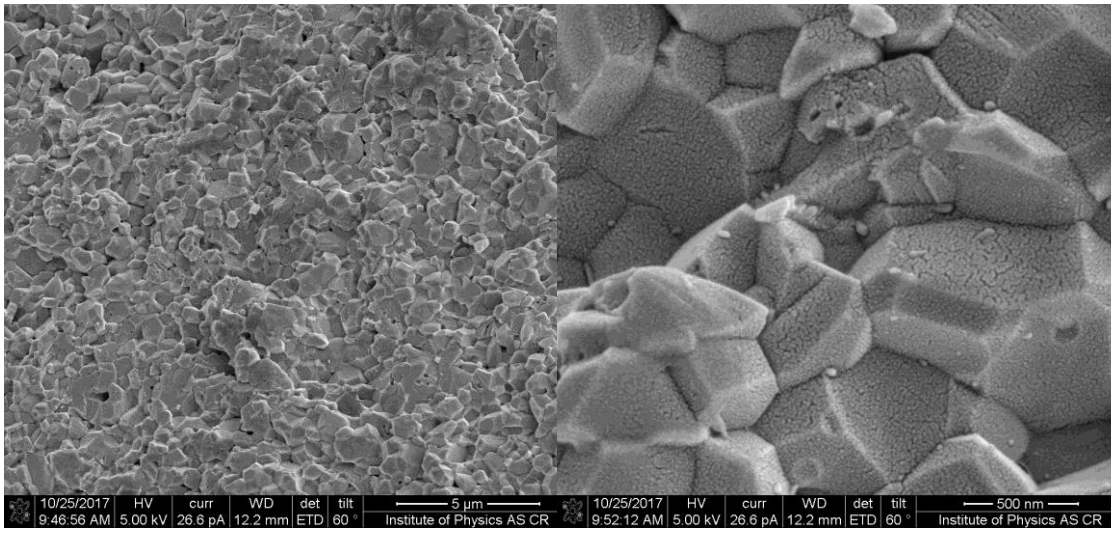

Figure 4-88 SEM image of Al_2O_3 sample sintered at the temperature of 1350 °C with DPC of 50-50 ms

4.9 Effect of sequence of pressure and heating

4.9.1 Al7075

The flexural stress of three different SPS processes is evaluated in *Figure 4-89*. Three sintered conditions are compared in the graph. The samples "*pressure before temperature*" were sintered according to *Figure 4-22* at the temperature 425°C. The powder was pressed by uniaxial pressure and after the maximal pressure was achieved, the sintering temperature was increased. The samples "*pressure after temperature*" were prepared in reversed order of applied uniaxial pressure and heating (the samples were first heated to the maximum temperature and then pressed). For the samples "*pressure and temperature*", the uniaxial pressure was slowly increased together with the increasing temperature.

The highest flexural stress (412±9 MPa) was achieved in the case of samples where the uniaxial pressure was applied before the maximal temperature and the lowest flexural stress (392±6 MPa) for the sample where the uniaxial pressure was applied after reaching the maximum temperature. The flexural stress of the sample that is simultaneously pressed and heated is (400±8 MPa) seen in *Figure 4-89*.

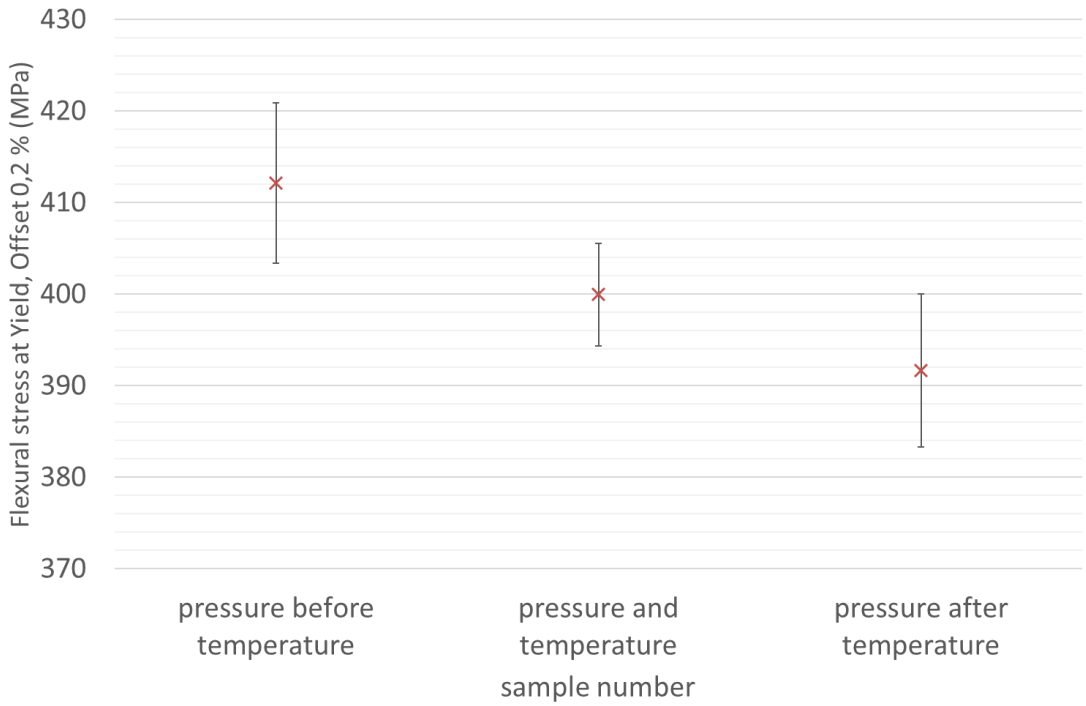

Figure 4-89 Effect of sequence of pressure and heating, Al7075 samples sintered at the temperature of 425 °C by non-pulsed DC

4.9.2 Al_2O_3

The influence of the sequence of pressure and temperature was investigated for non-conductive samples (corundum) as well. The flexural stress of corundum samples prepared by various sintering conditions is compared in *Figure 4-90*. The flexural stress of samples is lower when the uniaxial pressure is applied after the maximum temperature is reached.

The fracture surface of the corundum "pressure after temperature" sample is in *Figure 4-91*. It is obvious that the microstructure contains more areas, which are more porous than in the case of samples in *Figure 4-87*.

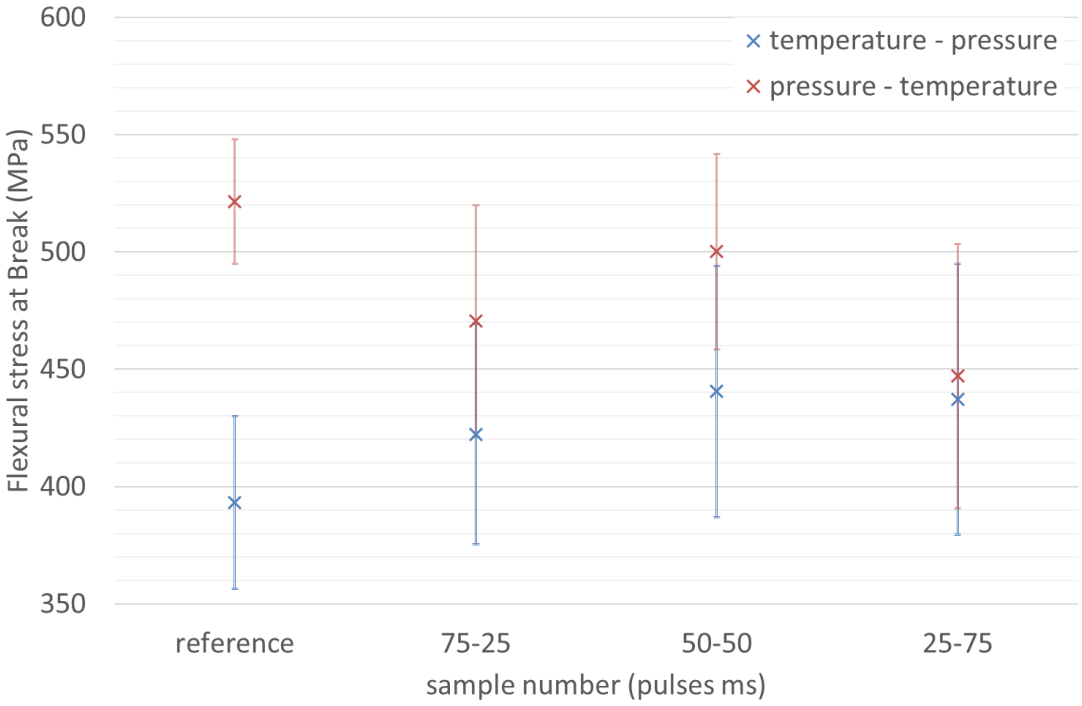

Figure 4-90 Effect of sequence of pressure and heating, Al_2O_3 samples sintered at the temperature of 1350 °C by non-pulsed DC and by pulsed current

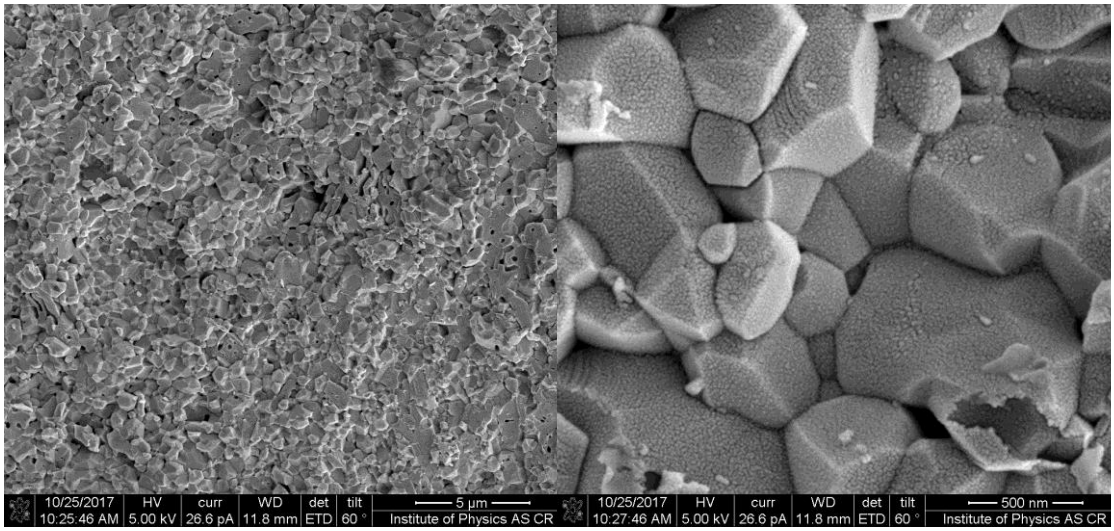

Figure 4-91 SEM image of Al_2O_3 sample sintered at the temperature of 1350 °C with non-pulsed current, the powder was pressured after reaching the maximal temperature

5 Discussion

5.1 Sintering temperatures

It was proved that the temperatures inside of the sintered compact and the temperature measured by pyrometer are different, as seen in *Figure 4-1*. In most cases the temperature measured by a pyrometer is lower than the temperature of compacted powder as shown in *Chap. 4.2*. Moreover, the temperature overshoot depends on the resistivity of the powder and on the SPS heating rate. Therefore, when the SPS process is regulated by a pyrometer, the true process temperature is higher than the set point temperature as was proved on the ground of the temperature measurement in *Chapter 4.2*.

The biggest issue with comparing the obtained results with other publications is different particle-size distribution of used powders. Mo powders with particle size of 47 μm [78], was sintered at the temperature of 1650 °C under various conditions (dwell time of 1-2 min, uniaxial pressure 40 and 48 MPa) to the density around 98.5 %. The hardness of the samples sintered using dwell time of 1 min and uniaxial pressure of 48 MPa was 220.42 HV10 (pulsed current) and 231.40 HV10 (non-pulsed current). Hardness of samples sintered with longer dwell time (1.5 min) are 217.20 HV10 (pulsed current) and 210.00 HV10 (non-pulsed current). However, the values were calculated as an average of only five indents on one sample and the pulse length is not mentioned. The hardness of the samples is different to samples sintered in this work. Hardness of molybdenum samples presented in this work is 415±12 HV2 (reference sample) and the sample with a biggest difference is 429±7 HV2 (both values are calculated as an average of 27 indents). It is obvious that the difference between samples compacted by non-pulsed and pulsed current is similar as published in [78]. However, the difference in hardness is a consequence of a poor reproducibility (*Chapter 4.7.2*) rather than the influence of pulsed current.

5.2 Repeatability of the sintering process

The experiment of the repeatability of the sintering process was carried out with AlNi and nMo powders. In all cases, a relatively good repeatability of sintering processes using non-pulsed DC current as seen in *Figure 4-39* and *Figure 4-44*. However, the measurement of sintering reparability with using pulsed DC current showed significant differences through repeated sintering cycles shown in *Figure 4-41* and *Figure 4-46*. The use of DC pulsed instead of non-pulsed current leads to a deterioration of the process regulation, thus the reproducibility of the SPS process becomes poor. This results in a larger difference between the true process temperatures and the set point temperature.

The reliability of the measured material properties of the sintered samples is described in *Chapter 4.6.* Vickers hardness mapping was performed on the cross section of the sintered samples. It was shown that the hardness is not homogeneously distributed through the cross-sections of samples. Therefore, the values obtained from mapping and from the horizontal axis of the

samples were compared. Obtained data of both types of hardness measurement (from mapping and from the horizontal axis) are in agreement, even when small differences between hardness values are observable in the case of nMo.

The repeatability of the sintering process was verified by a hardness measurement of the samples described in *Chapter 4.7.* The hardness of samples sintered under the same conditions was compared with regard to the results of reliability of material properties measurements shown in Table 4-5 and Table 4-6. It is obvious that the reproducibility of a SPS process is a big issue of sintering. Although temperature courses are similar and there are no significant difference (for sintering by non-pulsed current), the measured hardness of three AlNi and Mo samples is in the range of 404±21 HV2 to 415±12 HV2 (Mo) respective 331±7 HV2 to 346±13 HV2. A relatively big variance of measured values is given by inhomogeneity of the sintered samples. However, the difference in hardness of samples compacted by pulsed current is even bigger. Hardness of Mo samples is in the range of 404±22 HV2 to 423±10 HV2 and hardness of AlNi samples is from 328±7 HV2 to 341±14 HV2. If any influence of pulsed current might be proved, the change in measured hardness must be higher than this difference.

5.3 **Influence of pulsed DC current**

The results of the influence of pulsed DC current measurements can be divided in to two categories: a SPS process controlled by a thermocouple and a SPS process controlled by a pyrometer.

5.3.1 SPS processes controlled by thermocouple

Higher temperature exceeding over the set-point temperatures was observed for the pulse patterns with low duty cycles of 25 % (5-15ms and 25-75ms) while the courses of duty cycle of 75 % are very similar to the reference courses. The measurement of samples porosity is with agreement with the measured temperature exceeding. Samples sintered with the 25 % duty cycles of current have higher density compared to samples sintered with 75 % duty cycles of current. No influence of current pulses on uNi and nNi hardness was observed. The biggest influence of pulsed current on mechanical properties was observed for Al7075 powder. The temperature exceeding caused change of the phase compounds resulted in decrease in samples' flexural strength and also in hardness. As seen from *Figure 4-67* the best mechanical properties were achieved by using of non-pulsed DC current.

5.3.2 SPS processes controlled by pyrometer

DC pulsed current parameters did not have an influence on AlNi materials parameters. The measured hardness of all samples was in the range from 330±10 HV2 to 322±8 HV2, which was also in the range of statistical error and of the SPS process repeatability. No change in the chemical phase compounds of AlNi samples was observed. This is evidence that the sintering temperature was

not higher than 1638 °C and thus no discharge or plasma take place between sintered particles.

No significant difference in hardness for nMo samples sintered at 1200 °C by various pulse patterns was observed in *Figure 4-83*.The lowest density (*Figure 4-82*) of the sample 75-25ms responds to the higher temperature overshoot of the setpoint temperature.

The effect of pulse current in the publication [58] shows the difference in hardness and porosity of samples compacted by non-pulsed and pulsed current. But all the measured differences are in the range of the samples repeatability and in the reliability of measurements as follows from the results in this work.

5.3.3 Sintering of non-conductive powder

Al_2O_3 powder was sintered at the temperature of 1350 °C. The flexural strength of samples compacted by non-pulsed DC current is higher with lower variance of values compared to samples compacted by using pulsed DC current. A type C thermocouple was not available for this measurement thus any temperature overshooting or exceeding over the set point temperature were not measured.

5.4 **Effect of sequence of pressure and heating and electro plastic effect**

The sequence of heating and applying of a uniaxial pressure was investigated on Al7075 powder (*Figure 4-89*) and on Al_2O_3 powder (*Figure 4-90*). The samples which were first pressed and then heated, have higher flexural stress (at yield and at break) in all cases. However, when a powder is heated under the maximum uniaxial pressure of 100 MPa, the sintered powder is not in a point-touch as is very often published by nearly identical pictures *Figure 1-6* (for example by Nouari Saheb [36]).

The powder loaded typically by a pressure in the range of 50 - 100 MPa is more dense and the touch surface between particles is not a single point, but is deformed by the pressure. When a SPS sample with a diameter of 20 mm (surface of the specimen is 314 mm^2) is sintered in the SPS which was used in this work, the maximum sintered current is 4 kA. Assuming that the current flows only through the sintered sample, the maximal current density is around 12.7 $A.mm^{-2}$ (if the sample is fully sintered). Thanks to that the current density flowing through the sample is definitely lower than 1000 $A.mm^{-2}$ [79] or 3000 $A.mm^{-2}$ [40] which is a current density when the electro plastic effect was proved. Therefore, I considered the occurrence of electro plastic effect during sintering by the SPS technique as absolutely excluded.

5.5 **Effect of discharge or a plasma effect**

The presence of plasma or discharge has not been observed from the change of phase compounds Al7075 and AlNi. Yet, plasma is explained as "*Plasma can only be artificially generated by heating or subjecting a neutral gas to a strong electromagnetic field to the point an ionised gaseous substance becomes*

increasingly electrically conductive, and long-range electromagnetic fields dominate the behavior of the matter"[80]. The sintering process takes place under the melting point of the sintered powder and in low pressure (< 10 Pa), there for plasma formation was not possible. However, the electric field in SPS machines is very low - the voltage of power supplies is relatively low (10 V). Since punches, die, and spacers are from the same material (graphite) and when an approximate current density is assumed in all mentioned parts, the voltage is uniformly distributed between upper and bottom electrode – between them are pressed two punches (2 x 30 mm), two spacers (2 x 20 mm) and pressed powder (~ 5 mm). This means that the maximal electric field between electrodes can be 0,095 V/mm (95 V/m), but the dielectric strength of air is 3 MV/m [81] and 1.32 x 10^{18} V/m (Schwinger limit) in the case of the ideal vacuum. As seen the electric field in the SPS machine is too low and thus no presence of discharges between particles is possible.

6 Conclusion

6.1 Temperature measurement of a SPS process

The SPS process is monitored and regulated by the temperature measured by a thermocouple in the bottom punch or by an optical pyrometer focused onto a hole located in the side of the die. However, temperature measurements carried out by the pyrometer and thermocouples provide different results. The temperature value obtained by the thermocouple is consistently higher than that obtained by the pyrometer, as demonstrated by the series of measurement in this work. The non-homogeneous temperature distribution in punches and the die was investigated on the basis of measurements using a Ni strip with an exactly defined melting point temperature. It was found out that the Ni strip was melted at the process temperature of 1353 °C as measured by a pyrometer whereas the true melting temperature of Nickel is 1455 °C. It was proved that measured process temperatures are different from the temperature experienced by a sample inside the die. However, the temperature measured by the thermocouple is much more accurate than the temperature measured by the pyrometer. The biggest issue is the very limited usage of thermocouples which is given by their maximum operating temperature range to 1200 °C for the K-type thermocouple (its melting point), or around 1500 °C for the C-type thermocouple (due to the reaction of Mo thermocouple sleeve with SPS graphite parts). Therefore, only a pyrometer can be used for monitoring and regulating a high temperature sintering cycle above 1500 °C.

As proved, the measured temperature on the die surface is lower than the temperature experienced by a sintered powder inside the die. Since the relation between the measured process temperature and the temperature inside the die is crucial for controlling the sintering process, several additional experiments were performed. The sintering process was regulated by the pyrometer and the temperature inside the die was verified by a thermocouple. The temperature overshoot over the set temperature was investigated by compacting electrically conductive and non-conductive powders with different heating rates of 50 °C/min and 150 °C/min.

The electrically conductive powder is heated directly by the passing current and the heat is generated in the middle of the die from where the heat is conducted to the surface of the die. Due to this the temperature measured by the pyrometer in a hole located on the side of the die is lower than the temperature in the middle of die. This temperature gradient depends on the heating rate and on the sintering temperature. It is noticeable that the temperature overshoot depends on the heating rate and on the sintering temperature and it is bigger with increasing heating rate. The stable sintering temperature difference above the set point temperature grows with higher sintering temperature for the heating rate of 50 °C/min, but it is constant at all temperatures for the heating rate of 150 °C.

Temperature overshoot above the set point temperature is significant during the sintering of non-conductive powder. It is noticeable that the die is heated from the surface and the heat is conducted to inside of the die. The inner and surface temperatures are equalised at the temperature of 1000 °C. It is above this temperature than the inner temperature becomes higher than the surface temperature, but this difference is not crucial.

On the grounds of temperature measurements, where temperatures overshoots above the set point temperature were studied in detail, an optimised temperature evolution was designed. The optimised sintering temperature evolution led to the decreasing of the temperature overshooting above the set point temperature.

It was found, on the grounds of published papers, that there is only a small noticeable difference in material properties of the SPSed samples compacted by various pulse conditions. Therefore, a reproducibility of the sintering process was investigated and the results were taken into account during forthcoming measurements. The reproducibility of the SPS process was investigated by compacting of two powder types AlNi and nMo. Each powder was sintered three times under the same conditions by non-pulsed current and three times with pulsed current. The SPS process was monitored and regulated by the pyrometer and the process temperature was verified by the type C thermocouple (placed in the bottom punches). While the SPS processes were regulated by a pyrometer, no significant temperature difference above the set point temperature (measured by the thermocouple) was observed between individual SPS processes when non pulsed current was used. But significant differences in temperature (measured by the thermocouple) between individual SPS processes were proved during sintering by pulsed current. **Thus the sintering process has a very poor reproducibility when the pulsed current is applied**.

6.2 Non-homogeneity of sintered samples

In order to determine the material properties of sintered samples, SPS samples were cut and prepared for the metallographic test. The hardness of the samples was measured by the Vickers indentation technique. One half of a sample was mapped by indentation. It was found that the hardness is not distributed homogeneously through the sample cross section, but there are areas with higher hardness and hardness value are decreasing in the direction to the samples edge. This finding is in common with the [67] where the higher porosity of SPSed samples around their circumference and their lower porosity in the middle of the samples are described. Because the measurement of the non-homogeneous distribution by Vickers mapping is a time-consuming measurement, a comparable method was used. The hardness was measured in the horizontal axis as a series of indents. The average values of hardness obtained by mapping of a half of a metallographic sample and in horizontal axis were compared and the average hardness values of two measurements were in good match. This comparison of hardness was measured for more samples and it was found as a good method for evaluation of hardness of samples. In many

publications hardness is evaluated as an average of several indents, which gives an inaccurate result.

6.3 Study of the pulse current effect

If the pulse current has any advantage over non-pulsed current, the samples compacted by pulse current would have lower porosity and better mechanical properties. Thus the effect of the pulsing current was carried out on not fully dense samples, because the influence is not observable on fully dense samples. All powders were compacted at various temperatures in order to determine the dependence of samples porosity on the temperature of sintering. The temperature of sintering where the samples porosity was around 5 % was chosen as the reference temperature. Powders were compacted at the reference temperatures by non-pulsed current and by pulsed current with several pulse conditions. Changes in the porosity, hardness and microstructure of samples were studied.

The results can be categorised into two groups: the process regulated by a thermocouple and the process regulated by a pyrometer.

nNi, uNi and Al7075 powders were compacted at temperatures lower than 1200 °C, therefore the process temperature was measured and regulated by a thermocouple inserted into the bottom punch. It was found that the process temperature overshoot above the set point temperature depends on a current duty cycle. The temperature overshoot is higher in the case of lower current duty cycle (pulses 5-15 ms and 25-75 ms) and it decreases with increasing duty cycle. **Sintering by pulse current results in momentary overshoot of the process value (temperature) over the desired value or set point,** as was observed during all measurements. It is especially significant for the nNi sample compacted with the current of pulse pattern 25-75 ms. The temperature overshoot had an impact on the sample porosity which was lower in comparison to other nNi samples. The change in measured hardness of uNi and nNi samples compacted by various pulse patterns is within a statistical error variance. Al7075 Samples compacted by pulsed current have different phase compounds as evident from SEM pictures. All microstructure of samples compacted by pulse current have a higher ratio of visible precipitates compared to the reference sample compacted by non-pulse current. The higher ratio of visible precipitates (thus lower ratio of precipitates is dissolved in sub grains) results in lower hardness and also lower flexural strength.

The SPS process was regulated by the pyrometer, in the case of sintering nMo, AlNi and Al_2O_3 powders. A type C thermocouple, placed in the bottom punch, measured the temperature that is closer to the real temperature of a sample. It is obvious that the difference of “sample” temperature from the set point temperature is around ±50 °C. The mechanical properties of the SPSed samples were measured and it is evident that the porosity of a sample also depended on the temperature overshoot above the set point temperature. Thus the lower porosity of several samples sintered by pulse current compared to the

reference sample sintered by non-pulse current is not a result of a pulse current, but is caused by the temperature overshoot

Pulse current has no impact on material properties of samples compacted by the spark plasma sintering technique. All measured differences in material properties between samples compacted by pulsed or non-pulse current resulted from a poor reproducibility of SPS process and process temperature differences.

6.4 Effect of sequence of applied uniaxial pressure and heating

The effect of sequence of applied uniaxial pressure and heating on material properties has been verified on Al_2O_3 and Al7075 powders. The powders were sintered under various conditions; powders were pressed by the maximal uniaxial pressure and then heated, powders were heated up to the maximal sintering temperature and then pressed, the powder Al7075 was also heated and pressed at the same time. The effect of sequence of applied uniaxial pressure and heating was investigated by measuring flexural stress. **Samples which were first pressed and then heated had a higher flexural strength (at yield or at break) than the samples which were first heated and pressed after. This dependence was in common for all tested samples.**

6.5 Evaluation results of measurement hardness and flexural strength

Material properties of SPSed samples can be evaluated by measurement of hardness or by evaluation of flexural stress. Hardness and flexural strength were measured on Al7075 samples. As seen from the measured values, both methods are well comparable. However, to achieve a good accuracy of measurement, the flexural measurement had to be measured at least on 10 testing beams, which requires at least five sintered samples. The hardness measurement must be measured by enough indentions (in this thesis by 27 indentions) on the horizontal axis of a sample cross section. Both measurements are time-consuming; however, they provide reliable and comparable results.

7 Appendix

7.1 Hardness evaluation on cross sections of the samples

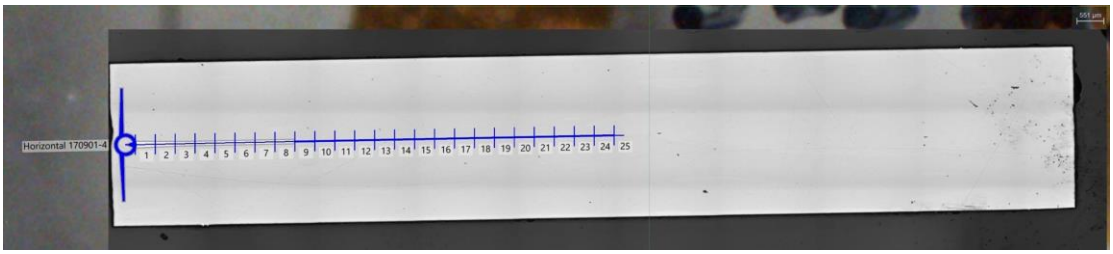

Figure 7-1 Cross section of a sample with highlighted hardness grid

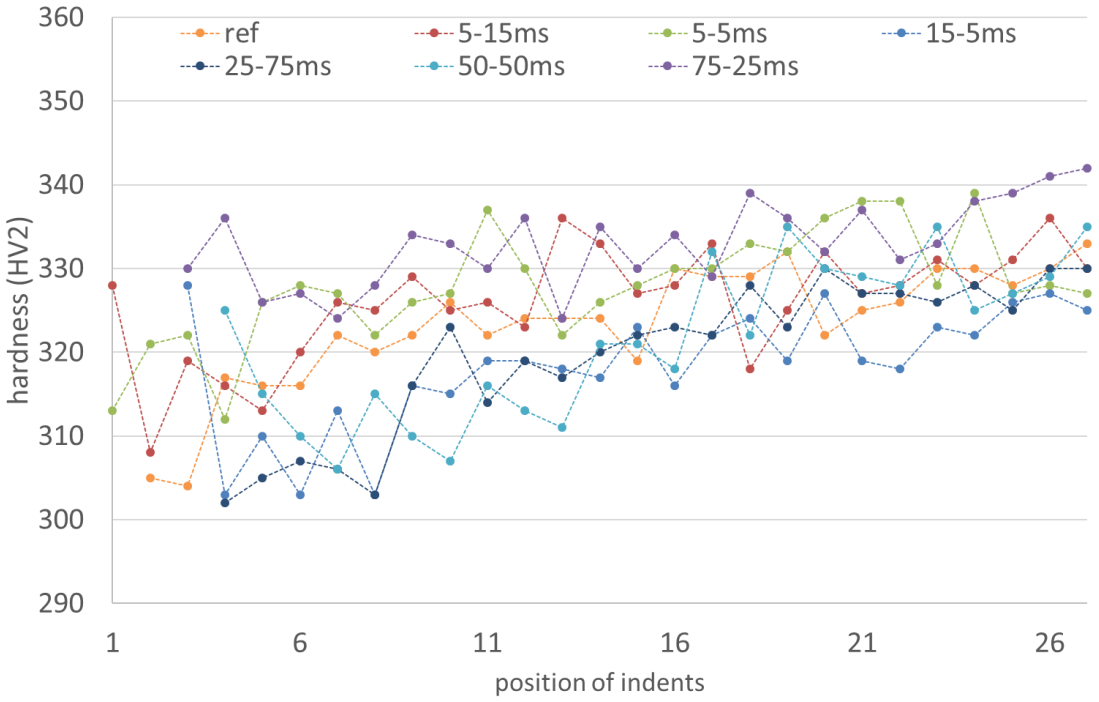

Figure 7-2 Distribution of hardness on nNi metallographic cross section

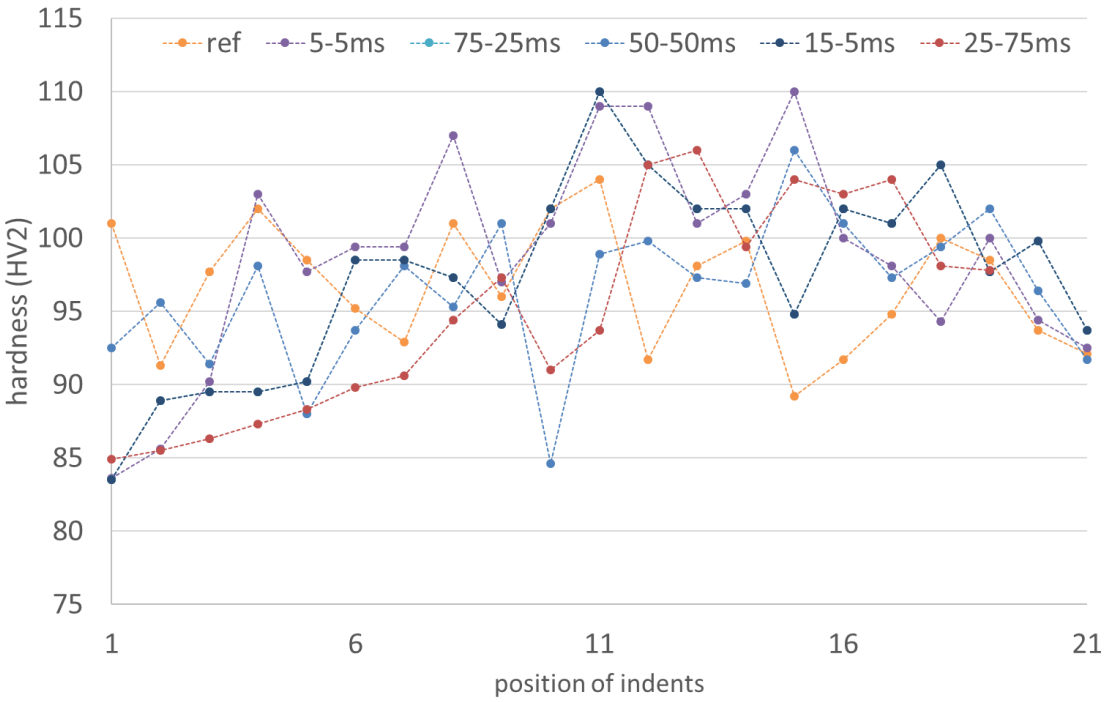

Figure 7-3 Distribution of hardness on uNi metallographic cross section

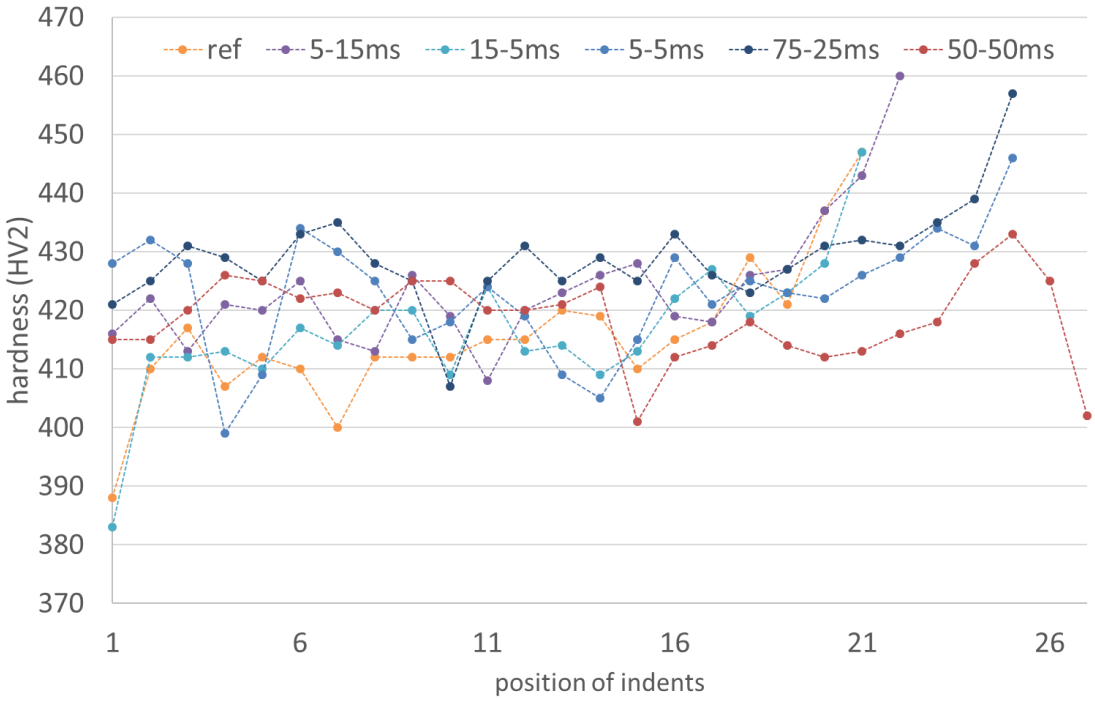

Figure 7-4 Distribution of hardness on nMo 1200 °C metallographic cross section

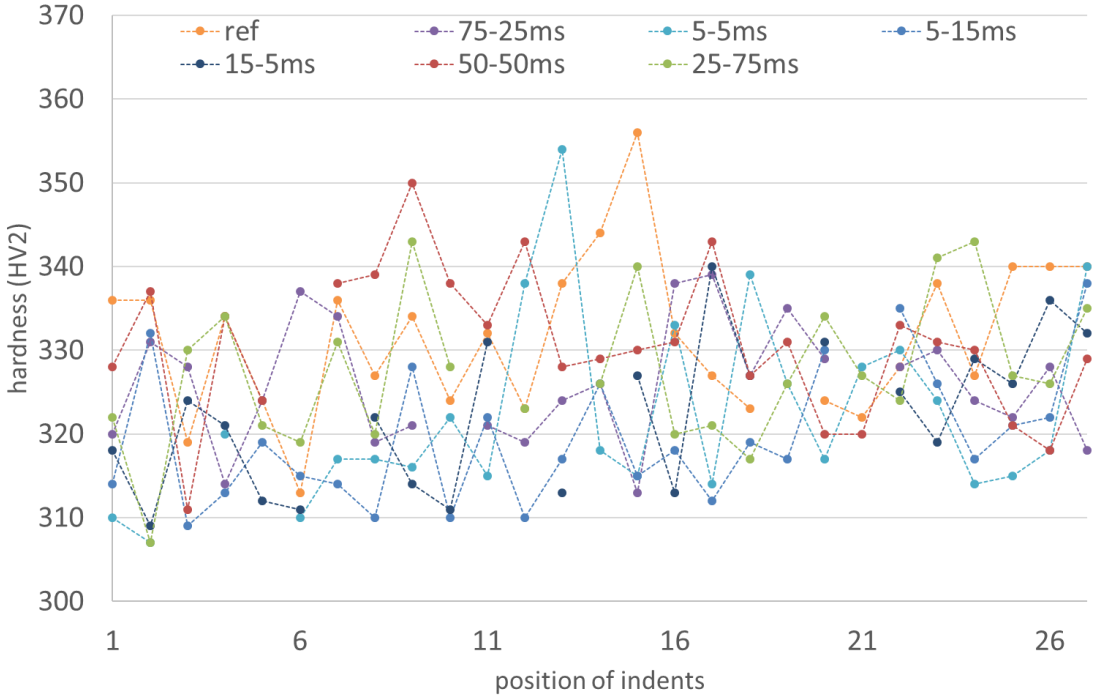

Figure 7-5 Distribution of hardness on AlNi metallographic cross section

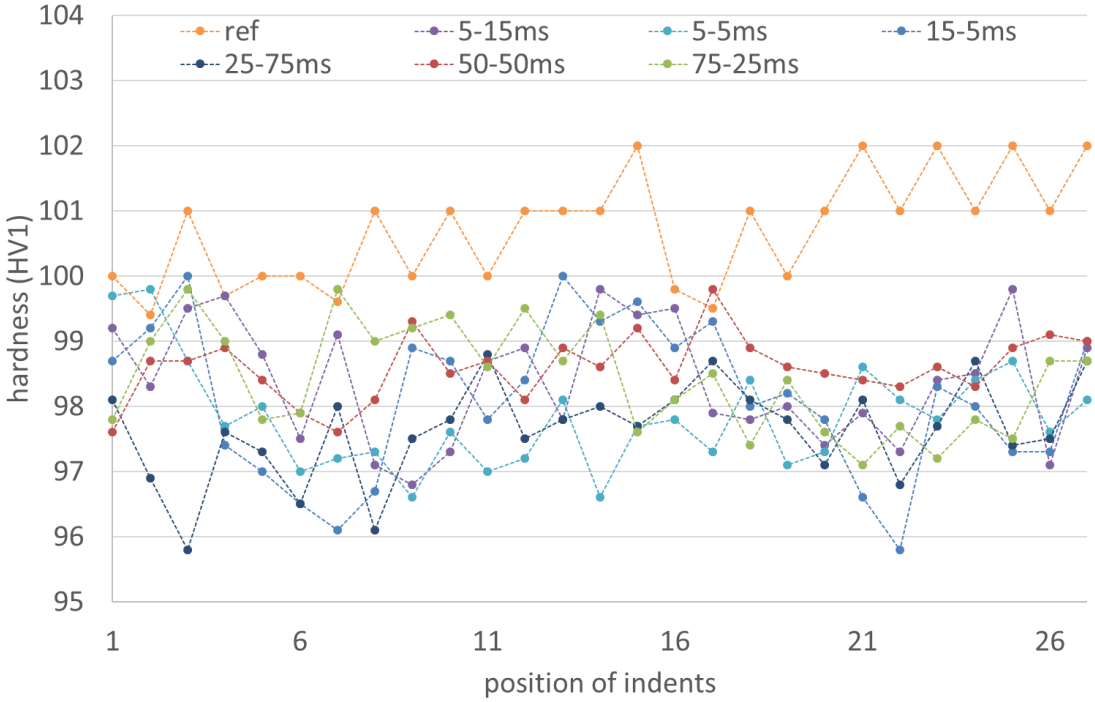

Figure 7-6 Distribution of hardness on Al7075 metallographic cross section

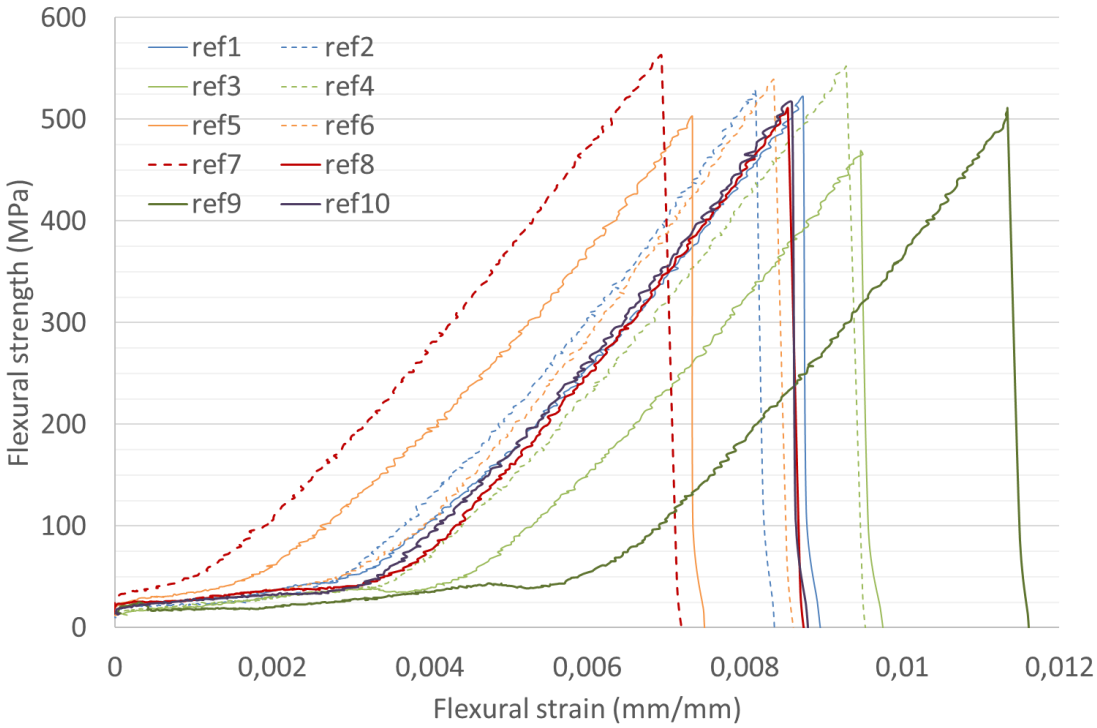

Figure 7-7 Flexural strength of Al2O3 samples sintered by non pulsed current

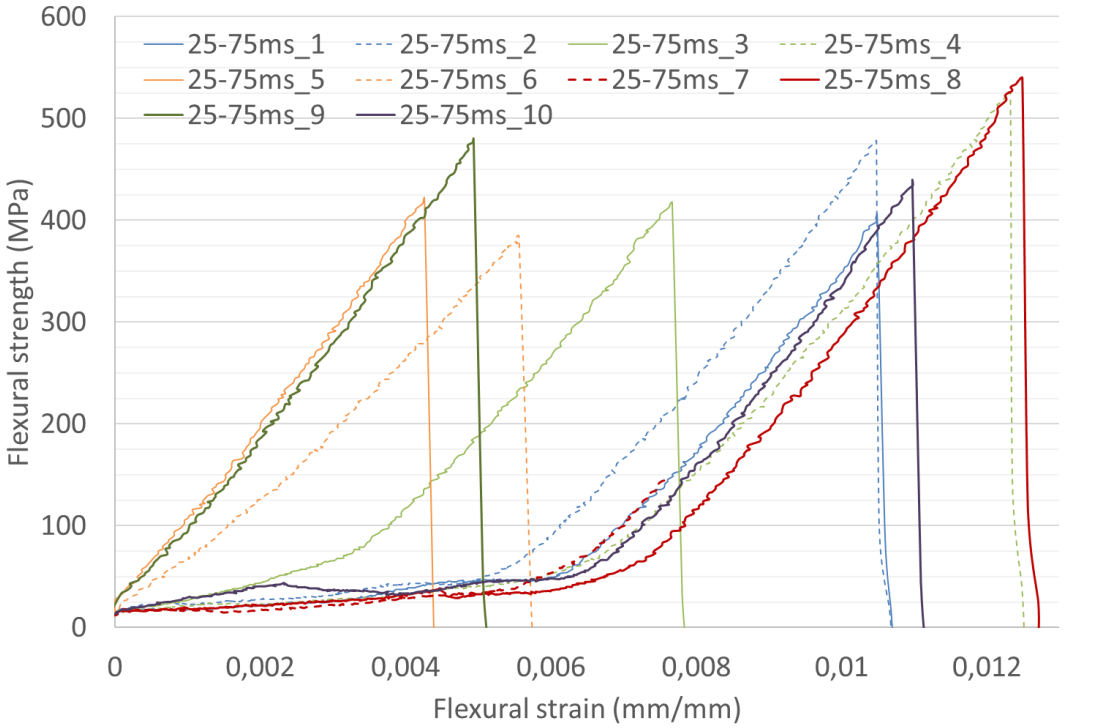

Figure 7-8 Flexural strength of Al2O3 samples sintered by 25-75ms pulsed current

8 List of publications

List of Publications related to Spark plasma sintering, all authors have the same contribution for all papers.

- Papers in Impacted Journals

2017

(Accepted December, 2017 in the journal Ceramics-Silikáty, ISSN 1804-5847) J. Cinert, P. Ctibor, V. Brozek, V. Bouda, L. Mastny, "Preparation of ZrB_2 by boro/carbothermal reduction in SPS device"

M. Koller, T. Chraska, J. Cinert, O. Heczko, J. Kopecek, M. Landa, R. Musalek, M. Remes, H. Seiner, J. Stransky, M. Janecek, "Mechanical and magnetic properties of semi-Heusler/light-metal composites consolidated by spark plasma sintering," *Mater. Des.*, vol. 126, pp. 351–357, Jul. 2017.

F. Lukac, T. Chraska, O. Molnarova, P. Malek, and J. Cinert, "Effect of cryogenic milling on Al7075 prepared by spark plasma sintering method," *Powder Diffr.*, vol. 32, no. S1, pp. S221–S224, Sep. 2017.

2016

P. Pokorny, J. Cinert, and Z. Pala, "Fe-Zn intermetallic phases prepared by diffusion annealing and spark-plasma sintering," *Mater. Tehnol.*, vol. 50, no. 2, pp. 253–256, Apr. 2016.

P. Ctibor, J. Sedlacek, V. Ryukhtin, J. Cinert, and F. Lukac, "Barium titanate nanometric polycrystalline ceramics fired by spark plasma sintering," *Ceram. Int.*, vol. 42, no. 14, pp. 15989–15993, Nov. 2016.

- Other Publications

2017

P. Malek, O. Molnarová, J. Cinert, F. Lukac, and T. Chraska, "Processing of bulk Al7075 alloy by spark plasma sintering," *IOP Conf. Ser. Mater. Sci. Eng.*, vol. 179, no. 1, p. 12050, Feb. 2017.

2016

O. Molnarová, P. Malek, G. Nemeth, J. Kozlik , F. Lukač, T. Chraska, J. Cinert, "THE INVESTIGATION OF AN Al7075 ALLOY PREPARED BY SPARK PLASMA SINTERING OF MILLED POWDERS". METAL 2016 – Conference proceedings: 25th Anniversary International Conference on Metallurgy and Materials. Ostrava: TANGER Ltd., Ostrava, 2016, s. 1200-1205. METAL. ISBN 978-80-87294-67-3.

2014

T. Chraska, J. Medrický, R. Musálek, M. Vilemova, Z. Pala, J. Cinert, “Post-treatment of plasma sprayed amorphous ceramic coatings by spark plasma sintering”. ITSC 2014 :Interational Thermal Spray Conference and Exposition, Abstracts (including manuscripts on CD-ROM). Düsseldorf : DVS Media GmbH, 2014, s. 617-622. ISBN 978-3-87155-574-9. - (DVS-Berichte. 302).

9 References

[1] E. A. OLEVSKY, "SINTERING THEORY," *SAN DIEGO STATE Univ. CALIFORNIA, USA*.

[2] J. Kazior, "Fundamentals of Sintering," *Cracow University of Technology, Department of material engineering*. [Online]. Available: http://riad.pk.edu.pl/~mnykiel/iim/KTM/MP/DOWNLOAD/pdf/CHAPT06.PDF.

[3] E. a. Olevsky, "Theory of sintering: from discrete to continuum," *Mater. Sci. Eng. R Reports*, vol. 23, no. 2, pp. 41–100, Jun. 1998.

[4] A. Lakshmanan, *SINTERING OF CERAMICS – NEW EMERGING Edited by Arunachalam Lakshmanan*. Rijeka, Crotia: InTech, 2012.

[5] T. Kraft and H. Riedel, "Numerical simulation of solid state sintering; model and application," *J. Eur. Ceram. Soc.*, vol. 24, no. 2, pp. 345–361, Jan. 2004.

[6] "The library of manufacturing." [Online]. Available: http://thelibraryofmanufacturing.com/index.html.

[7] H. M. Lee, C. Y. Huang, and C. J. Wang, "Forming and sintering behaviors of commercial α-Al2O3 powders with different particle size distribution and agglomeration," *J. Mater. Process. Technol.*, vol. 209, no. 2, pp. 714–722, Jan. 2009.

[8] Q. Chang *et al.*, "Effect of particle size distribution of raw powders on pore size distribution and bending strength of Al2O3 microfiltration membrane supports," *J. Eur. Ceram. Soc.*, vol. 34, no. 15, pp. 3819–3825, Dec. 2014.

[9] F. Parhami, R. M. McMeeking, a. C. F. Cocks, and Z. Suo, "A model for the sintering and coarsening of rows of spherical particles," *Mech. Mater.*, vol. 31, no. 1, pp. 43–61, Jan. 1999.

[10] V. Kumar, "Simulations and Modeling of Unequal Sized Particles Sintering," 2011.

[11] K. Takagi, S. Masuda, H. Suzuki, and A. Kawasaki, "Preparation of Monosized Copper Micro Particles by Pulsated Orifice Ejection Method," *Mater. Trans.*, vol. 47, no. 5, pp. 1380–1385, 2006.

[12] "【Spark Plasma Sintering】What's SPS," *Fuji Electronic Industrial Co., Ltd.* [Online]. Available: http://sps.fdc.co.jp/whats/whats1.html.

[13] "Metal Sintering Processes Powder metal forming." [Online]. Available: http://www.roymech.co.uk/Useful_Tables/Manufacturing/Sintering.html.

[14] M. Mashhadi, E. Taheri-Nassaj, and V. M. Sglavo, "Pressureless sintering of boron carbide," *Ceram. Int.*, vol. 36, no. 1, pp. 151–159, Jan. 2010.

[15] T. K. Roy, C. Subramanian, and a. K. Suri, "Pressureless sintering of boron carbide," *Ceram. Int.*, vol. 32, no. 3, pp. 227–233, Jan. 2006.

[16] B. S. Mitchell, *An Introduction To Materials Engineering And Science: For Chemical And Materials Engineers*. 2005.

[17] M. L. Pines, “PRESSURELESS SI NTERING OF POWDER PROCESSED FUNCTIONALLY GRADED METAL-CERAMIC PLATES,” University of Maryland, 2004.

[18] Dinesh Agrawal (The Pennsylvania State University), “Microwave Sintering of Ceramics, Composites and Metallic Materials, and Melting of Glasses,” *Trans. Indian Ceram. Soc.*, vol. 65, pp. 129–144, 2006.

[19] T. Street, “COUPLED SURFACE A N D G R A I N - B O U N D A R Y,” vol. 43, no. 4, pp. 1395–1406, 1995.

[20] K. A. Khalil, “Advanced Sintering of Nano-Ceramic Materials,” no. 1.

[21] Z. Z. Fang, X. Wang, T. Ryu, K. S. Hwang, and H. Y. Sohn, “Synthesis, sintering, and mechanical properties of nanocrystalline cemented tungsten carbide – A review,” *Int. J. Refract. Met. Hard Mater.*, vol. 27, no. 2, pp. 288–299, Mar. 2009.

[22] N. U. Yoshihiko Doi, Nobuhito Kuroishi, Shigeki Ochi, “Cold pressing, then sintering,” US4710345 A, 1987.

[23] L. Martin, “Development of Hot Pressing as a Low Cost Processing Technique for Fuel Cell Fabrication,” pp. 1–41, 2003.

[24] P. Antona and C. Mapelli, “Hot Isostatic Pressing (HIP): the State of the Art & Improvement on Two Steels,” *Metall. Sci. Tecnol.*, pp. 3–7, 2013.

[25] Spotlight, “High Performance Parts Using by Hot Isostatic Pressing Process,” *nippon steel & summito metal*, no. 92, pp. 39–41, 2005.

[26] C. D., “Origin of the Liquid Hot Isostatic Pressing process,” *Metall. Sci. Technol.*, pp. 3–5, 2000.

[27] R. Seshadri, B. D. Rao, V. Narayanaswamy, and L. Rangaraj, “Design and fabrication of a laboratory model uniaxial hot press,” *Mater. Sci.*, 1994.

[28] GT advanced technology, “Laboratory Furnace - Graphite.” .

[29] Pascal Schreyer and F. M. Sonder, “Direct Hot-pressing Makes Sintering of Near-net-shape Parts Quick and Easy,” *2009*, pp. 39–40, 2009.

[30] R. Tremblay and R. Angers, “Abnormal grain growth at the curie point during hot-pressing of iron,” *Metallurgical Transactions*, vol. 3. pp. 2711–2712, 1972.

[31] E. O. Hall, “The Deformation and Ageing of Mild Steel: III Discussion of Results,” *Proceedings of the Physical Society. Section B*, vol. 64, no. 9. pp. 747–753, 2002.

[32] S. Grasso, Y. Sakka, and G. Maizza, “Electric current activated/assisted sintering (ECAS): a review of patents 1906–2008,” *Sci. Technol. Adv. Mater.*, vol. 10, no. 5, p. 53001, Oct. 2009.

[33] J. Langer, M. J. Hoffmann, and O. Guillon, “Direct comparison between hot pressing and electric field-assisted sintering of submicron alumina,” *Acta Mater.*, vol. 57, no. 18, pp. 5454–5465, Oct. 2009.

[34] R. Orrù, R. Licheri, A. M. Locci, A. Cincotti, and G. Cao, “Consolidation/synthesis of materials by electric current activated/assisted sintering,” *Mater. Sci. Eng. R*

Reports, vol. 63, no. 4–6, pp. 127–287, Feb. 2009.

[35] M. Nygren and Z. Shen, "On the preparation of bio-, nano- and structural ceramics and composites by spark plasma sintering," *Solid State Sci.*, vol. 5, no. 1, pp. 125–131, Jan. 2003.

[36] N. Saheb *et al.*, "Spark Plasma Sintering of Metals and Metal Matrix Nanocomposites: A Review," *J. Nanomater.*, vol. 2012, pp. 1–13, 2012.

[37] D. Tiwari, B. Basu, and K. Biswas, "Simulation of thermal and electric field evolution during spark plasma sintering," *Ceram. Int.*, vol. 35, pp. 699–708, 2009.

[38] Z. H. Zhang, Z. F. Liu, J. F. Lu, X. B. Shen, F. C. Wang, and Y. D. Wang, "The sintering mechanism in spark plasma sintering - Proof of the occurrence of spark discharge," *Scr. Mater.*, vol. 81, pp. 56–59, 2014.

[39] M. Suárez *et al.*, "Challenges and Opportunities for Spark Plasma Sintering : A Key Technology for a New Generation of Materials," in *Sintering Applications*, 2013, pp. 319–342.

[40] D. Li, E. Yu, and Z. Liu, "Microscopic mechanism and numerical calculation of electroplastic effect on metal's flow stress," *Mater. Sci. Eng. A*, vol. 580, pp. 410–413, 2013.

[41] M. Molotskii and V. Fleurov, "Magnetic effects in electroplasticity of metals," *Phys. Rev. B*, vol. 52, no. 22, pp. 15829–15834, 1995.

[42] H. Conrad, "Electroplasticity in metals and ceramics," *Mater. Sci. Eng. A*, vol. 287, pp. 276–287, 2000.

[43] U. Anselmi-Tamburini, S. Gennari, J. E. Garay, and Z. a. Munir, "Fundamental investigations on the spark plasma sintering/synthesis process," *Mater. Sci. Eng. A*, vol. 394, no. 1–2, pp. 139–148, Mar. 2005.

[44] M. Tokita, "Mechanism of Spark Plasma Sintering," *NEDO Int. Symp. Funct. Graded Mater.*, vol. Kyoto, Jap, no. Mmc, 1999.

[45] N. Tamari, T. Tanaka, K. Tanaka, I. Kondoh, M. Kawahara, and M. Tokita, "Effect of Spark Plasma Sintering on Densification and Mechanical Properties of Silicon Carbide," *J. Ceram. Soc. Japan*, vol. 742, no. 1995, pp. 740–742, 2000.

[46] M. Tokita, "Trends in Advanced SPS Spark Plasma Sintering Systems and Technology," *Journal of the Society of Powder Technology, Japan*, vol. 30, no. 11. pp. 790–804, 1993.

[47] O. Yanagisawa, T. Hatayama, and K. Matsugi, "Recent Research on Spark Sintering Process.," *Mater. Japan*, vol. 33, no. 12, pp. 1489–1496, 1994.

[48] Y. MAKINO, "Characteristics of sintering process based on pulsed high current," *New Ceramics 10*, p. 39, 1997.

[49] H. Tomino, H. Watanabe, and Y. Kondo, "Electric current path and temperature distribution for spark sintering," *Funtai Oyobi Fummatsu Yakin/Journal Japan Soc. Powder Powder Metall.*, vol. 44, no. 10, pp. 974–979, 1997.

[50] G. Xie *et al.*, "Effect of Interface Behavior between Particles on Properties of Pure

Al Powder Compacts by Spark Plasma Sintering.," *Materials Transactions*, vol. 42, no. 9. pp. 1846–1849, 2001.

[51] C. Romaric *et al.*, "Effect of current on the sintering of pre-oxidized copper powders by SPS," *J. Alloys Compd.*, vol. 692, pp. 478–484, Jan. 2017.

[52] C. Collard, Z. Trzaska, L. Durand, J. M. Chaix, and J. P. Monchoux, "Theoretical and experimental investigations of local overheating at particle contacts in spark plasma sintering," *Powder Technol.*, vol. 321, pp. 458–470, Nov. 2017.

[53] K. Vanmeensel, A. Laptev, S. G. Huang, J. Vleugels, and O. Van der Biest, "The Role of the Electric Current and Field during Pulsed Electric Current Sintering," in *Ceramics and Composites Processing Methods*, Hoboken, NJ, USA: John Wiley & Sons, Inc., 2012, pp. 43–73.

[54] O. Yanagisawa, H. Kuramoto, K. Matsugi, and M. Komatsu, "Observation of particle behavior in copper powder compact during pulsed electric discharge," *Mater. Sci. Eng. A*, vol. 350, no. 1–2, pp. 184–189, 2003.

[55] D. M. Hulbert, A. Anders, J. Andersson, E. J. Lavernia, and A. K. Mukherjee, "A discussion on the absence of plasma in spark plasma sintering," *Scr. Mater.*, vol. 60, no. 10, pp. 835–838, 2009.

[56] J. G. Santanach *et al.*, "Influence of pulse current during Spark Plasma Sintering evidenced on reactive alumina–hematite powders," *J. Eur. Ceram. Soc.*, vol. 31, no. 13, pp. 2247–2254, 2011.

[57] U. Anselmi-Tamburini, J. E. Garay, and Z. A. Munir, "Fundamental investigations on the spark plasma sintering/synthesis process," *Mater. Sci. Eng. A*, vol. 407, no. 1–2, pp. 24–30, Oct. 2005.

[58] S. Chakraborty, A. R. Mallick, D. Debnath, and P. K. Das, "Densification, mechanical and tribological properties of ZrB2 by SPS: Effect of pulsed current," *Int. J. Refract. Met. Hard Mater.*, vol. 48, pp. 150–156, Jan. 2015.

[59] N. Orlovskaya and M. Lugovy, Eds., *Boron Rich Solids*. Dordrecht: Springer Netherlands, 2011.

[60] G. Lalet, H. Kurita, T. Miyazaki, A. Kawasaki, and J. F. Silvain, "Thermomechanical stability of a carbon fiber-reinforced aluminum matrix composite fabricated by spark plasma sintering in various pulse conditions," *Mater. Lett.*, vol. 130, pp. 32–35, 2014.

[61] J. Laszkiewicz-Łukasik, L. Jaworska, P. Putyra, P. Klimczyk, and G. Garzeł, "The influence of SPS heating rates on the synthesis reaction of tantalum diboride," *Bol. la Soc. Esp. Ceram. y Vidr.*, vol. 55, no. 4, pp. 159–168, 2016.

[62] G. Aldica, M. Burdusel, S. Popa, M. Enculescu, I. Pasuk, and P. Badica, "The influence of heating rate on superconducting characteristics of MgB2 obtained by spark plasma sintering technique," *Phys. C Supercond. its Appl.*, vol. 519, pp. 184–189, 2015.

[63] L. A. Stanciu, V. Y. Kodash, and J. R. Groza, "Effects of heating rate on densification and grain growth during field-assisted sintering of α-Al2O3 and MoSi2 powders," *Metall. Mater. Trans. A*, vol. 32, no. 10, pp. 2633–2638, Oct. 2001.

[64] Z. Shen, M. Johnsson, Z. Zhao, and M. Nygren, “Spark Plasma Sintering of Alumina,” *J. Am. Ceram. Soc.*, vol. 85, no. 8, pp. 1921–1927, Aug. 2002.

[65] S. R. Bakshi, V. Musaramthota, D. Lahiri, V. Singh, S. Seal, and A. Agarwal, “Spark plasma sintered tantalum carbide: Effect of pressure and nano-boron carbide addition on microstructure and mechanical properties,” *Mater. Sci. Eng. A*, vol. 528, no. 3, pp. 1287–1295, 2011.

[66] M. KAWAHARA, T. SHIROSAWA, T. YASUNO, M. ITO, Y. MAKINO, and Y. KOGO, “Observation and Control of Pore Formation in SPS-Synthesized Alumina,” *J. Japan Soc. Powder Powder Metall.*, vol. 62, no. 5, pp. 228–233, 2015.

[67] L. Minier, S. Le Gallet, Y. Grin, and F. Bernard, “A comparative study of nickel and alumina sintering using spark plasma sintering (SPS),” *Mater. Chem. Phys.*, vol. 134, no. 1, pp. 243–253, May 2012.

[68] B. N. Taylor and C. E. Kuyatt, “Guidelines for Evaluating and Expressing the Uncertainty of NIST Measurement Results,” *NIST Tech. Note*, vol. 1297, p. 20, 1994.

[69] H. Zhang *et al.*, “Processing and microstructure characterisation of oxide dispersion strengthened Fe–14Cr–0.4Ti–0.25Y 2 O 3 ferritic steels fabricated by spark plasma sintering,” *J. Nucl. Mater.*, vol. 464, pp. 61–68, Sep. 2015.

[70] L. Luo *et al.*, “Microstructure and performance of rare earth element-strengthened plasma-facing tungsten material,” *Sci. Rep.*, vol. 6, no. 1, p. 32701, Dec. 2016.

[71] H. M. Rietveld, “Line profiles of neutron powder-diffraction peaks for structure refinement,” *Acta Crystallogr.*, vol. 22, no. 1, pp. 151–152, Jan. 1967.

[72] “A. A. Coelho, (Computer Software), Coelho Software. Brisbane, (2016).”

[73] P. Málek, O. Molnárová, J. Cinert, F. Lukáč, and T. Chráska, “Processing of bulk Al7075 alloy by spark plasma sintering,” in *IOP Conference Series: Materials Science and Engineering*, 2017, vol. 179, no. 1.

[74] L. Gao, J. . Hong, H. Miyamoto, and S. D. D. . Torre, “Bending strength and microstructure of Al2O3 ceramics densified by spark plasma sintering,” *J. Eur. Ceram. Soc.*, vol. 20, no. 12, pp. 2149–2152, Nov. 2000.

[75] T. Borkar and R. Banerjee, “Influence of spark plasma sintering (SPS) processing parameters on microstructure and mechanical properties of nickel,” *Mater. Sci. Eng. A*, vol. 618, pp. 176–181, 2014.

[76] R. Ohser-Wiedemann, U. Martin, H. J. Seifert, and A. Müller, “Densification behaviour of pure molybdenum powder by spark plasma sintering,” *Int. J. Refract. Met. Hard Mater.*, vol. 28, no. 4, pp. 550–557, 2010.

[77] M. T. Tsai and H. C. Shih, “Effects of powder processing on the characterization of magnesia derived from alkoxide precursors,” *J. Mater. Sci.*, vol. 28, no. 16, pp. 4530–4535, 1993.

[78] T. . Srivatsan, B. . Ravi, A. . Naruka, L. Riester, M. Petraroli, and T. . Sudarshan, “The microstructure and hardness of molybdenum powders consolidated by plasma

pressure compaction," *Powder Technol.*, vol. 114, no. 1–3, pp. 136–144, Jan. 2001.

[79] V. V Stolyarov, "Electroplastic effect in nanocrystalline and amorphous alloys," *Mater. Sci. Technol.*, vol. 31, no. 13, pp. 1536–1540, Oct. 2015.

[80] A. I. (Alekseĭ I. Morozov, *Introduction to plasma dynamics*. 2013.

[81] A. Russell, "The Dielectric Strength of Air," *Proc. Phys. Soc. London*, vol. 20, no. 1, pp. 49–91, Jan. 1906.